DEPOSITIONAL TEXTURES AND STABLE ISOTOPIC COMPOSITION

OF THE RILEY TRAVERTINE

Submitted by

ROBERT BOLTON

to

Department of Geoscience

In partial fulfillment for the degree of Master's in Science

May 10, 1993

TABLE OF CONTENTS

LIST OF FIGURES

PAGE

ABSTRACT

A drill core from the Riley travertine, which is an informal member of the Santa Fe Formation, was investigated petrographically and isotopically. Drill core NRDC#1 was chosen for study because it contains a large variety of textures and features. Given the detail needed for petrological observations and precise isotopic sampling, analysis was limited to the upper 12 ft (4 m).

NRDC#1 exhibits many petrographic textures. The most common is intrasparrudite that contains micrite-rich intraclasts. Shrubs, travertine rafts, rhizoliths and translucent laminated bands each comprise a small percentage of NRDC#1. Orange horizontal layers are also seen which are interpreted to represent terra rossa horizons. The textural diversity of the upper portion of NRDC#1 reflects changing depositional environments.

NRDC#1 was sampled isotopically to examine if travertine textures were isotopically sensitive or not. Post-depositional processes affected some of the samples, however a trend of decreasing $\delta^{18}O$ but increasing $\delta^{13}C$ composition is preserved among intrasparrudite and terra rossa horizons. This might be interpreted as either a paleoclimatic warming trend or a changing depositional environment. Another trend seen in a linear traverse of intrasparrudite samples and a specimen of banded travertine from the Riley appears to be a seasonal trend of rise then fall in $\delta^{18}O$ composition during deposition.

INTRODUCTION

THE RILEY TRAVERTINE

LOCATION

The Plio-Pleistocene (?) Riley travertine is approximately 25 mi (40 km) north of Socorro, NM and about 10 mi (16 km) west of Bernardo, NM. The center of the deposit is 10.5 mi (17 km) south of Ladron Peak (Fig 1, Barker, 1984). Access to the Riley travertine is from US-60 or from I-25 (Exit 175) via county ranch roads. The Rio Salado has eroded through the upper members of the Santa Fe Group including the Riley travertine (Massingill, 1977). This has unevenly split the Riley travertine into a northern and a southern region. The northern region of the Riley travertine underlies 17.8 mi^2 (46 km^2) and the southern region underlies 8.1 mi^2 (21 km^2) and the lateral extent before erosion covered at least 58 mi^2 (150 km^2) (Barker, 1984).

GEOLOGY OF THE RILEY TRAVERTINE

The Riley travertine has been examined by several authors with differing opinions on its origin and classification. The Riley travertine was first described by Denny (1940, 1941) who considered it to be a Recent surficial and pedogenic caliche deposit containing a considerable number of gray colored specks which he interpreted to be detrital particles of silt and clay. Bachman and Machette (1977) also consider the Riley a pedogenic calcium carbonate deposit, although they believe the Riley travertine to be a calcrete deposit.

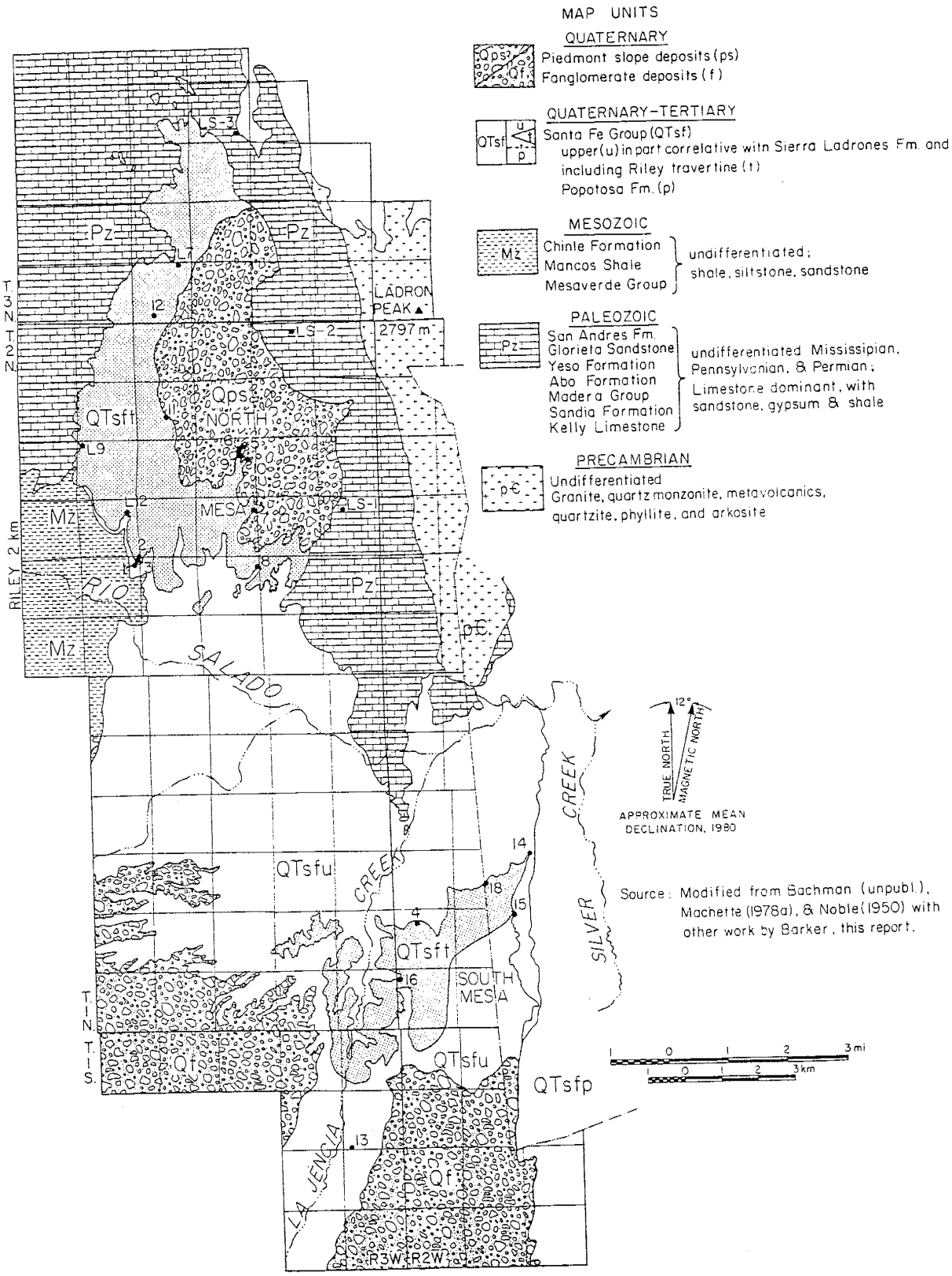

FIGURE 1. Location of the Riley travertine and surrounding regional geology (after Barker, 1983).

Kottlowski (1962) recognized the Riley travertine as a separate geological unit, described it and named it for nearby Riley, New Mexico. He measured a section of it on the north mesa at the NE corner of sec. 22, T2N, R3W where more than 55 ft (17m) of conglomerate and sedimentary breccia is tightly cemented by calcite and contains Paleozoic and Precambrian clasts. Overlying this is up to 20 ft (6 m) in thickness of light-brown to light-gray, laminated, algal limestone in beds 1 to 2 ft (0.3 to 0.6 m) thick. The uppermost layer is loosely consolidated, calichified gravel and sand. Kottlowski's (1962) recognition of the occurrence of "algal-limestones" within the Riley travertine led him to propose a lacustrine origin for the deposit. He envisioned widespread Cenozoic spring-fed pools that precipitated travertine of the overall dimension of the present day extent of the Riley travertine.

Other authors also recognized lacustrine and biogenic features in the Riley travertine. Massingill (1979) mapped a very small portion of the Riley travertine and noticed "laminated, algal-like and oncolite-like" textures. He also detected secondary manganiferous zones in the underlying Popotosa Formation, of the Santa Fe Group, which are vertically aligned and possibly represented conduits for surface springs. Barker (1983) recognized massive, laminated and vuggy physical features along with calcite-cemented breccias which prompted a hypothesis that the Riley travertine is a dynamic system of calcium carbonate accumulation. He demonstrated the geochemical and isotopic

differences between the north mesa and south mesa of the Riley travertine and differentiated between the "North Riley" and "South Riley" travertine. The model of travertine deposition proposed by Barker (1983) was a nonpedogenic process that produced surface and subsurface "carbonate deposits related primarily to lateral groundwater flow." The strength of this proposal is twofold: First, the model not only allows, but requires, the deposition of spring-deposited travertine and biogenic deposits. Secondly, the model accounts for lateral and geographically dependent changes in the morphology of calcium carbonate deposition. Barker (1983) aided understanding of the origin of the Riley travertine by moving away from simple models.

PRE-RILEY GEOLOGY

The geology of the pre-Riley units is varied. Massingill (1979) considers the Riley travertine to be younger than the underlying Popotosa Formation of the Santa Fe Group, but older than the upper Santa Fe Group (Sierra Ladrones Formation) which is found on top of the South Riley travertine. Barker (1983) considers the Riley to be diachronous within the Santa Fe Group and observed that the Riley travertine descends in elevation from the north to the south. The northern base of the Riley rests on Paleozoic rocks while the southern base rests on Cenozoic rocks and the Riley travertine is only seen in depositional contact with underlying units (Barker, 1983). The very subtle synclinal form of the Riley results from the "deposition on

inclined substrates rather than tectonism" (Barker, 1983).

POST-RILEY GEOLOGY

The Sierra Ladrones Formation of the Santa Fe Group continued to be deposited after the termination of deposition of the Riley. This was followed by Quaternary alluvium and most recently, pediment sediments from drainage of the Sierra Ladrones continued to cover the Riley travertine (Massingill, 1979; Barker, 1983). Erosion by the Rio Salado and arroyos that merge with the Rio Salado have exposed the Riley travertine in some places.

The precise time period of deposition of the Riley is not known. Dating of the Riley travertine is handicapped by the lack of an upper radiogenically or biochronographically datable unit. A basalt flow stratigraphically beneath the Riley travertine is dated at 3 m.y. old (Chamberlin and others, 1982) and a stage 6 caliche overprints the South Riley travertine (John Hawley, 1989, personal communication). These bracket the age of the Riley travertine to probably between 1 to 3 m.y. old.

TRAVERTINE FORMATION

The deposition of travertine from natural waters is a complex geochemical process made more complex when biological processes are involved. The deposition of calcium carbonate in springs and spring-fed streams has been studied by many authors (see, for example Friedman, 1970). The formation of travertine

is the result "of inorganically and/or organically caused precipitation from spring waters" (Chafetz and Folk, 1984). Differences of opinion exist on the factors of deposition, such as the significance of biogenic influence on the geochemistry of travertine-precipitating waters (Chafetz et al., 1991; Usdowski et al., 1979). However most workers do agree that a large variety of components play significant roles depositing travertine.

INORGANIC MECHANICS OF DEPOSITION

Natural waters with an elevated carbonate concentration are essential for the accumulation of travertine. Water is the critical component needed to initiate a travertine deposit. The source of the water is commonly meteoric, it can however be surficial meteoric (Slack, 1967), meteoric waters circulating at depth (Herman and Lorah, 1987), or phreatomagmatic waters (Friedman, 1970). Water moving slowly through soil horizons dissolves carbon dioxide which is produced by plants and microorganisms and the fluid becomes CO_2 enriched (Dandurand et al., 1982). This CO_2-rich groundwater can scavenge calcium from granitic or volcanic terrains (Feth and Barnes, 1979 in Chafetz and Folk, 1984), or it can react "with limestone, forming a solution containing Ca^{+2}, HCO_3^- and CO_3^{-2}, as well as H_2CO_3 " (Friedman, 1970).

Carbon Isotopes In Travertine

The complex nature of travertine accumulation also affects

the isotopic systems. At a given temperature, there is a distinct and consistent equilibrium $\delta^{13}C$ difference between the isotopic composition of a fluid and the $\delta^{13}C$ of the calcium carbonate precipitated from the fluid. However, the carbon isotopic composition of the precipitate has been seen to vary with respect to the fluid, at a given temperature. This disequilibrium geochemistry of carbonate precipitating fluids has been recorded by many researchers (for example, see Chafetz et al., 1991; Usdowski et al., 1979). Detailed sampling has shown a large range in the difference of carbon values between travertine and the solution that precipitated it ($\Delta^{13}C$), whereas the difference for oxygen ($\Delta^{18}O$) in most cases is negligible (Chafetz et al., 1991; Friedman, 1970). The cause of the isotopic disequilibria in travertine has been explained as a kinetic effect related to both the inhibition of nucleation of calcite and the supersaturation of $CaCO_3$ in solution before precipitation can occur (Usdowski et al., (1979). In highly supersaturated $CaCO_3$ travertine depositing systems, carbon and oxygen isotopic equilibrium does not exist between the fluid and the precipitate.

Dandurand et al., (1982) simplified the explanation of the kinetic effect to: "precipitation is faster than equilibrium with respect to the isotope". Kinetics affect the site of nucleation and precipitation of $CaCO_3$. As CO_2 is released into the atmosphere, $CaCO_3$ is formed in the solution, but the $CaCO_3$ that is produced stays in solution until a high degree of supersaturation occurs (Usdowski et al., 1979). Studies have shown wide ranges

in the level of calcium carbonate supersaturation before precipitation such as 1 to 16 times supersaturated (Lorah and Herman, 1988), and 2.1 to 48 times supersaturated (Chafetz et al., 1991) in calcium carbonate. The supersaturated solution will eventually overcome an energy barrier to nucleation and precipitate calcium carbonate (Lorah and Herman, 1988). The supersaturated solution is not at chemical equilibrium and this affects the carbon isotopic composition between the carbon compounds in solution (H_2CO_3, HCO_3^-, CO_3^{-2} and dissolved CO_2) and the $CaCO_3$ formed, which includes $CaCO_3$ in solution and $CaCO_3$ precipitated. When the fluid approaches chemical equilibrium, which can be 2 mi (3.2 km) downstream from the vent (Lorah and Herman, 1988), carbon isotopes are nearly in equilibrium, but almost all of the $CaCO_3$ has already precipitated.

Oxygen Isotopes in Travertine

The use of oxygen isotopes in carbonates was pioneered by Clayton (1962) when he published an isotopic fractionation equation of $^{18}O/^{16}O$ between $CaCO_3$ and water. However, his calculations did not take into account the complexity of the geochemistry of travertine depositing systems. While later researchers would discover that oxygen isotopes did not show the variability of carbon isotopes (Chafetz et al., 1991), there was disequilibrium between the oxygen isotopes in the fluid and the mineral precipitate (Dandurand et al., 1982; Usdowski et al., 1979). However this effect is minor oxygen isotopes appear to be

near equilibrium and the variation in ^{18}O has consistently proven to be narrow (Chafetz et al., 1991). The process of evaporation (Amundson and Kelly, 1987) and decreasing kinetic factors (Friedman, 1970) have been invoked as the cause for the small difference between calculated and field measured equilibrium values for the fluid-$CaCO_3$. While the cause is still unclear (Amundson and Kelly, 1987), most studies indicate that oxygen isotopes in the deposited travertine are not at equilibrium.

Oxygen isotopes in travertine are used as paleoclimatic indicators. Two different oxygen isotopic techniques are used in paleoclimatic research. One involves the direct calculation of paleoclimatic temperatures at the time of mineral deposition using $^{18}O/^{16}O$ fractionation equations if the $\delta^{18}O$ of the fluid is known or assumed (Lambert and Harvey, 1987). Another approach is to compare ^{18}O trends between the deposited $CaCO_3$ and known ^{18}O trends from cores such as marine and arctic ice cores to match the trends and thereby gain an understanding of the paleo-climate (Winograd et al., 1988). The near equilibrium of$\delta^{18}O$ fluid with $\delta^{18}O$ $CaCO_3$ (deposited) allows the use of oxygen isotopes as a two-dimensional paleoclimatic indicator.

BIOGENIC DEPOSITION

The geochemistry of travertine waters can be altered by biological organisms that do not directly produce travertine. Photosynthetic plants including algae and cyanobacteria consume CO_2 and produce O_2. By consuming CO_2, organisms remove it from

the aqueous environment which has the same effect as degassing. This effect has been referred to as biogenic modification by Golubic (1991). Slack (1967) observed biological activity changing the CO_2 content of a slow moving creek. The production of oxygen bubbles by photosynthetic organisms that absorb CO_2 can lead to the accumulation of calcium carbonate coated "bubbles" (Chafetz et al., 1991). The oxygen bubbles absorb CO_2 from the surrounding waters which effectively degasses the solution in the "microenvironment" and leads to encasement of the bubble in calcium carbonate (Chafetz et al., 1991). Biogenic influenced degassing of carbonate-rich fluid will alter the geochemistry of that fluid and lead to the deposition of travertine.

Micro-organisms can directly deposit travertine in streams and springs. Alga (red and green) are known to indirectly "trap" $CaCO_3$ on their filaments (Golubic, 1991). Golubic, (1991) noticed that multiple species of micro-organisms interact within stromatolites to deposit $CaCO_3$. Chafetz et al., (1991) found cyanobacteria that produce $CaCO_3$ and encase themselves, forming microscopic, nondirectional, calcite crystals with organic material in their centers (Chafetz et al., 1991). Emeis et al., (1987) described an example where diatom blooms produce dissolved organic carbon which encourages nucleation of micritic $CaCO_3$ in the euphotic zone. Epiphytes (diatoms and prokaryotes) colonize on other organisms, such as mosses, bind the micritic particles and biologically induce deposition of the particles (Emeis et

al., 1987). The particles become nucleation sites for chemically deposited $CaCO_3$. These different forms of biogenic deposition display the diversity of biogenic accumulations in travertine.

MORPHOLOGY

Various depositional environments exist in a travertine system including vents, waterfalls, channels, deep ponds and rimstone dams. The combined inorganic and organic processes of deposition cause a variety of textures. Many names such as tufa, sinter, calcareous tufa, and marl were used previously to distinguish textures that were assumed to be produced by a specific type of nonmarine biotic or non-biotic process (see, for example, Irion and Muller, 1968). A modern classification correlating different morphologies of travertine to specific depositional environments was proposed by Chafetz and Folk (1984). Fissure ridges form "irregular, thin layers parallel to the surface morphology" and sloping mounds, cones and fans that are non-horizontal form deposits of variable strata thickness. Another environment is the shallow lakefill deposits that are horizontally stratified and contain massive and dense carbonate mud and bacterial growths known as "shrubs". The strength of this classification system developed by Chafetz and Folk (1984) is that it is jointly based on field and petrographic observations.

Many textures and features are seen in the Riley travertine. A list of definitions of petrological terms used in this thesis is presented in Table 1. Many terms are derived from the

TABLE 1 - GEOLOGIC TERMS TO THE TRAVERTINE IN NRDC#1

Clast:	An individual grain or fragment of a [sediment of] rock, produced by weathering.
Coated grain:	A sedimentary particle possessing concentric or enclosing spherical to lensoidal layers of calcium carbonate around a nucleus.
Intraclast:	A general term for a component of limestone representing a torn-up and reworked fragment of a penecontemporaneous sediment (having any degree of lithification) that has been eroded within the basin of deposition and redeposited there to form a new sediment.
Micrite:	A matrix (or material) of semiopaque micro-crystalline carbonate having a crystal size of 4 microns or less in diameter (Folk, 1962).
Neomorphism:	A term for the transformation of a mineral grain. Neomorphism can be caused by the processes of inversion, recrystallization and strain recrystallization. The new grain can be larger (aggradational) or smaller.
Ooid:	A grain that has the structure of a pisoid but is smaller than 0.8 in. (2 mm).
Peloid:	A small (0.3 to 0.15 mm, usually rounded to elliptical aggregate of accretionary composed of almost exclusively clay-sized (micritic) material. Peloids can be a product of algae and/or cyano-bacteria (Friedman et al., 1973), (Chafetz, 1986) although peloids may be formed in other ways.
Pisoid:	A pisolith. A spherical or ellipsoidal accretionary body composed of calcium carbonate. The nucleus of a pisoid is surrounded by concentric laminations which may be due to biogenic activity. The size of a pisoid is usually 0.8 in (2 mm) or greater. The larger size of the pisoid separates it from ooids.
Pseudospar:	A neomorphic calcite cement that forms grains 20 microns or larger in diameter.

Rafts: A calcium carbonate feature that forms at the aqueous surface as elongate micrite core. After it sinks below the fluid surface, micritic and/or spar cements coat the core, and commonly found with iron-stained carbonate. (Jones, 1989).

Rhizolith: A feature caused by the existence of a plant stem or root that produces a moldic pore after deposition stops. The rhizolith can be filled-in latter by spar or micritic cements. (Mount and Cohen, 1984).

Shrubs: A bacterially-produced calcium carbonate feature 0.4 - 2.0 in. (1 - 5 cm) found in travertine that resembles "trees in the forest" (Chafetz and Folk, 1984).

Spar: A calcite cement that forms grains 10 μm or larger in diameter. Spar cement differs from neomorphic spar in that spar cement is a void-filling post-deposition product. (Folk, 1962).

Tepee Structure: A sedimentary structure consisting of a fold which in cross section resembles a chevron or an "inverted depressed v" (Leslie et al., 1992).

Terra Rossa: Orange to red-brown, iron-stained sparry calcium carbonate in as horizontal bands; a remnant of subaerial exposure and/or depositional hiatus (Allan and Matthews, 1982).

Glossary of Geology some terms however, have been modified specifically for the context of travertine, with the appropriate author(s) listed.

NORTH RILEY TRAVERTINE

DESCRIPTION OF NORTH RILEY TRAVERTINE

The North Riley drill core number one (NRDC#1) was chosen for detailed examination because it is the best example of the diversity of textures within this unit available. The other prime consideration for choosing NRDC#1 was that this is the most complete drill core. As there are significant geochemical and textural differences between the north mesa and south mesa of the Riley travertine (Barker, 1983), it was decided to study only one region. The core was drilled vertically and the first recovered travertine of NRDC#1 begins at 27 ft (8.2 m) below the surface. Each 10 ft (3.1 m) of NRDC#1 is considered an interval (27-37 ft or 8.2-11.3 m) and only the upper or first interval was examined in detail. A few small sections, 2 in. (51 mm) or less, of the core are missing. Some small gaps within the core are found within an oxidized iron-rich zone. Rarely, calcite crystals are found filling in a vug or in a perimeter of these gaps. The direction of crystal growth is inward, toward the missing material which indicates later void-filling spar. The base of the NRDC#1 is 96 ft (29.2 m) below the surface. Within the lower region of the core, the travertine is more iron-stained and friable.

Detailed inspection of the NRDC#1 revealed regions of the core that displayed periods of reworking and non-deposition. Because NRDC#1 does not represent a continuously depositing, unaltered core, isotopic sampling of NRDC#1 could mix data from primary and secondary material. Before the NRDC#1 was sampled for isotopic analysis, a travertine specimen from North Riley that appeared, in thin section, to be largely unaffected by secondary processes was used as a baseline to measure "typical" isotopic variations. The Riley banded travertine specimen (RBTS) was chosen to provide isotopic data that could display the variation of $\delta^{18}O$ and $\delta^{13}C$ that would be expected from primary processes, although RBTS would not directly indicate whether NRDC#1 was unaltered and continuous. RBTS is comprised of lamellae that appear similar to banded epithermal ore veins (Fig. 2). The lamellae averaged 0.08 in. (2 mm) although some layers were under 0.04 in. (1 mm). The total height of the sample was about 2.0 in. (51 mm). RBTS was analyzed isotopically to set a baseline for comparison to regions within NRDC#1.

The depositional model for travertine advanced by Chafetz and Folk (1984) implies that a multitude of textures demonstrates multiple depositional environments. The North Riley travertine exhibits "shrubs", peloids, rhizoliths, micrite layers, terra rossa horizons and other features. These textures are produced by different depositional environments. This indicates that the travertine that comprises NRDC#1 lies within a highly dynamic

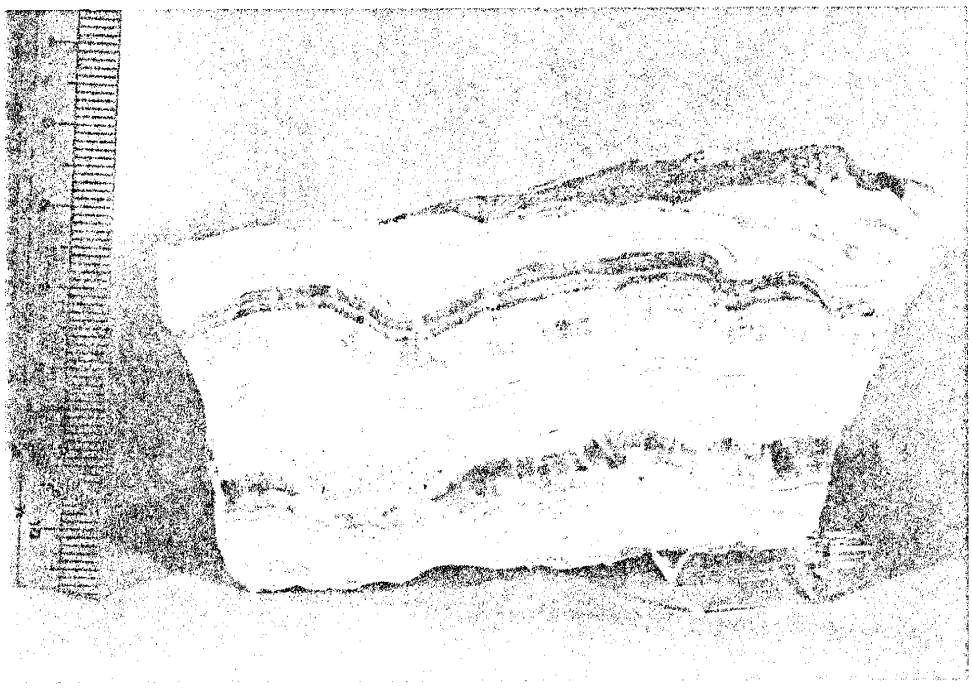

FIG. 2 - Photograph of the Riley banded travertine specimen (RBTS), wet surface for contrast. Centimeter scale on left side.

system of travertine deposition.

The rate of travertine accumulation in NRDC#1 was highly variable. The rate of travertine deposition can effect which textures will form. At Tivoli, Italy, deposition rates of about 3 ft/yr (1 m/yr) have been measured for dense micritic $CaCO_3$, whereas shrub accumulation only form in areas of low, 2-4 in. (5-10 cm), accumulation (Folk, personal communication, 1991). In the first ten feet of NRDC#1, there are 8 in. (20 cm) thick unbroken micrite layers, but there are also shrub layers and travertine rafts which imply a period of slower deposition. The abundance of intraclasts that indicate reworking of previously deposited travertine was common. The existence of orange horizontal layers within NRDC#1 are most likely subaerial exposure surfaces which imply a hiatus in carbonate deposition. The many textures are evidence of changing depositional environments with differing accumulation rates within the North Riley travertine.

ISOTOPIC DATA COLLECTION

An isotopic sampling program was developed to examine minute features in the North Riley travertine. A Fordham variable-speed flexible-shaft power drill on a stand was equipped with a tungsten carbide bit. The RBTS was sampled first, and 57 samples were collected over the 2 in. (51 mm) width of the specimen. Then 100 samples from the upper 14 ft (4.3 m) of NRDC#1 were collected. All samples were treated with pure H_3PO_4 for at least 4 hr on a

standard carbonate isotopic vacuum line. The CO_2 produced from the reaction was analyzed on a Finnegan-MAT Delta E mass spectrometer. The $\delta^{13}C$ values are reported relative to PDB and the ^{18}O values are measured relative to SMOW, but SMOW and PDB values for ^{18}O can be found in the appendix. Samples were rerun on the mass spectrometer if the standard deviation of 0.08 $^{0}/_{00}$ or greater was encountered for carbon and/or oxygen. A comparison of five samples extracted twice on the carbonate vacuum line showed an average error of $0.11^{0}/_{00}$ $\delta^{13}C$ and $0.09^{0}/_{00}$ $\delta^{18}O$. The RBTS samples averaged $22.9^{0}/_{00}$ for $\delta^{18}O$ and $3.7^{0}/_{00}$ for $\delta^{13}C$ while the NRDC#1 samples averaged $22.6^{0}/_{00}$ for $\delta^{18}O$ and $6.7^{0}/_{00}$ for $\delta^{13}C$.

Samples were chosen to represent the diverse textures and features in NRDC#1. Textures such as intrasparrudite, terra rossa horizons, rafts, shrubs and translucent laminated bands were sampled as well as features such as micro-stalactites and void-filling spar. The number of samples taken from any texture or feature loosely represents the abundance of that material. Other samples were taken in sets to examine the isotopic systematics. Samples were collected above and below a terra rossa horizon to see if there was a trend in the isotopic data, and void-filling spar samples along with the adjacent material were collected to see if the spar was derived from the adjacent material. Similar textures from different regions of NRDC#1 were sampled and compared to one another to examine the possibility of a long-term trend. Some samples were taken randomly in an attempt to find a cryptic trend and prevent sample bias.

PETROLOGY OF NRDC#1

OVERVIEW

The upper 20 ft (6.1 m) of NRDC#1, from 27 to 47 ft (8.2 to 14.3 m), was chosen for detailed study because it displays the largest variety of textures seen in the core. The upper portion of NRDC#1 contains primary sedimentary particles such as peloids and pisoids. Authigenic material, including shrubs, and sedimentary features such as rhizoliths and terra rossa horizons are also found in NRDC#1. The upper portion of NRDC#1 has undergone diagenetic alteration, that produced void-filling cements and neomorphism.

Approximately 70% of the upper 20 ft (6.1 m) NRDC#1 is composed of brownish-orange to beige fine grain calcite that appears micritic in hand sample. Using the carbonate classification proposed by Folk (1962), this material would be classified as an intrasparrudite. Intraclasts, which are commonly composed of peloids, are far more prevalent than coated grains in NRDC#1. Because some of NRDC#1, such as peloids, probably was produced by micro-organisms, the Burne and Moore (1987) classification system represents an advance in differentiating microbial carbonates. However, their system relies on knowing the precise role of microbes, which is beyond the scope of this study. Therefore, the travertine that comprises NRDC#1 can only be assigned to the larger classification "microbialite".

PRIMARY TEXTURES

SEDIMENTARY PARTICLES

Peloids

Peloids are a very common component of the total allochems within the intrasparrudite of NRDC#1. The shape of peloids varies from spherical to ellipsoidal, though most are nearly spherical. Peloids are often found together in clumps surrounded by first a fine grain, opaque, isopachous cement, then sparry cements (Fig. 3). More commonly, multiple groups of peloids are found together and then further recemented, forming intraclasts (Fig. 4). Rarely, individual or small groups of peloids are found "free floating" in sparry cement. The peloids in NRDC#1 were once carbonate mud that has now become micrite.

Coated Grains

Some allochems have a multiple laminated rim which strongly suggests that they are coated grains. The size of the coated grains in NRDC#1 range from 0.004 in (0.1 mm) to 0.12 in. (3 mm), so thereby both pisoids and ooids are found in the Riley. Almost all the coated grains in the upper portion of NRDC#1 are deformed ellipses to lensoidal in shape and compare favorably with the travertine pisoids (Folk and Chafetz, 1983) or travertine vadoids (Peryt, 1983). Many coated grains have peloids or rarely travertine clasts as nuclei, surrounded by a few concentric laminations. Only a few oncoids, irregularly laminated grains, have been recognized in the upper portion of NRDC#1. Very different from the other coated grains in NRDC#1 are large, over

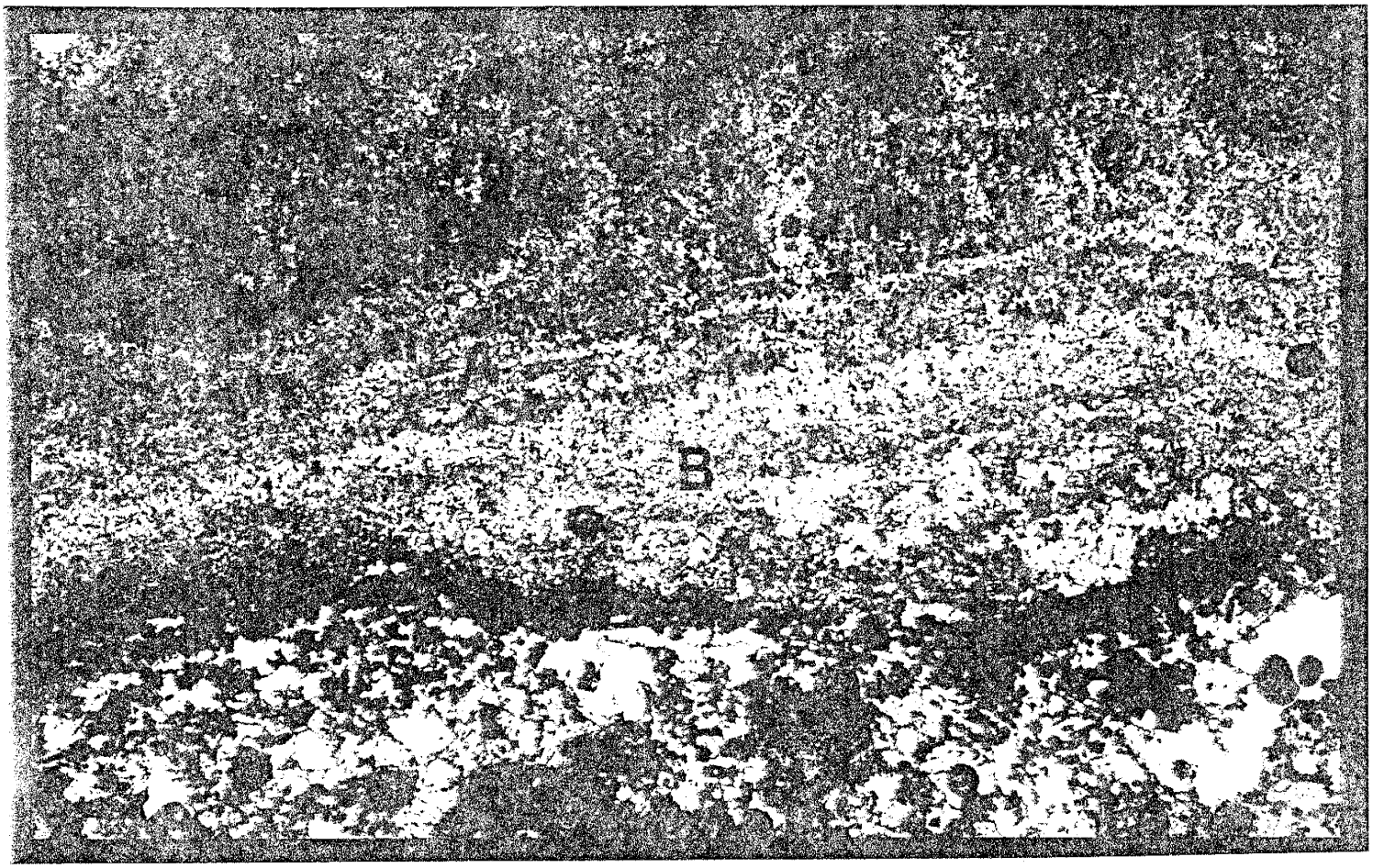

FIG. 3 - A grain composed of opaque peloids (A) (upper portion of photograph) that has discontinuous spar/micrite layers (B). An isopachous micritic cement separates the grain from the spar cement. Field of view is 2mm.

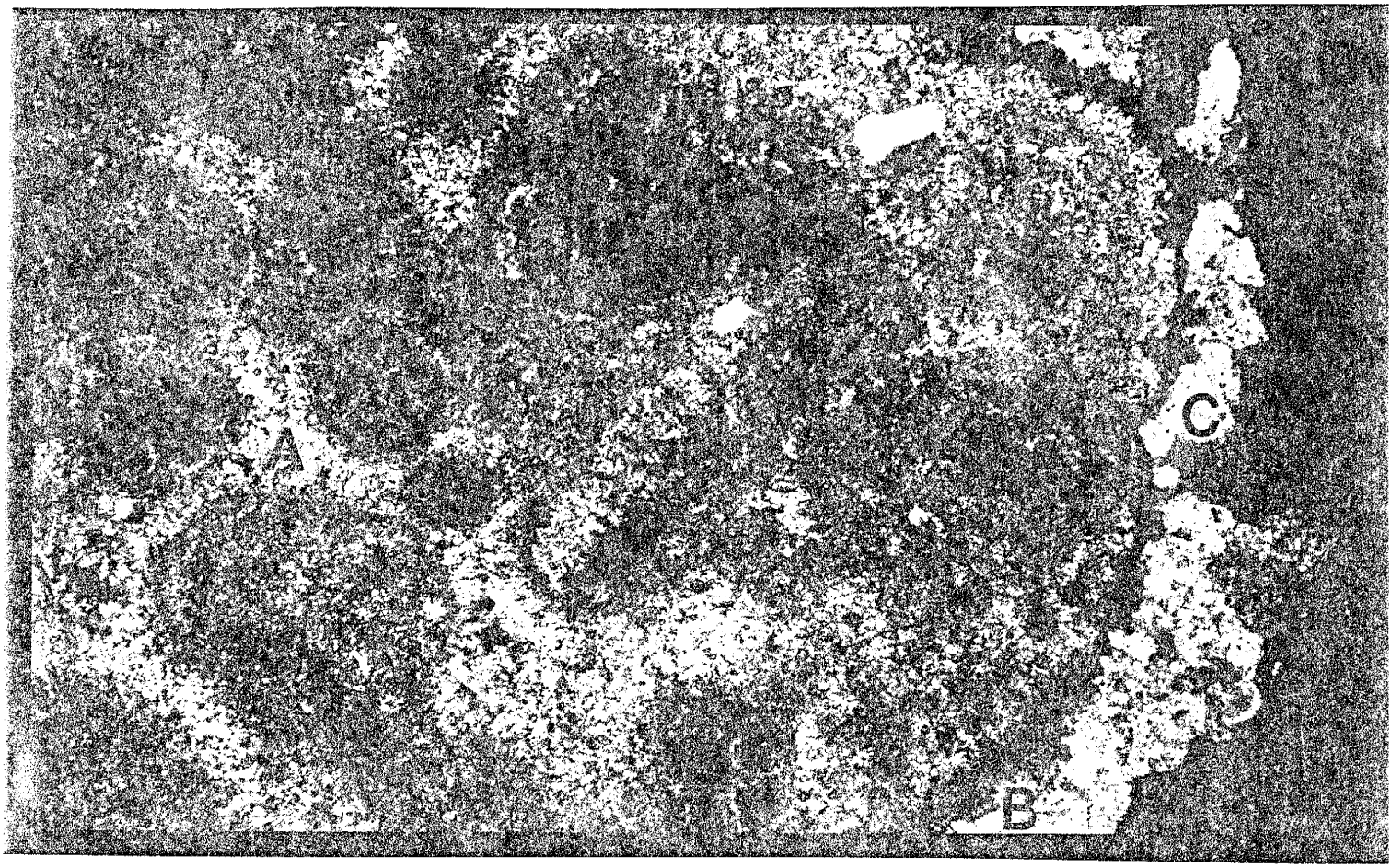

FIG. 4 - An intraclast showing multiple peloids (A) cemented together and coated by an isopachous micrite cement (B), then an outer void filling spar cement (C). Field of view is 2 mm, the photograph was taken with crossed polars.

0.5 in. (12 mm), nearly spherical with many well-defined concentric laminations. These large pisoids are found in the 37 to 38 ft (11.3 to 11.6 m) section of NRDC#1, and are very similar to inorganic pisoids described by Folk and Chafetz (1983).

Intraclasts

Intraclasts are the most abundant allochem in NRDC#1. They comprise approximately 50%, by volume, of the allochems in the first 10 ft (3.1 m) of the core and about 70% of the upper 20 ft (6.2 m) of NRDC#1. The size of these intraclasts is variable, but most are larger than 0.02 in. (0.5 mm) and many are visible as pinkish-beige crescent shaped grains. Most intraclasts contain peloids in clumps surrounded by two stages of cement. The first is an opaque, isopachous micrite followed by a sparry, bladed pore-filling cement (Fig. 4). This sequence of erosion then cementation is repeated in the formation of intraclasts, except that the sparry cement is usually scalenohedral or rhombohedral. Commonly travertine clasts are incorporated into intraclasts, and some intraclasts are composed of smaller intraclasts, indicating multiple periods of deposition then weathering and/or rip-up and redeposition.

Travertine Rafts

A few groups of travertine rafts occur in the 32.5 to 34 ft (9.9 to 10.4 m) section of NRDC#1. Rafts are seen as opaque, white, slightly curved rods, that average 0.5 to 1.0 in. (1 to 2.5 cm) long by a few millimeters wide. The rafts are either coated by or directly associated with orange iron-stained

calcite. The start of the raft region and the terra rossa capping can be seen in Fig. 5. Rafts comprise about 5% of the first 10 ft (3.1 m) of NRDC#1 and they are not found in the second 10 ft (3.1 m) section of core. Most rafts in NRDC#1 have been modified by post-depositional cements, which surround the rafts accentuating visibility.

The initial, raft core is a thin, tabular, opaque core composed of very fine grain carbonate that is commonly 0.0004 in. (10 microns) wide and 0.004 in. (100 microns) long. These raft cores have been recognized in other travertine deposits as forming at the fluid surface where degassing is rapid (Chafetz et al., 1991). Fig. 6 displays multiple raft cores with very fine grained, opaque material emanating from the cores in one direction. This direction corresponds to the upward direction of NRDC#1 and seems to indicate the growth direction of the material. A recent article about rafts by Jones (1989) describes similar thin, tabular raft cores with directional growth features. A more detailed comparison of raft morphology can be found under "Raft Modification".

AUTHIGENIC MATERIAL

Shrubs

Shrubs are a feature described by Chafetz and Folk (1984) from Bagni di Tivoli, Italy. Shrubs resemble "fernlike arborescent growths that branch upward to form colonies 1 to 3 in. (2-8 cm) high, giving a sawn slab the appearance of a

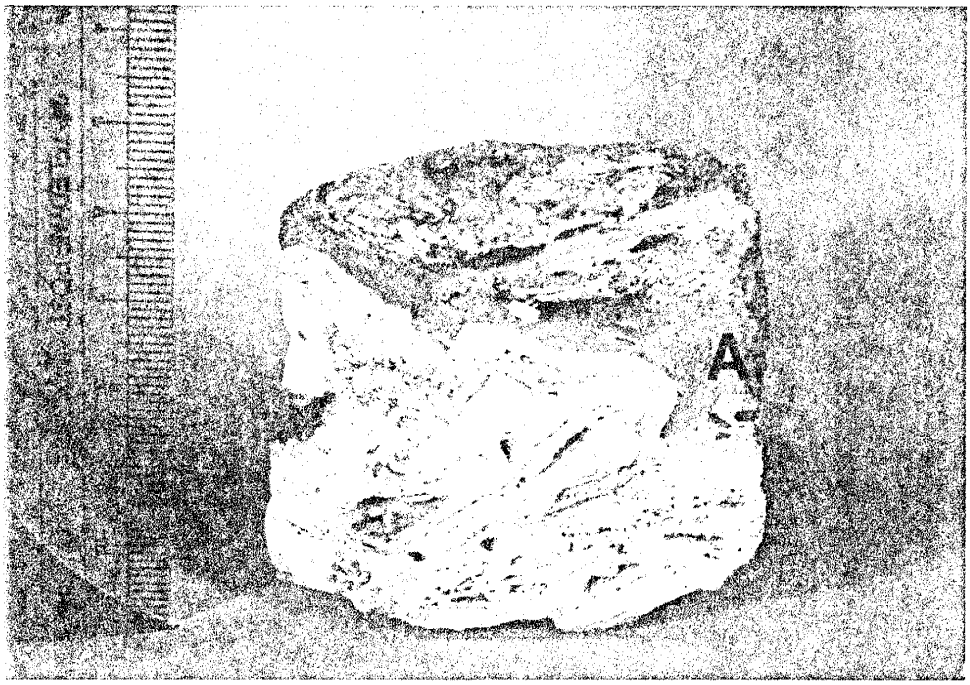

FIG. 5 - Photograph of a terra rosa horizon (A) capping the uppermost rafts in the raft region in NRDC#1. Wetted surface, centimeter scale on left side.

FIG. 6 - Linear, opaque rafts (A) "floating" in a spar matrix. The raft cores are very thin and linear with a fine-grain opaque material emanating from the cores in the upward direction within NRDC#1. Elongated micrite sutures point toward the surface. Field of view 2 mm, the photomicrograph was taken in plain light.

succession of miniature forests (Chafetz and Folk, 1984)" Shrubs are formed by bacteria, especially cyanobacteria in quiescent pools characteristic of shallow lake-fill deposits and "are the result of extracellular encrustation of bacterial bodies by crystals of calcite (Chafetz and Folk, 1984)". Shrub layers are commonly horizontal and laterally continuous for many meters and can exhibit vertical accumulations of more than 16 ft (5 m) (Chafetz and Folk, 1984). The morphology and depositional pattern of these shrubs are the type reference for shrub accumulations.

Shrub accumulations in NRDC#1 are poor in comparison to the classic shrub morphology described above. Shrubs occur in two separate and distinct regions within the first 10 ft (3.1 m) of NRDC#1. Both shrub regions combined are less than 10% of the upper interval. They are almost nonexistent in the second interval. The calcite that comprises shrubs is dark brown micrite. Shrubs are branch upward toward the top of the core, which indicates the direction of growth (Fig. 7). Many of the individual shrubs have an overgrowth of isopachous spar cement (Fig. 8). The base of each shrub is usually "anchored" in thin micritic laminations. Shrub clasts are also found in NRDC#1. Shrubs represent a small, but important texture in understanding the depositional conditions of the North Riley travertine.

Shrub Regions

The upper shrub region contains abundant peloids and intraclasts. The layer is found 31 to 32 ft (9.4 to 9.8 m) below the

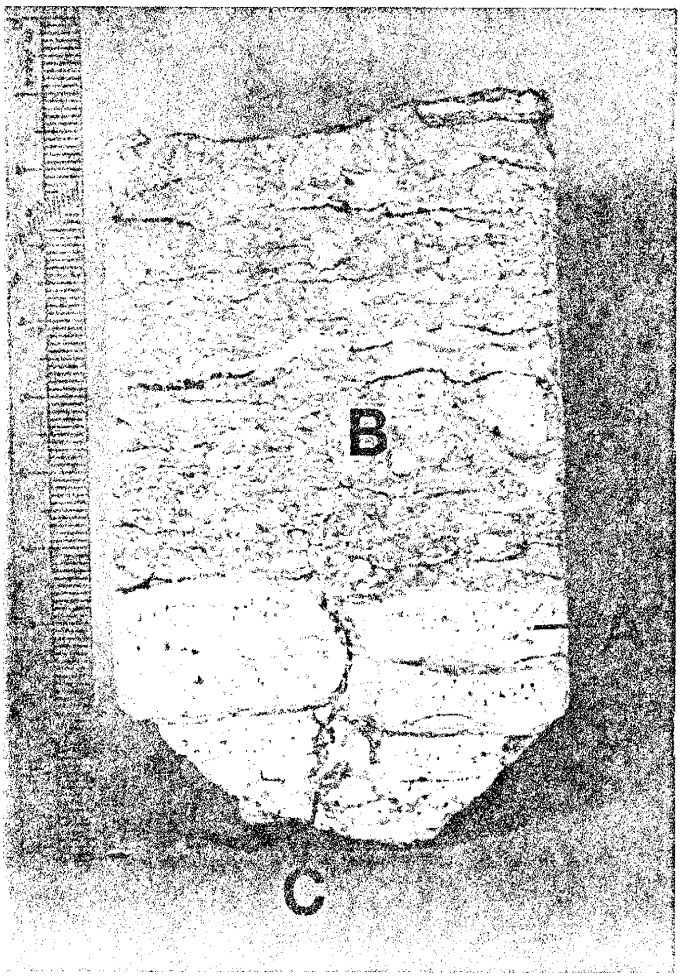

FIG. 7 - Photograph of part of the lower shrub layer (A) showing "trees in the forest" layering. Micritic allochems in intrasparrudite cap (B) the shrub layer, which has been bisected by a desiccation crack (C). Centimeter scale on left.

FIG. 8 - Shrubs (A) growing vertically on a micritic lamination (M). In the upper photograph some of the shrubs have a thin spar rim (S) coating them. Field of view 2 mm, the upper photomicrograph was taken in plain light, while the lower was taken with crossed polars.

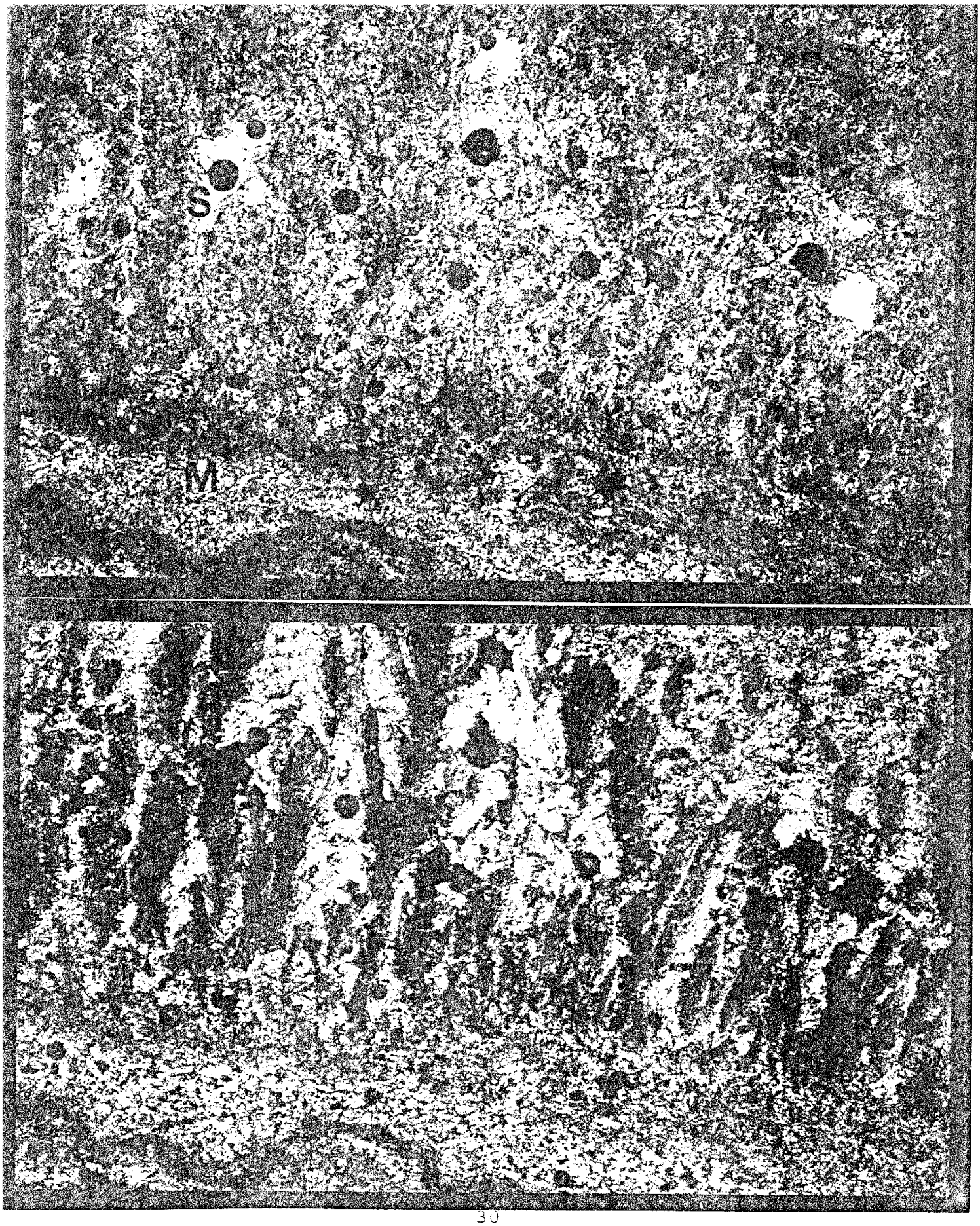
S
M

surface. The shrub layer is directly overlain by a thin terra rossa horizon and grades downward into intrasparrudite. The shrub layers have erratic layering and have lost their characteristic "miniature forest" look. Individual shrub layers are sinuous, disjointed and bounded by allochem layers. Highly elongated lensoidal pores that are parallel to the shrub layers are very common in the upper shrub region. The upper shrub region of NRDC#1 does not resemble typical shrub accumulations.

The lower shrub region in NRDC#1 resembles travertine shrubs as described by Chafetz and Folk (1984). This region is approximately 37 ft (11.3 m) below the surface. There are five distinct horizontal layers of shrubs, each bounded by micrite layers. A vertical desiccation crack splits the layers nearly evenly and slightly offsets them (Fig. 10). The individual shrub layers have very rich micrite allochems that fills in between the "trees in the forest" and between the shrub layers. Fig. 12 shows the upward direction of shrub growth which is also the upward direction of NRDC#1. This strongly suggests that the shrub horizons are due to authigenic carbonate deposition.

SEDIMENTARY FEATURES

TRANSLUCENT LAMINATED BANDS

Within the upper 10 ft (3.1 m) of NRDC#1, there are five different regions, 4 in. (10 cm) or less, composed of translucent laminated bands(TLB). The color of the TLB varies from colorless to tan and even light green. The TLB are directly associated

with terra rossa horizons and pinkish-brown intrasparrudite. Within each TLB region, the individual laminations are distorted by macroscopic moldic pores. The laminations alternate between translucent spar and a whitish, opaque, micrite. Together, these laminations vaguely resemble stromatolites, but the laminations are too continuous and consistent to be stromatolites.

Microscopically, these laminations are composed of calcite crystals acting as void-filling spar. The alternating laminations that appear to be separate layers actually are different layers of crystal growth or zoning within a much larger calcite crystals. These crystals are usually 0.1 in. (2 mm) or larger, and can have four horizons of zoned crystal growth (Fig. 9). Using cathodoluminescence, many of the petrographic crystal horizons also show distinct luminescing horizons. However, the alternating horizons of impurities seen petrographically do not show a consist pattern of cathodoluminescent horizons. This indicates that while zoned crystal growth was occurring, the geochemical aspects of the impurities where changing in a geochemically open system.

RHIZOLITHS

Moldic pores found in travertine are commonly caused by previous presence of plant stems or roots (Julia, 1983). Recent terminology uses rhizolith for paleo-root pores in lithified

FIG. 9 - A section of translucent laminated bands (TLB) showing zoned crystal growth across two horizons of impurities (I). The impurities were incorporated into the crystal's growth and now display the crystals morphology. Field of view is 2 mm and the upper picture was taken in plain light while the lower picture was taken with crossed polars. The lower picture shows uniform extinction of individual calcite crystals indicating each crystal crosses the different laminations.

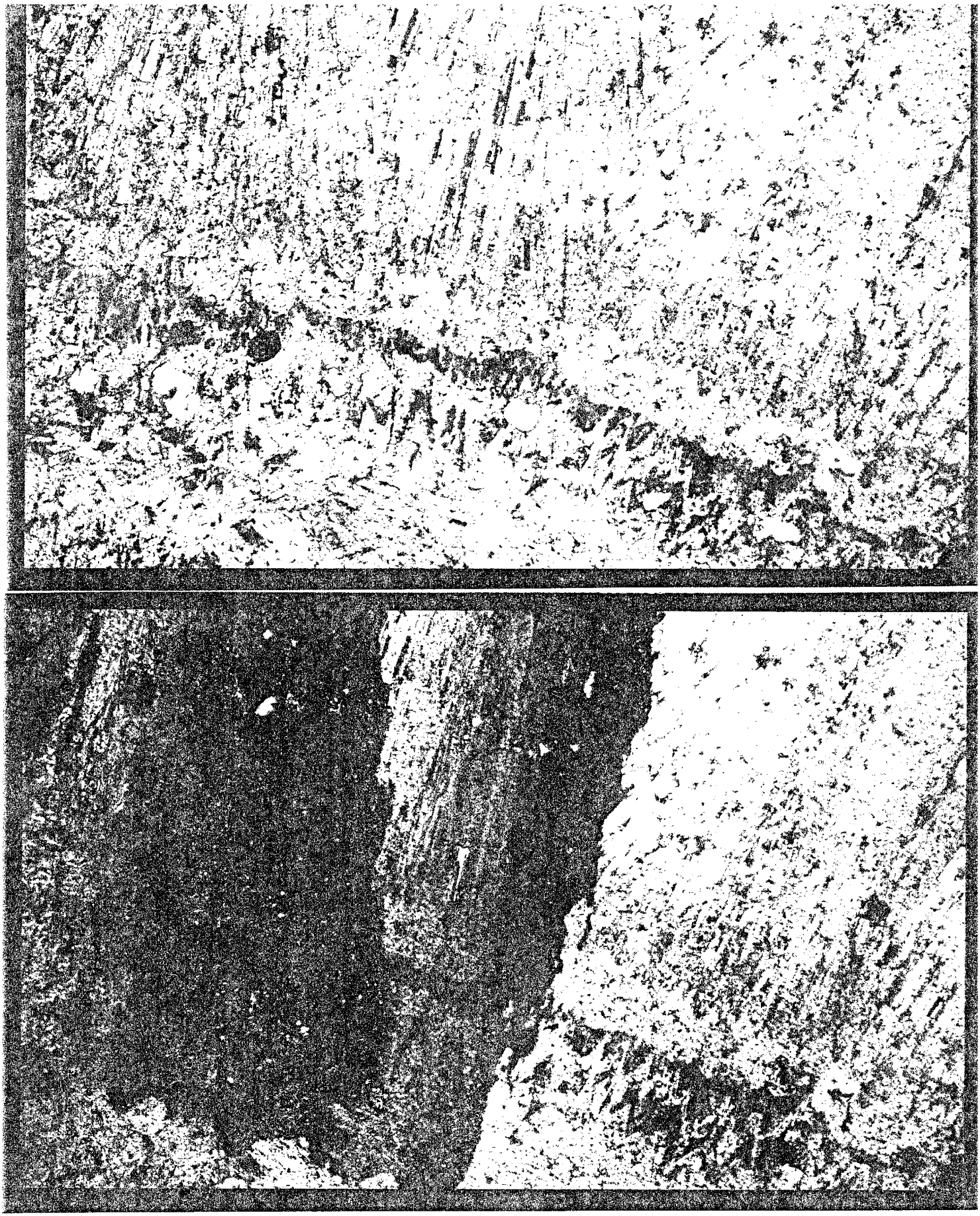

sediments (Klappa, 1980, in Mount and Cohen, 1984). Within NRDC#1 are voids or filled cavities which have similar features to the root casts of Mount and Cohen (1984). The rhizoliths they described by were found to occur in distinct patterns including discrete vertical roots and horizontal roots. Both horizontal and vertical rhizoliths are lithified and preserved in a process in which microstalactitic cements outline the edge of the pore, then micritic cement may be deposited in the pore and finally void filling spar may complete the lithification (Mount and Cohen, 1984). Both types of rhizoliths can have anomalous iron and/or manganese present in the spar. They can also have micrite infilling of the root cavity which is due to the decay of organic matter that alters the Eh in the microenvironment of precipitation (Mount and Cohen, 1984).

Both vertical and horizontal rhizoliths are found within NRDC#1. Rhizoliths comprise at most 1% of the upper portion of NRDC#1. Two types of vertical rhizoliths are seen in NRDC#1. A few large, nearly vertical rhizoliths are found in some regions such as within the upper TLB layers. The inside of a large pore 4 in. (10 cm) from the top of the NRDC#1 is iron-stained, and both equant and acicular spar partially fill the void. NRDC#1 also contains many 0.5 in. (0.4 cm) "half-moon" shaped vertical rhizoliths. These smaller rhizoliths have been damaged during polishing, leaving an iron-stained rind to define the border (Fig. 10). The horizontal rhizoliths are either spar filled or are still void and can best be seen in thin sections of NRDC#1.

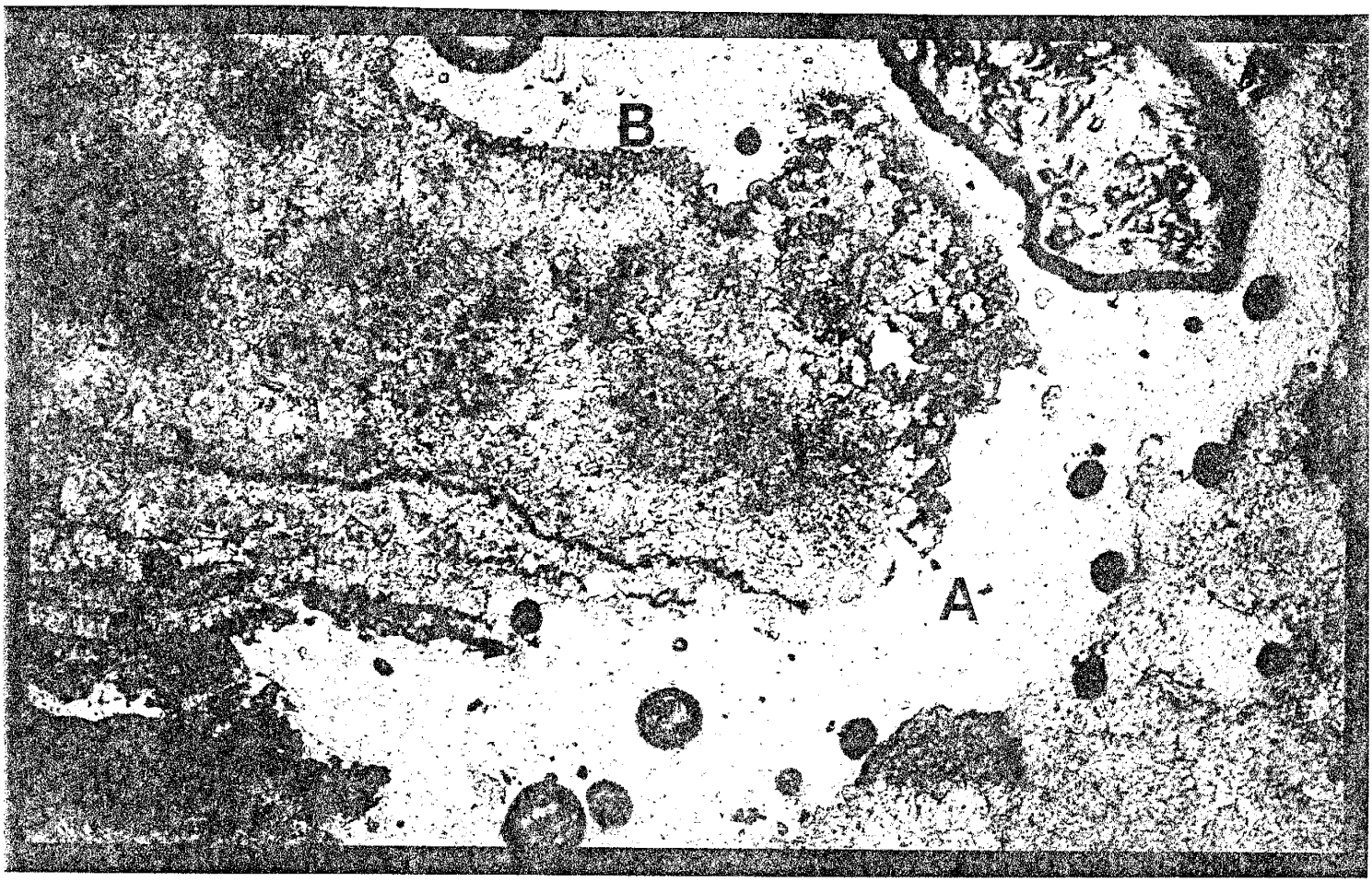

FIG. 10 - A crescent-shaped mold (A) of a vertical rhizolith with a partially iron-stained border (B). Field of view 2 mm and the photomicrograph was taken in plainlight. The rhizolith was plucked during slide preparation but is clearly defined in hand specimen.

The spar filled horizontal rhizoliths have a definitive sequence of acicular and then equant spar. Iron is frequently associated with the spar filled horizontal rhizoliths. The features that Mount and Cohen (1984) have described as horizontal and vertical rhizoliths are manifested in some regions of NRDC#1.

TERRA ROSSA

Prominent within the core are thin bands, between 0.1 to 2 in. (0.25 to 5 cm), of orange-brown, iron-rich carbonate that are nearly horizontal (Fig. 8). X-ray diffraction analysis indicates that calcite comprises 90% or more of the material in these iron-stained zones. The other 10% is composed of siderite and/or colloidal iron minerals. The morphology of calcite in the iron-stained regions is equant or blocky spar. Optically, the spar is clear with a yellow tinge, however, it is the nearly isopachous coating of iron (hydroxide?) around the spar that gives the terra rossa horizons their color.

The dark orange bands are usually homogeneous although sometimes cobble sized breccias of intrasparrudite are cemented by the terra rossa carbonate. These bands occur throughout NRDC#1 and comprise between 5 to 10% of the upper portion of it. The bands are almost always linear on their upper horizon and range in thickness from 2 in. (5 cm) to barely visible. However, the thinner bands have more irregular surfaces. These bands commonly terminate a sequence of deposition (TLBs and shrubs)

or are directly associated with rhizoliths and breccias.

Chafetz and Butler (1980) noticed a pale reddish brown feature associated with travertine that capped accumulations and filled the space between fractures. They noted that theses features were composed almost entirely of carbonate and are analogous to an immature terra rossa soil. The iron rich bands in NRDC#1 are also similar to dark brown, horizontal, red laminated crusts of variable thickness seen by Allan and Matthews (1982). The red laminated crusts are associated with moldic pores, root tubes and breccias and occur between two different formations or a period of non-deposition (Allan and Matthews, 1982). These crusts were believed to represent subaerial exposure features (Allan and Matthews, 1982). The laminated crusts and terra rossa discussed by Chafetz and Butler (1980) are similar to iron-stained horizontal bands in NRDC#1 strongly suggesting that orange horizontal bands in NRDC#1 are also terra rossa horizons.

OTHER SEDIMENTARY FEATURES

Clasts exist within NRDC#1 that were transported from outside the deposit. These clasts in NRDC#1 are very rare (under 0.1%) and are seen as either minute felsic or quartz grains in thin section or very rarely as dispersed, fine to coarse sand sized, subangular to subrounded grains associated with sections of terra rossa in NRDC#1. Previous work by McLemore and Barker (1987) found a few thin siliclastic horizons in the North Riley travertine that were not seen in the upper 10 ft (3.1 m) of NRDC#1. Because of the

constantly changing morphology of travertine deposits, the number of clasts deposited will differ from site to site at any moment within the accumulation. Non-travertine clasts in the North Riley travertine are represented in very localized and limited horizons.

Other sedimentary features, such as desiccation cracks, teepee structures and rip-up clasts exist in NRDC#1. Desiccation cracks are found in a few regions of the upper portion of NRDC#1, such as in the lower shrub layers (Fig. 8). Desiccation cracks indicate fluctuation of depositional conditions. Macroscopic rip-up clasts are found in breccia-like zones associated with terra rossa. The rip-up clasts are usually subrounded indicating abrasion or possibly soft sediment deformation. A single structure in the core 37 ft (11.3 m) below the surface appears similar to tepee structures associated with travertine by Leslie et al., (1992). A teepee structure is the border between polygons, in which each side is curved upward steeply and is created by evaporation of upwelling ground water generating polygonal cracking in algal mats (Warren, 1982). Although they comprise a minute percentage of the upper portion of NRDC#1, desiccation cracks, rip-up clasts and teepee structures are significant depositional indicators.

DIAGENESIS

There are many examples of diagenesis in NRDC#1. In many instances, acicular and/or equant spar forms a separate post-depositional cement and both types of spar are seen growing from the edge of a pore toward the center of a pore. Isopachous

micritic cement encases many allochems. Later spar cement deposit upon the micritic cement can give a grain the appearance of being coated. Stalactites occur in large pores and the terra rossa bands are composed of equant spar. Some of the equant spar that fills vugs has regions of zoned luminescence indicating multiple generations of spar. Desiccation cracks are commonly filled with spar.

TWO STAGE CEMENTS

Two different stages of void-filling spar are typically observed in thin sections (Fig. 11). One stage is scalenohedral or drusy crystals of calcite lining the perimeter of the void and the other is rhombohedral or equant spar which occupies the center of the cavity. Together, both stages resemble a drusy calcite mosaic (Friedman, 1967) from a freshwater tufa. Rarely, equant spar crystals are 0.001 in. (50 microns) or more in length and the drusy crystals are large and distinct enough to be recognized as dogtooth spar.

An extremely thin orange (iron hydroxide?) layer sometimes coats the perimeter of scalenohedra separating the twostages (Fig. 11). This orange layer is not within either cement mor-phology, but is seen coating or partially coating some primary grains, or it can coat the edges of spar that partially fill a void. So, this orange material is seen at the beginning of cementation, a distinct change in a cement's morphology, or at the end of cementation.

FIGURE 11. In the lower right corner of the photomicrograph an scalenohedral calcite "dogtooth spar" crystal (S) with a thin coat of a Fe-mineraloid (F). Later rhombohedral (equant) spar (R) then continued to fill the region. Filed of view is 2 mm and the upper picture was taken in plain light. The lower picture was taken with crossed polars and shows the uniform extinction of the dogtooth crystal indicating a single crystal.

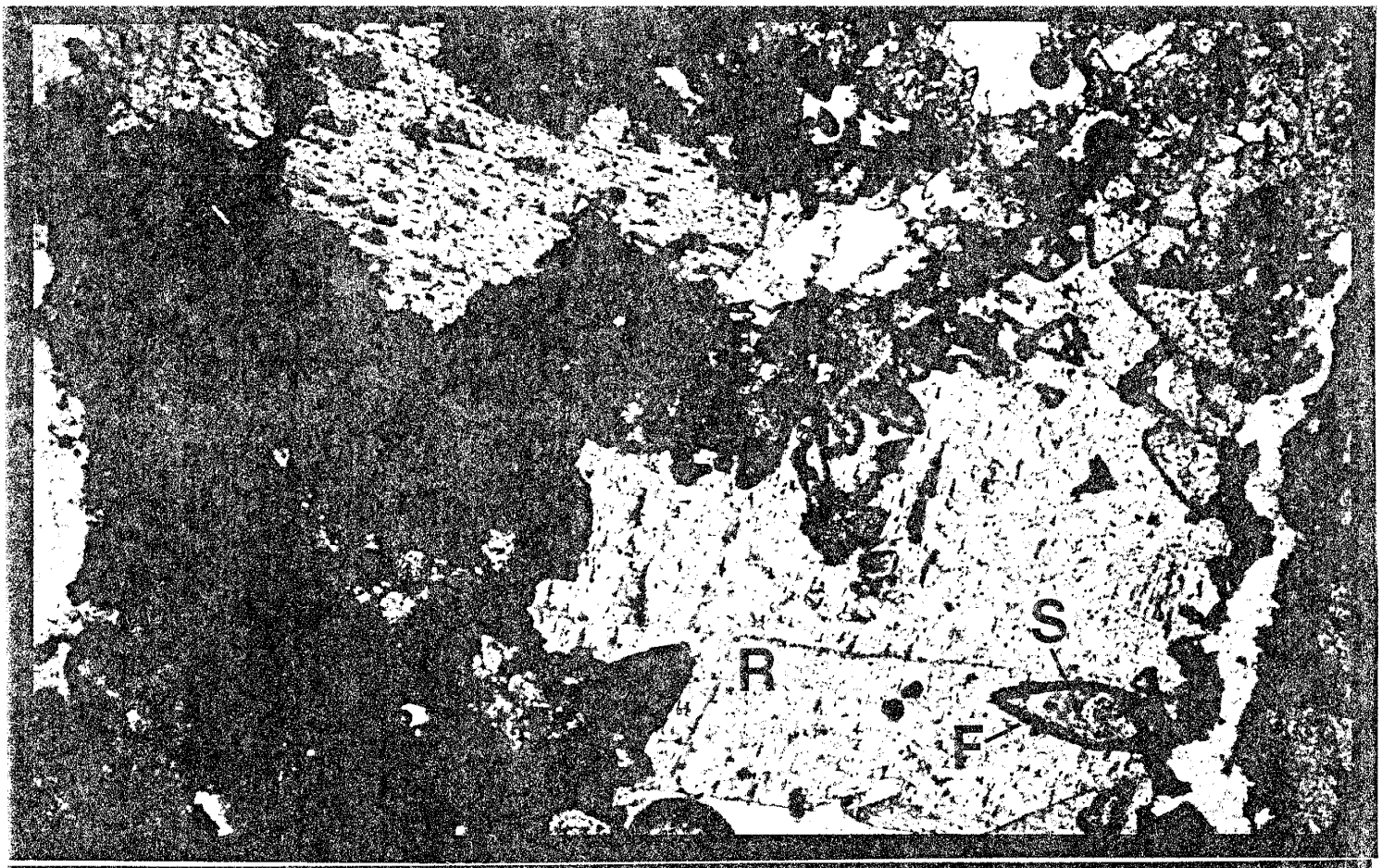
S
R
F

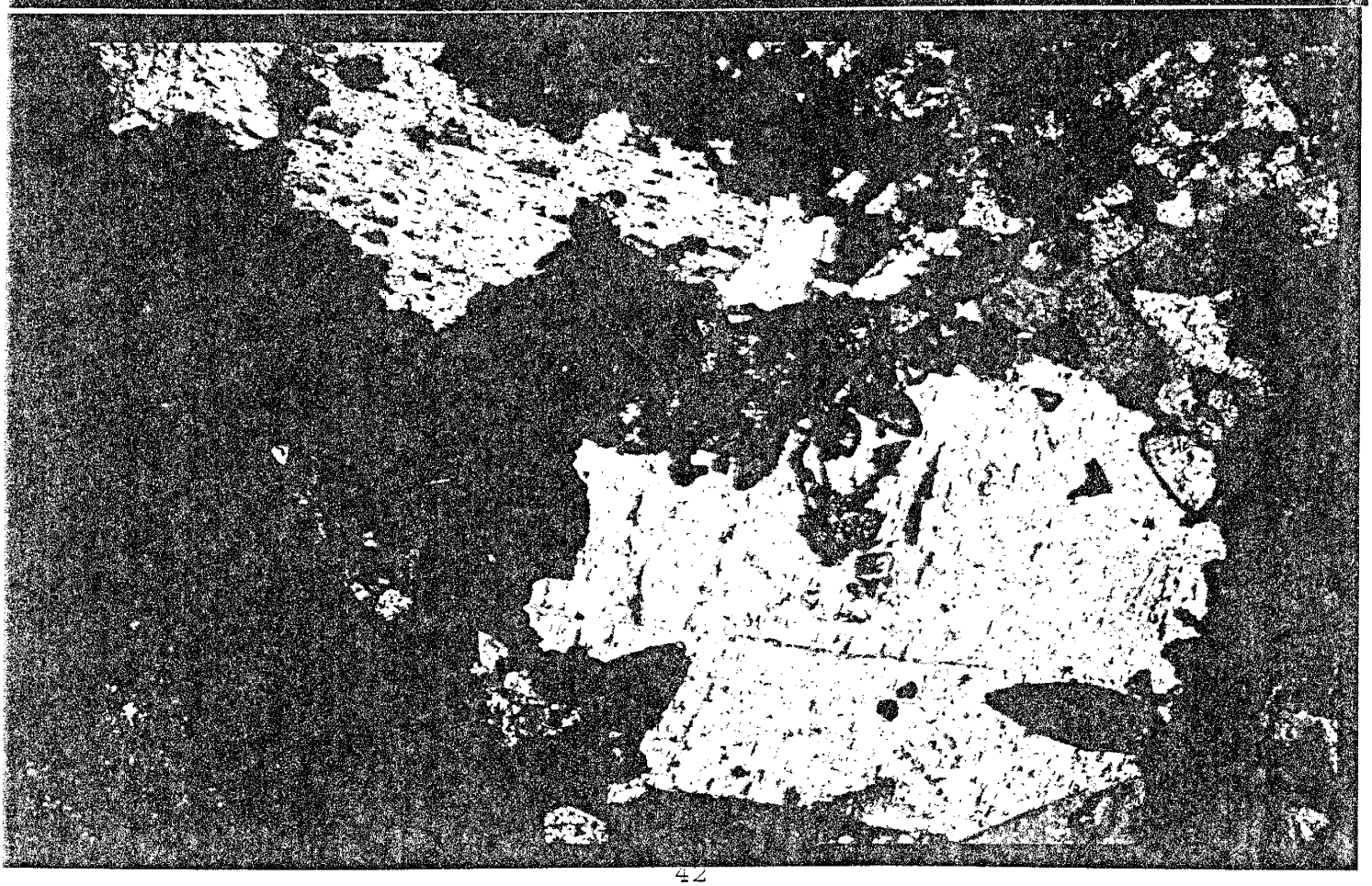

Thereby, the thin orange layers indicate a change in the solutions that lithified NRDC#1.

RAFT MODIFICATION

After rafts have formed at the aqueous surface and a central, nearly perfect tabular micritic core has developed, agitation of the water's surface sinks the rafts (Jones, 1989). A thin cement layer usually spar, forms around the micrite core followed by an outer alternating cement layer which usually completely coats the previous layer. Layers of spar-then-micrite are considered to be an isopachous cement and commonly the micrite-spar couplet occurs twice around the micritic core and the spar is commonly iron stained (Jones, 1989). Travertine raft cementation or modification seen in NRDC#1 is similar in morphology to the rafts described by Jones (1989). However, some rafts seem to be composed of just micrite, where a micrite core could be overlain by micrite cement. The micritic cement is opaque and resembles micrite seen in shrub layers. In most rafts examined in NRDC#1 the same relationship of spar-micrite laminations noted by Jones (1989) is seen. A raft from NRDC#1 is shown (Fig. 15) with two distinct micrite/spar couplets and part of a third, coating the micrite core. There, the inner most spar layer is very small and dwarfed by the micrite layer and the second spar layer is iron-stained. Elongated cavities found with rafts (upper right of Fig. 15) in NRDC#1 also provide further good evidence of the similarity between rafts

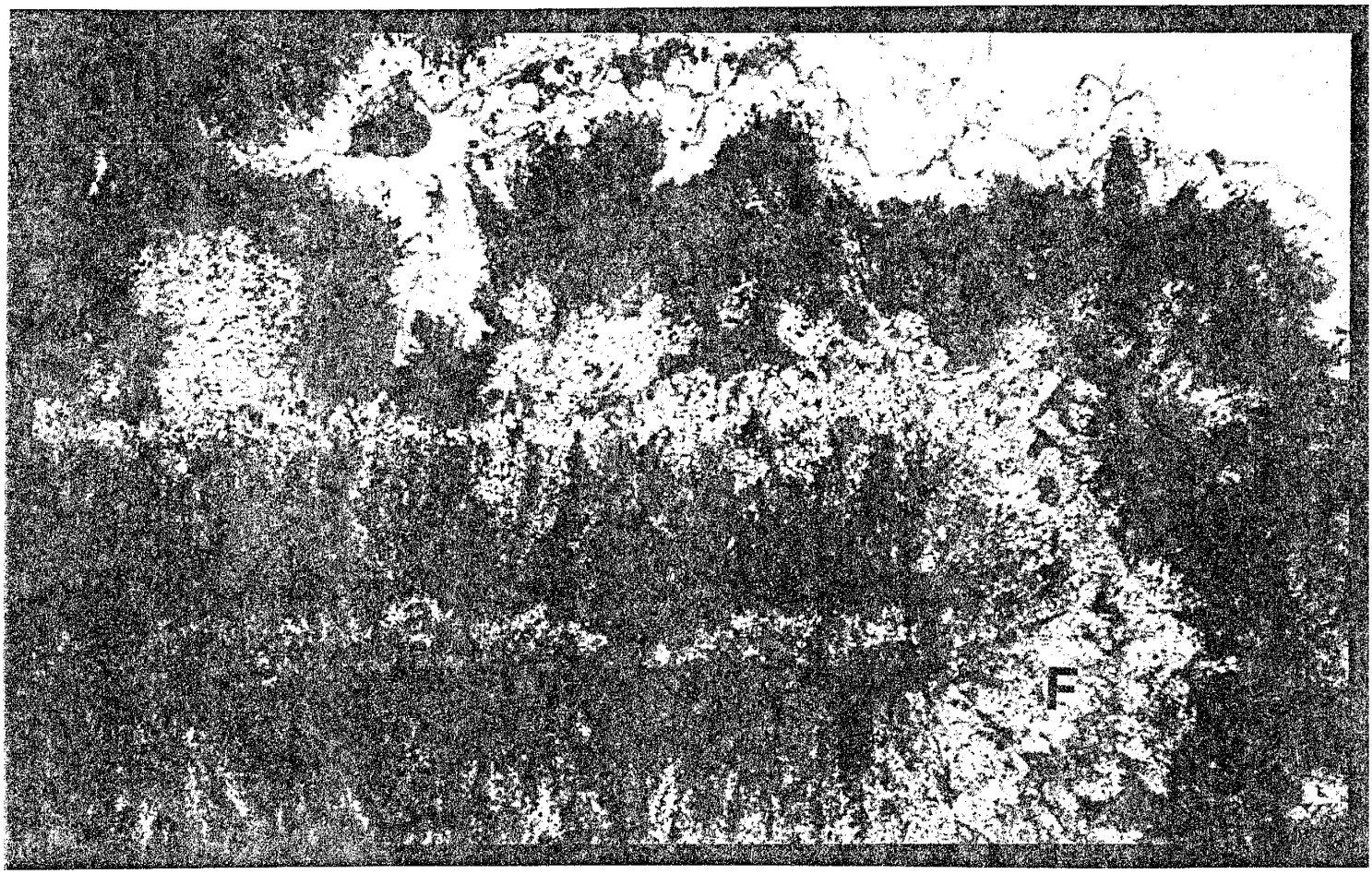

FIG. 12 - A raft showing two layers of spar/micrite overgrowths. The inner most spar layer is very thin and difficult to see (a), as is the faint iron-stained spar layer (F). Field of view is 2 mm, the photomicrograph was taken in plain light.

in NRDC#1 and rafts examined by Jones (1989)

NEOMORPHISM

Aggradational neomorphism is seen crossing raft cement layers and stalactitic columns in NRDC#1. A few examples are seen in NRDC#1 of neomorphic crystals in the cement layers that surround raft cores. The crystals cross cut the micrite/spar cement layers when seen at their extinction angle. Small, less than 0.2 in. (0.5 cm), stalactitic columns are found in pores at 27.5 ft (8.4 m) and 31.0 ft (9.4 m) below the surface. The columns display concentric laminations of rhombohedral calcite in cross section. The spar is clear with no trace of iron-staining or clasts which suggests the generation of spar was formed well after lithification started. Post-depositional changes and cements are common in NRDC#1.

ISOTOPIC ANALYSIS

PREVIOUS WORK

Isotopic changes in travertine have been examined in previous paleoclimatic studies (Henning, 1983, Lambert and Harvey, 1987; Pazdur and Pazdur, 1988). Henning (1983) postulated a relationship between travertine deposition and paleoclimates. The warmer climatic conditions would enabled greater $CaCO_3$ production, and "the evident climatic stimulation of Quaternary calcite formation is controlled by paleoclimatic fluctuations." Lambert and Harvey, (1987) examined oxygen isotopes in travertine to reconstruct fluid temperatures. These paleoclimatic investigations involving travertine did not consider isotopic fractionation to vary with textures and features. Pazdur and Pazdur (1988) examined ^{18}O values to calculate the paleo-temperatures of deposition and analyzed the variations. They used spring travertine samples from four different sites and each site had one or two dominant textures, such as stromatolites and oncoids. They considered that different textures might affect their isotopic data, but concluded that:

> "The isotopic composition of oxygen in sediment is independent of the type of tufa (biogenic or abiogenic) precipitated in different zones of stream. The validity of this assumption seems to be confirmed by studies of recently deposited spring tufas."

They found a correlation of carbon and oxygen isotopes within the individual deposits that was interpreted to show the predominance of kinetic effects. This assumption that the isotopic composition. of travertine is independent of textures is the critical question that the investigation of NRDC#1 attempts to answer

RILEY BANDED TRAVERTINE SPECIMEN

As initial inspection of NRDC#1 showed non-uniform deposition, multiple textures and diagenesis, the Riley banded travertine specimen (RBTS), a textually more homogeneous sample, was analyzed to determine the magnitude of isotopic fluctuations due to temperature and composition. The choice of the RBTS was influenced by a paper on vein calcite (Winograd, 1988). RBTS appears similar to the vein calcite and consists of alternating light brown to beige layers with dark yellowish brown translucent layers, all with numerous laminations. However, there are three regions within RBTS of reddish-brown, sediment and it is the lack of sediment is one of the key criteria Winograd (1988) used to define vein calcite. Many laminations are truncated and later reappear along the profile of the specimen and a few laminations are elliptical and completely contained within the specimen. Reconsidering these observations it is most likey that RBTS is not an example of vein calcite.

Fig. 13 displays the scatter plot for $\delta^{13}C$ (PDB) versus $\delta 18O$ (SMOW) for the entire RBTS sample set. The RBTS samples were collected sequentially down the 57 different laminations. The $\delta^{18}O$ ranges from $21.7^0/_{00}$ to $24.3^0/_{00}$. The data is scattered fairly evenly with one potential separate population having values above $23.7^0/_{00}$. The only similarities within this group are that colorless to white

laminations appear three times within a collection of six points. Even this association must be hesitantly drawn, because two of the white laminations contain discontinuous smaller laminations. The

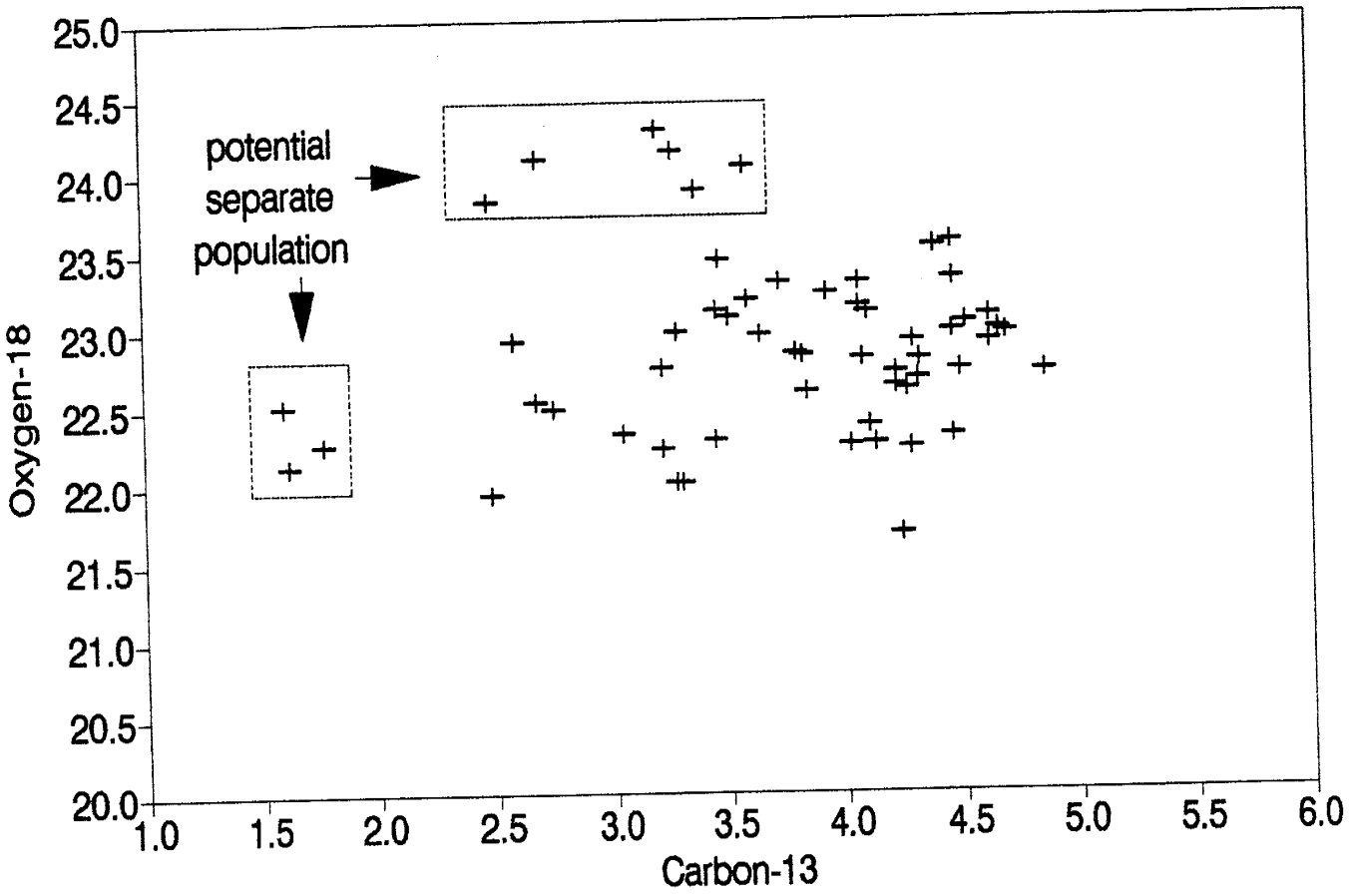

FIG. 13 - An isotopic scatter plot for all the RBTS samples. There exist two groups of data points that might be separate populations. However, there does not seem to be a correlation between coloration of the different layers and the seperate populations.

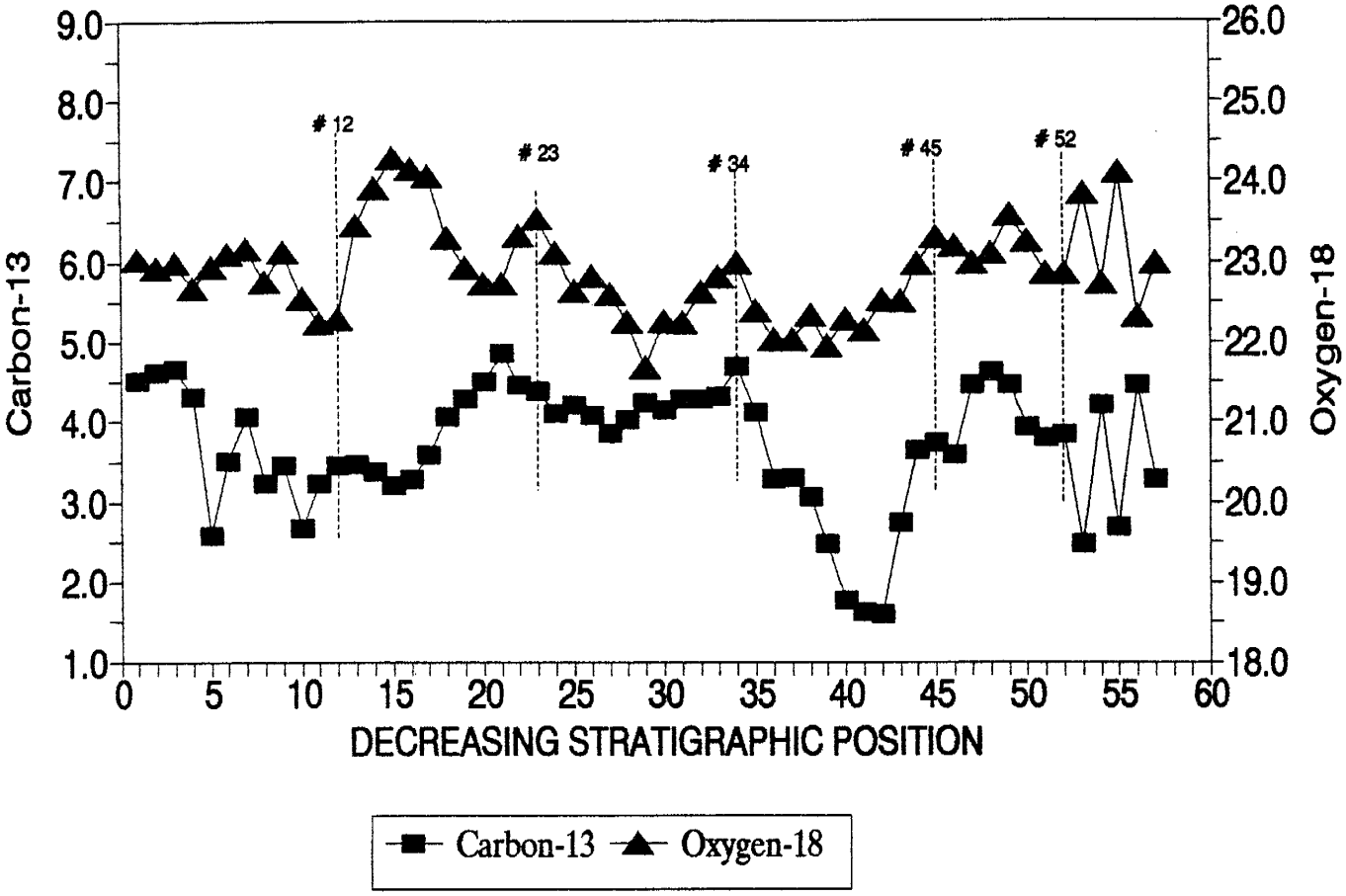

FIG. 14 - An isotopic profile of the RBTS data. The 57 sample points were taken perpendicualr to the horizontal layers. The vertical lines imposed on the graph mark the sample number where regions of similar $\delta^{13}C$ and $\delta^{18}0$ trends occur.

$\delta^{18}O$ data below $23.7^0/_{00}$ define a fairly homogeneous field and do not correlate to the macroscopic characteristics of the RBTS.

The $\delta^{13}C$ of RBTS ranges from $1.6^0/_{00}$ to $4.9^0/_{00}$. There is one potential separate population within the $\delta^{13}C$ data which falls below 20/00. The three samples are sequential, but include two brown onyx layers and a red sediment region. The other brown onyx layers and red sediment regions showed no ^{13}C depletion. The $\delta^{13}C$ data of RBTS do not reveal a correlation related to texture.

Delta ^{13}C and $\delta^{18}O$ RBTS isotopic data were plotted in relative decreasing stratigraphic position (Fig. 14). Within the isotopic data, there is some correlation between the $\delta^{13}C$ trend, and the $\delta^{18}O$ trend. Within each decreasing beige lamination, there is an increase in the $\delta^{18}O$ value. From points 16-21, there is a continuous rise of nearly $1.5^0/_{00}$, and samples 43-48 show also an increase of about $1.5^0/_{00}$, This trend is not displayed in the upper beige layer although there is no overlying sparry layer. The $\delta^{18}0$ trend does have four well-defined peak-valley cycles, 9- 15, 15-23, 23-34 and 34-45, but each group has a different sequence of textures. Many three to five point sequences within the $\delta^{13}C$ and $\delta^{18}O$ data correlate with a sequence of layer, however these "micro-trends" are not duplicated in other similar sequences. This might indicate that RBTS had a complex depositional history.

The twelve initial ^{13}C and ^{18}O samples show a general but vague similarity of decreasing per mil values. The trends then diverge

from each other and display a negative correlation for the following few samples. At point 23 within the $\delta^{18}O$ trend and $\delta^{13}C$ trend, the two trends exhibit covariation. Both trends peak in the low 20's, have a nadir around sample 28, and then rise nearly unabated to point 34. Both trends then show a small peak at point 49 of $\delta^{18}O$ and point 48 $\delta^{13}C$ then decrease in per mil values to point 52 followed by erratic spikes at the end of the data. About 60% of the $\delta^{13}C$ and $\delta^{18}O$ values display a well-defined covariation.

Despite general covariation there are parts of the sample which exhibit an inverse correlation between $\delta^{13}C$ and $\delta^{18}O$. The first 20 points show only a vague similarity to obviously opposite trends and the last few points also display a striking negative correlation. The cycles are not consistent with textures. Within the upper brown sparry layer, samples 10-15, the $\delta^{18}O$ trend shows a general increase in per mil value while $\delta^{13}C$ trend is fairly flat. However, within the lower brown sparry layer, samples 35-41, the $\delta^{13}C$ trend shows a decreasing trend while the $\delta^{18}O$ trend is fairly flat. The RBTS $\delta^{13}C$ and $\delta^{18}O$ trends do have similar, but not identical profiles.

There are factors that might have affected the consistency in the RBTS isotopic trends. Both trends (Fig. 14) show "spiked" regions at the end of the data, samples 53- 57, were taken from near an open cavity or pore at the base of the sample. Secondary or diagenetic changes may be responsible for the spikes, but this is speculative. Another possibility is that the distance the fluid

travelled before depositing the travertine of RBTS changed. Changing the distance could change the carbon isotopic content of the fluid in a manner seen by Chafetz et al., (1991) and the increased distance would also affect the amount of evaporation. This could alter the $\delta^{18}O$ of the fluid. The relative isotopic concentrations can also be affected by such factors as algal blooms, and temperature of the source fluid. Each isotope would be affected differently within a dynamic system. Because travertine deposits evolve over time, perfect synchronicity between different isotopic trends and cycles within the trends should not be expected.

It is possible that the lack of correlation between features and isotopic trends in RBTS is due to the sampling procedure. The samples were drilled based on the color changes that were used to define a lamination. Possibly non-isotopically fractionating processes controlled lamination coloration. Iron or other elements could vary in concentration causing colored laminations along surfaces that were continuous. The isotopic layering which could indicate depositional changes might be cryptic as with the UV fluorescent patterns in travertine recognized by Fitzmaurice (1990). Color-based segregation of laminations and identification of changes in travertine deposition might not be valid.

Although RBTS is not a perfect example of a vein calcite, it is a single-textured sample from one environment. Although some red sediment-like material is seen, there are no terra rossa

horizons that indicate an interruption of deposition. No other travertine textures are seen and RBTS resembles a laminated travertine crust described by Love and Chafetz (1988). However, the layering of RBTS lacks the symmetry of the laminated crust. RBTS appears to be a continuously deposited, singled textured specimen.

If RBTS is a continuously deposited, singled textured specimen, then it is a record of the changes that occurred within that environment. The data shows the fluctuation of isotopic values to be limited, the range of all δ18O values is $2.6^{0}/_{00}$, while that for the $\delta_{13}C$ range is $3.3^{0}/_{00}$. It is important to note that the changes in both $\delta^{18}O$ and $\delta^{13}C$ show some sort of systemic variation even through they don't always covary. This is very different than a set of random changes. The narrow ranges may reflect seasonal temperature variations. The seasonal variations affect biogenic production of travertine. The isotopic cycles in Fig. 14 may represent biogenic blooms. Seasonal variations can also effect the inorganic isotopic composition of the fluid that deposited RBTS because of changing evaporation rates and hydrologic precipitation cycles. The lack of correlation between the features and isotopic cycles implies multiple processes were involved with deposition.

NRDC#1 ISOTOPIC DATA

NRDC#1 SCATTER PLOT

The isotopic data from NRDC#1 plotted on a scatter diagram (Fig. 15) does not display a distinctive overall pattern or multiple distinct fields. The initial 82 samples were chosen to

fully represent the diversity seen within the 10 ft (3.1 m) interval, whereas the last 18 samples were taken within a single texture over a short distance. These last 18 samples will be discussed later. The isotopic data plotted in Fig. 15 display a range in $\delta^{13}C$ from 5.0 to $9.8^0/_{00}$ and 20.6 to $24.1^0/_{00}$ for $\delta^{18}O$. The standard deviation for $\delta^{13}C$ and $\delta^{18}O$ is about $0.6^0/_{00}$. Exactly 90% of the data lies in the "restricted range" region of Fig. 15. The variation in $\delta^{13}C$ is only $1.6^0/_{00}$ (6.0 to $7.6^0/_{00}$) and the variation in $\delta^{18}O$ is only $2.3^0/_{00}$ (21.7-$24.0^0/_{00}$). The 10% of the data lying outside the restricted range are clasts, secondary and altered samples that are not primary features of NRDC#1 (Fig. 15). The samples with a $\delta^{18}O$ under $21.7^0/_{00}$ are the translucent laminated bands that appear to be void-filling. The lone raft sample excluded from the restricted range displays neomorphic spar. Within the restricted range of Fig. 15 the NRDC#1 isotopic data from primary materials shows a single, distinct field.

In order to further investigate the data, the isotopic data from the first 10 ft (3.1 m) of NRDC#1 were graphed versus stratigraphic depth. The graphs of $\delta^{13}C$ versus depth (Fig. 16) and $\delta^{18}O$ versus depth (Fig. 17) show the variation in isotopic signatures down the length of the 10 ft (3.1 m) interval. These two figures display a wide variation in isotopic values of $\delta^{13}C$ and $\delta^{18}O$ within narrow 6 in. (15 cm) stratigraphic intervals compared to the deviation at 54 in. (137 cm) depth.

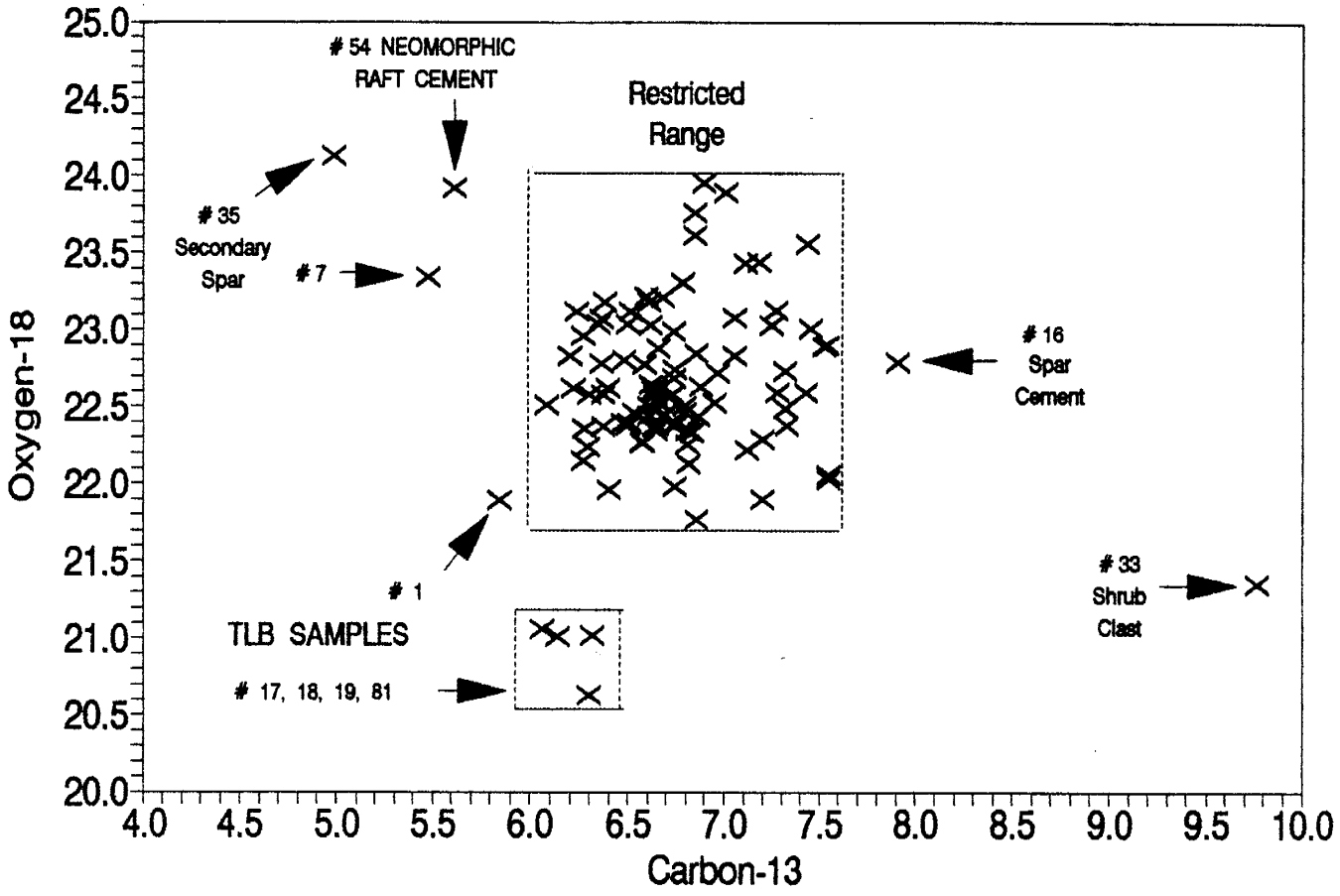

FIG. 15 - An isotopic scatter plot of NRDC#1 showing the initial 82 samples which were all taken from the first 10 ft. (3.1 m) of the core. The samples outside the "restricted range" are either post-depositional or show signs of alteration after deposition.

CARBON-13 PROFILE

The data in Fig. 16 does not portray a consistent trend. Samples 1-5 from the translucent laminated bands occur directly below a terra rossa horizon and reveal an increase in $\delta^{13}C$ values that is nearly linear with increasing depth. This agrees with Allan and Matthews (1982) observations about freshwater diagenesis of limestones. They observed that subaerial exposures surfaces had a relatively depleted $\delta^{13}C$ composition. However, below the subaerial exposure surface, there was a trend toward increasing $\delta^{13}C$ values with increasing depth. It is possible that samples 1-5 have been affected by freshwater diagenesis. However, sample group 37-45, seen in the 51.5 to 54 in. (1.3-1.4 m) interval, occurs under a terra rossa horizon, (sample 36). Samples 36-45 do not show an increase in $\delta^{13}C$ value and have a range of only $0.24^{0}/_{00}$.

Samples 24-32, from 28 to nearly 40 in. (0.7-1.0 m) in stratigraphic depth, show similar $\delta^{13}C$ value and range from 6.22 to $6.8^{0}/_{00}$. A wide range of textures are seen in the interval such as micritic rhizoliths, pinkish intrasparrudite in a highly porous zone, a terra rossa horizon and a spar cement sample. Samples 62-66, which include a terra rossa horizon, a large intraclast, a rhizolith, spar cement and a raft, also have a range of $\delta^{13}C$ values lower other areas of the core. Both sample groups, 24-32 and 62-66, include a terra rossa horizon, a rhizolith, micrite and spar cement sample. It is possible that the $\delta^{13}C$ values of both sample groups may have been homogenized by post-depositional processes.

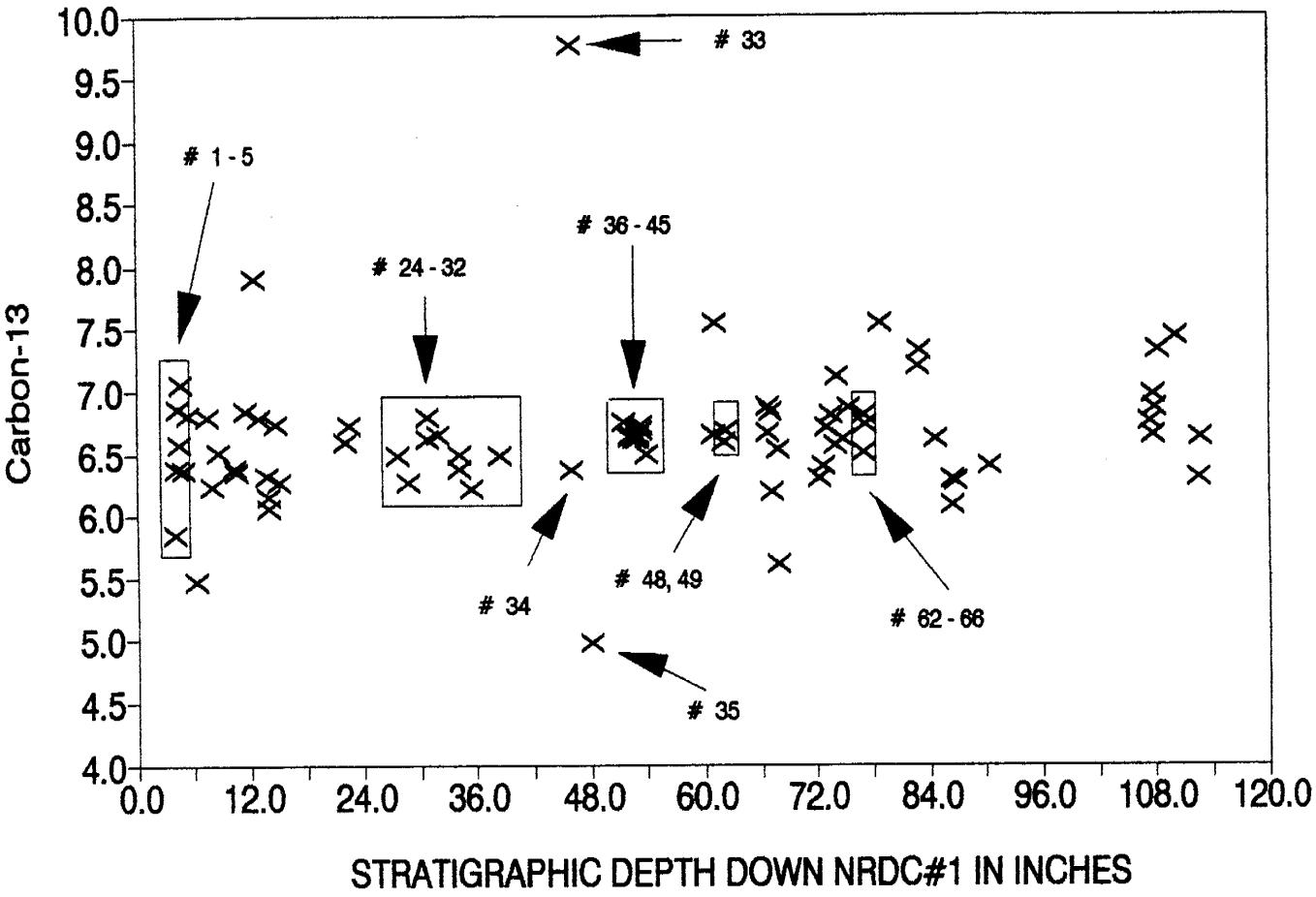

FIG. 16 - A $\delta^{13}C$ isotopic profile of the initial 82 samples taken from the first 10 ft (3.1 m) of NRDC#1. Samples were measured to within 0.25 in (6mm). The significance of the sample numbers indicated on the profile is discussed in the text.

The highest and lowest $\delta^{13}C$ isotopic values occur in just a 2 in. (5 cm) interval. Sample 33 is a small TLB clast with a $\delta^{13}C$ of $9.8^{0}/_{00}$. Sample 34 is a pinkish intrasparrudite that was collected next to sample 33. Sample 33 has a near average $\delta^{13}C$ value of $6.4^{0}/_{00}$. It is however, significant that the samples retain their distinctive composition and have not been homogenized. Sample 35 was taken from a void filling spar region surrounded by intrasparrudite. The sample is the most depleted in $\delta^{13}C$ in the entire NRDC#1 data set. However, a large travertine clast, sample 48, and the spar cement surrounding part of the clast, sample 49, have nearly identical $\delta^{13}C$ values. This implies that the carbon component of the spar was probably derived from the shrub clast although the spar and shrub could have formed under similar condition or that the shrub clast has been altered.

OXYGEN-18 PROFILE

Fig. 17 represents the $\delta^{18}O$ values for the first 10 ft (3.1m) of NRDC#1. The oxygen isotopic profile of the initial 82 samples of NRDC#1 (Fig. 17) is very similar to the carbon isotopic profile of NRDC#1. Within the first 10 ft (3.1 m) of the NRDC#1 are similar narrow intervals displaying large limited isotopic range. Like Fig. 16, samples 1-5 display a wide range of $\delta^{18}O$ values and the samples 33- 35 exhibit a very wide range in $\delta^{18}O$ values. Samples 36-45 show very limited variation in $\delta^{18}O$ composition, similar to the $\delta^{13}C$ data. The nearly identical $\delta^{18}O$ values along

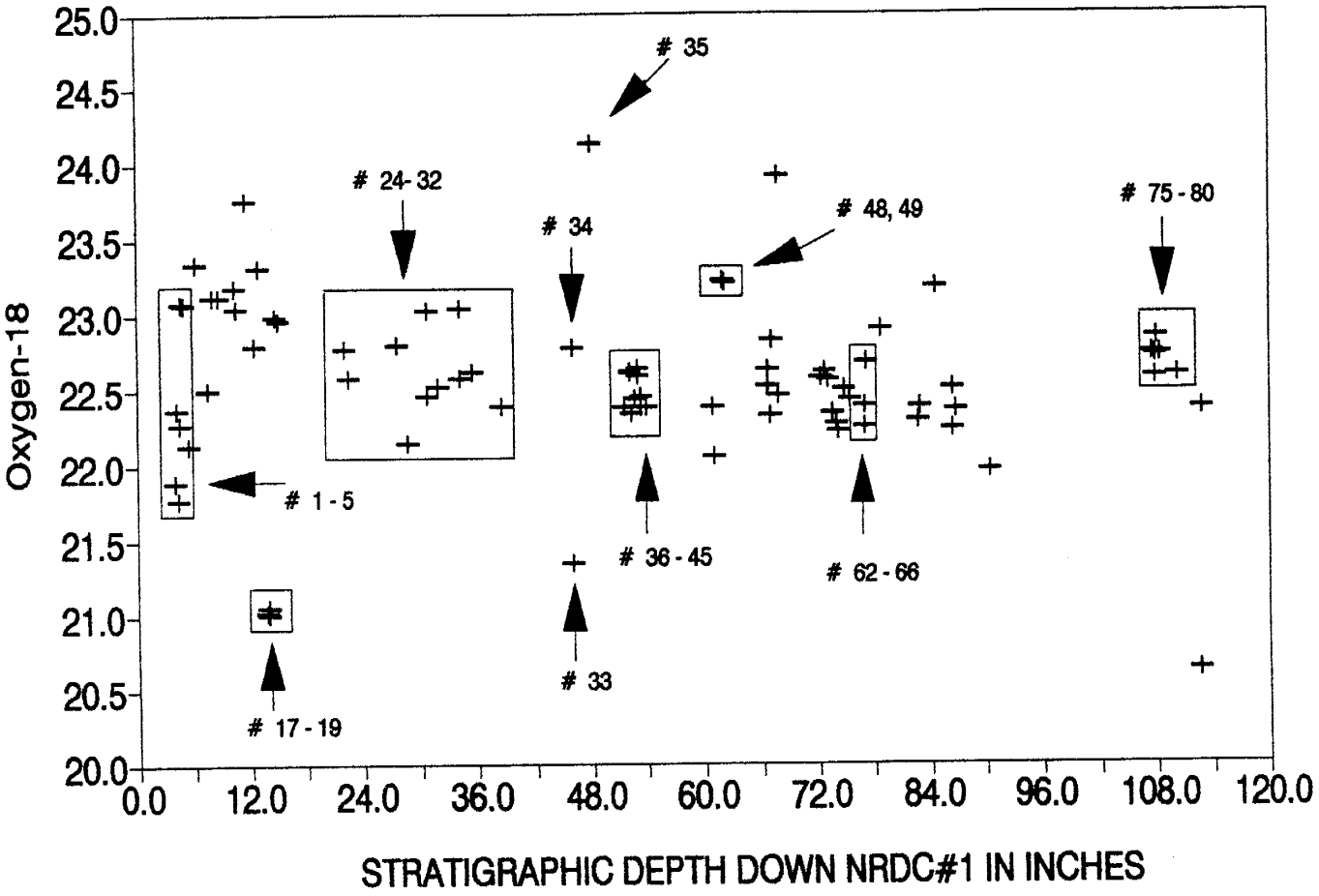

FIG. 17 - A $\delta^{18}O$ isotopic profile of the initial 82 samples taken from the first 10 ft (3.1 m) of NRDC#1. Samples were measured to within 0.25 in (6mm). The significance of the sample numbers indicated on the profile is discussed in the text.

with the $\delta^{13}C$ values of the shrub clast, sample 48 and adjacent spar sample 49, suggests the spar was derived locally. Sample group 62-66 exhibit a narrow $\delta^{18}O$ range of 0.40/00. Both the $\delta^{18}O$ and $\delta^{13}C$ values of this sample group display a range that is small.

There are differences between Fig. 16 and Fig. 17. A difference in the isotopic profiles is the very narrow $\delta^{18}O$ values ($0.3^{0}/_{00}$) of samples 75-80. The $\delta^{18}O$ value of the lower shrub samples is more homogeneous than the $\delta^{13}C$ data. Conversely, samples 24-32 have a $\delta^{18}O$ range of $0.9^{0}/_{00}$, which is greater than one standard deviation for $\delta^{18}O$ and $0.3^{0}/_{00}$ greater than the $\delta^{13}C$ range for the same samples. TLB samples 17-19 have slightly below average $\delta^{13}C$ values but extremely depleted $\delta^{18}O$ values. The extremely tight grouping of $\delta^{13}C$ values in samples 33-35 implies that the depletion affected all three samples. Samples 33-35 display a huge $\delta^{18}O$ range, $2.8^{0}/_{00}$. The TLB clast sample 33 is very depleted in $\delta^{18}O$ while spar sample 35, is enriched in $\delta^{18}O$. The micrite sample 34 adjacent to the TLB clast has a primary $\delta^{18}O$ value (within the restricted range) and is not affected by depleted or enriched nearby samples.

Trend analysis of $\delta^{18}O$ and $\delta^{13}C$ versus depth does not reveal any consistent trends. Sample groups 24-32 and 62-66 imply that terra rossa horizons homogenize underlying samples, but this is not seen with all terra rossa horizons. The spar samples can either show very similar $\delta^{13}C$ and $\delta^{18}O$ values (samples 48-49) or very different values (samples 34-35). Consistent isotopic values or cycles are not recognized with any texture within Fig. 16 and Fig. 17.

SINGLE TEXTURE TRAVERSE

In order to examine possibly of isotopic variation within a texture, sampling was done within a single texture. An interval representing continuous, very dense intrasparrudite at 39 ft (11.9 m) below the surface was sampled. Samples (87-95,97) were collected between the 39 to 41 ft region (11.9 - 12.5 m) to determine if an isotopic shift or cryptic layering was distinguishable within a single texture. Ten intrasparrudite samples were collected 1.0 in. (2.5 cm) apart over the 9 in. (23 cm) interval that has slightly variable porosity but no visible depositional hiatus. Other textures such as spar, a large clast, and a subaerial exposure surfaces were sampled in the 40 ft (12.2-12.5 m) interval to compare the isotopic variation.

By examining a single texture, an isotopic trends can be clarified. Segregating the adjacent samples from the intrasparrudite samples (Fig. 18), the $\delta^{18}O$ trend displays a well-defined peak similar to the RBTS isotopic trend (Fig. 14). These trends are compared because they are believed to occur on similar time scales. Peaks at sample 15,23,34 and 45 in the $\delta^{18}O$ trend of Fig. 14 are narrower than the micrite $\delta^{18}O$ trend (Fig. 18). The intrasparrudite accumulation is capped horizon by a dark-red thin layer with pebble-sized clasts and a lighter thin red layer without visible clast lies below the intrasparrudite accumulation. If these red layers are terra rossa horizons, they represent a cessation in deposition which could indicate a seasonal

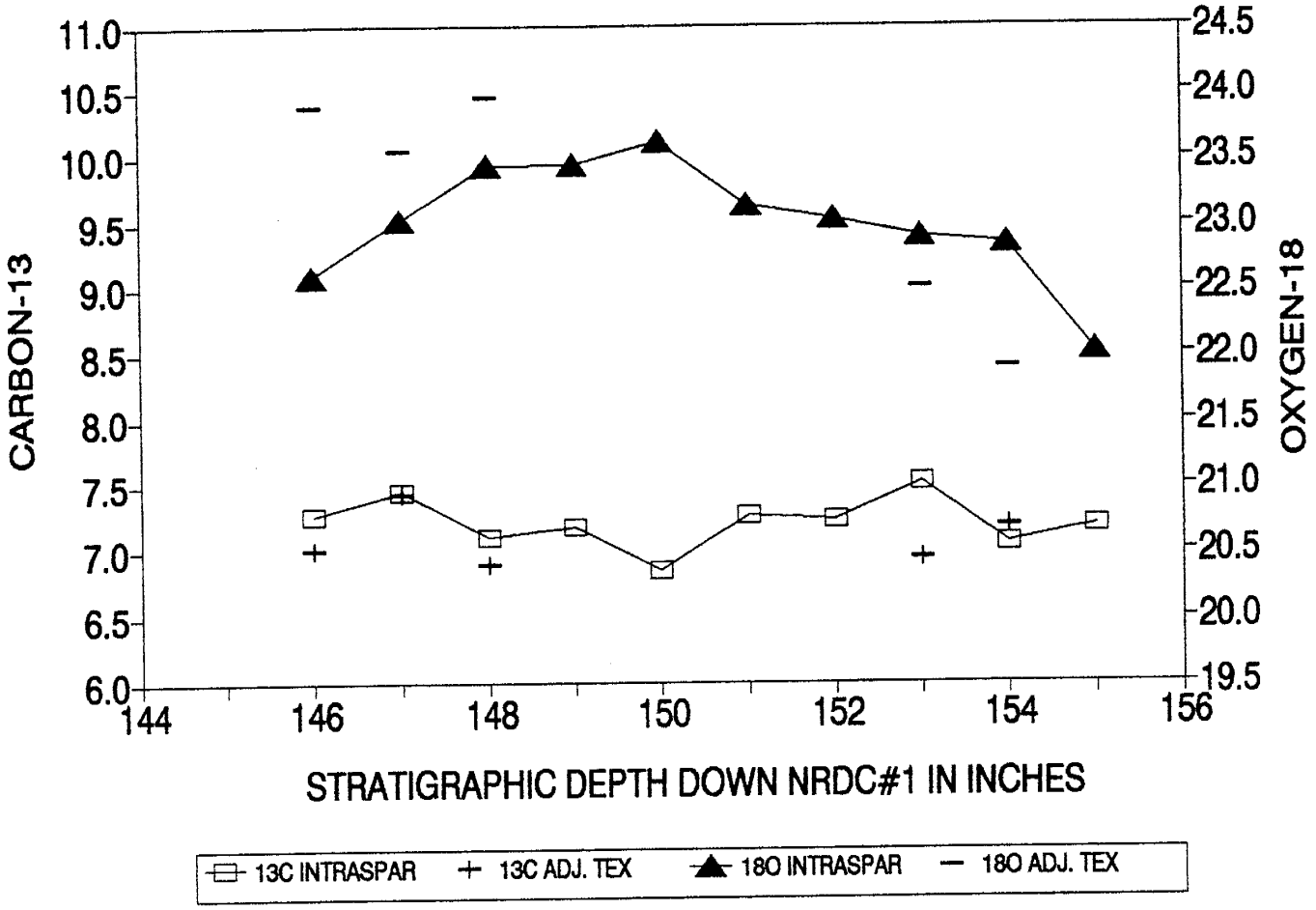

FIG. 18 - An isotopic profile of samples taken 39 to 40 ft (11.9 to 12.2 m) below the surface. Ten intrasparrudite samples were taken linearly 1.0 in (2.54 cm) apart to examine the possibility of cryptic and rhythmic layering. A few other adjacent samples were collected to observe the variation between textures.

(fall/winter) markers. The peak in Fig. 21 would then reflect paleoclimatic temperature changes and/or changes in the isotopic composition of the travertine depositing fluid. It appears evident that the same effectrecorded a few times in the RBTS sample is also recorded in the intrasparrudite accumulation in the 39 to 41 ft (11.9-12.5 m) region. The $\delta^{13}C$ data in Fig. 18 does not exhibit a broad trend. No two points consecutively show an increase or decrease in the $\delta^{13}C$ Value. However, there is a similarity with the RBTS data (Fig. 14) in that samples 23-31 show a very similar trend within a narrow $\delta^{13}C$ range. One difference between the carbon and oxygen isotopic trends in Fig. 18 is that the adjacent textures have similar $\delta^{13}C$ values. Linear sampling of the intrasparrudite accumulation displays natural fluctuations within a relatively flat $\delta^{13}C$ trend.

TEXTURE SEGREGATION OF NRDC#1

The detailed analysis and the isolation of texture among samples in the 39 to 41 ft (11.9-12.5 m) interval revealed probable trends. This trend was seen when textures and features were carefully grouped. To answer whether "simplifying assumptions" are valid between textural groups, further investigation of the first 82 samples was done. The NRDC#1 is a combination of primary and secondary carbonate, and only by selecting different samples group can the variety of effects be seen. The textures that comprise the NRDC#1 27-37 ft (8.2-11.3 m) region have been segregated to further identify isotopic trending.

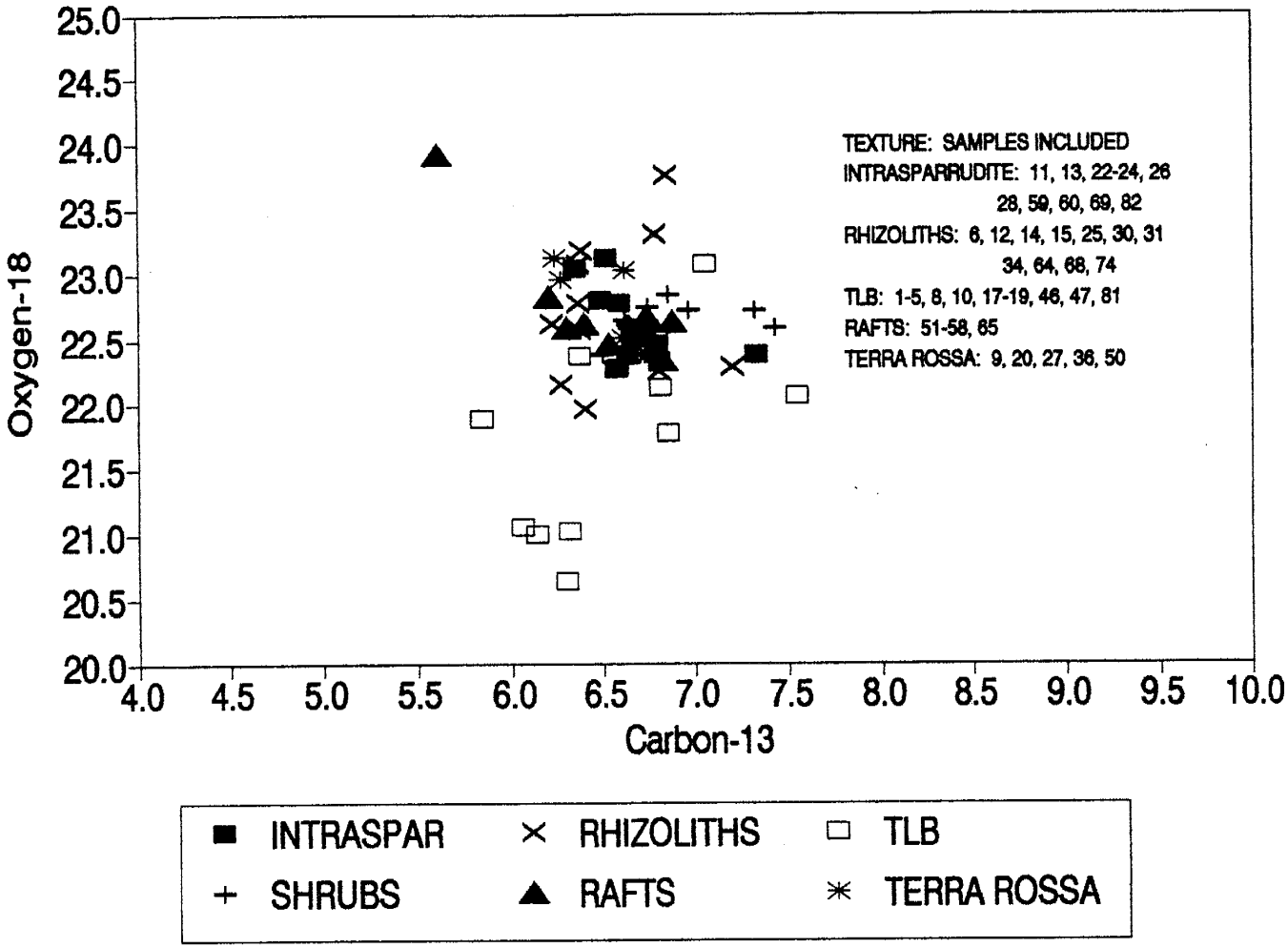

FIG. 19 - An isotopic scatter plot of the most common textures sampled in the first 10 ft (3.1 m) of NRDC#1. Both primary and secondary textures were sampled to examine the variation in isotopic composition among textures and features.

Six major textures, intrasparrudite, rhizoliths, shrubs, TLB, rafts and terra rossa horizons are seen in the initial 10 ft (3.1 m) interval (Fig. 19). Fig. 19 reveals that there is a largedegree of overlap relative to each textures' isotopic range of values. A complete overlap of textural isotopic ranges would imply that the "simplifying assumptions" of isotopic data to be independent of differing textures to be correct, but Fig. 19 does not show a complete overlap of textural isotopic ranges. Instead, some textures have samples clustered in one area of isotopic values. The intrasparrudites are found almost in the center region of Fig. 19 while the TLB generally show relatively depleted $\delta^{18}O$ values. Some terra rossa samples display relatively increased $\delta^{18}O$ values but slightly decreased $\delta^{13}C$ values. The shrubs exhibit a vague enrichment in $\delta^{18}O$ and a low variation in $\delta^{13}C$ values while the rhizoliths show a large $\delta^{13}C$ and $\delta^{18}O$ variation. Fig. 18 does not clearly display any texturally dependent isotopic trends, but it does not prove textural independence. Like Fig. 18, segregation of textures and detailed sample analysis should yield an answer to the question of texture dependent isotopic fractionation trends.

INTRASPARRUDITE

Within the intrasparrudite of NRCD#1, some regions are micrite rich (spar cement may comprise 15% or less of the sample). Micritic allochems were sampled because they are a major component of the

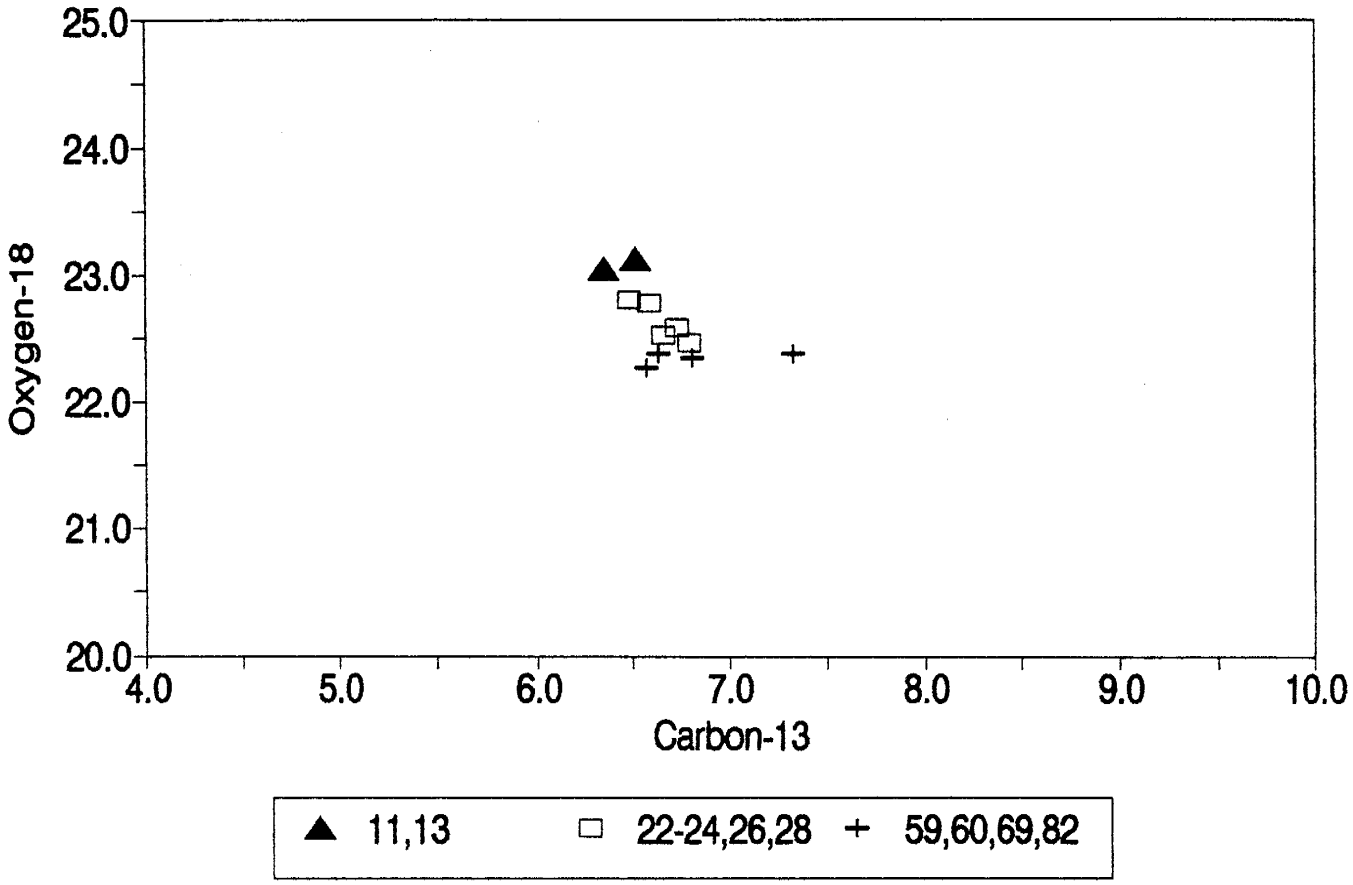

FIG. 20 - An isotopic scatter plot of micritic intrasparrudite samples (see text) not directly associated in with other textures in the upper 10 ft (3.1 m) of NRDC#1. The average of each groups composition displays a trend of decreasing $\delta^{18}O$ but increasing $\delta^{13}C$ with depth (decreasing sample number in this case).

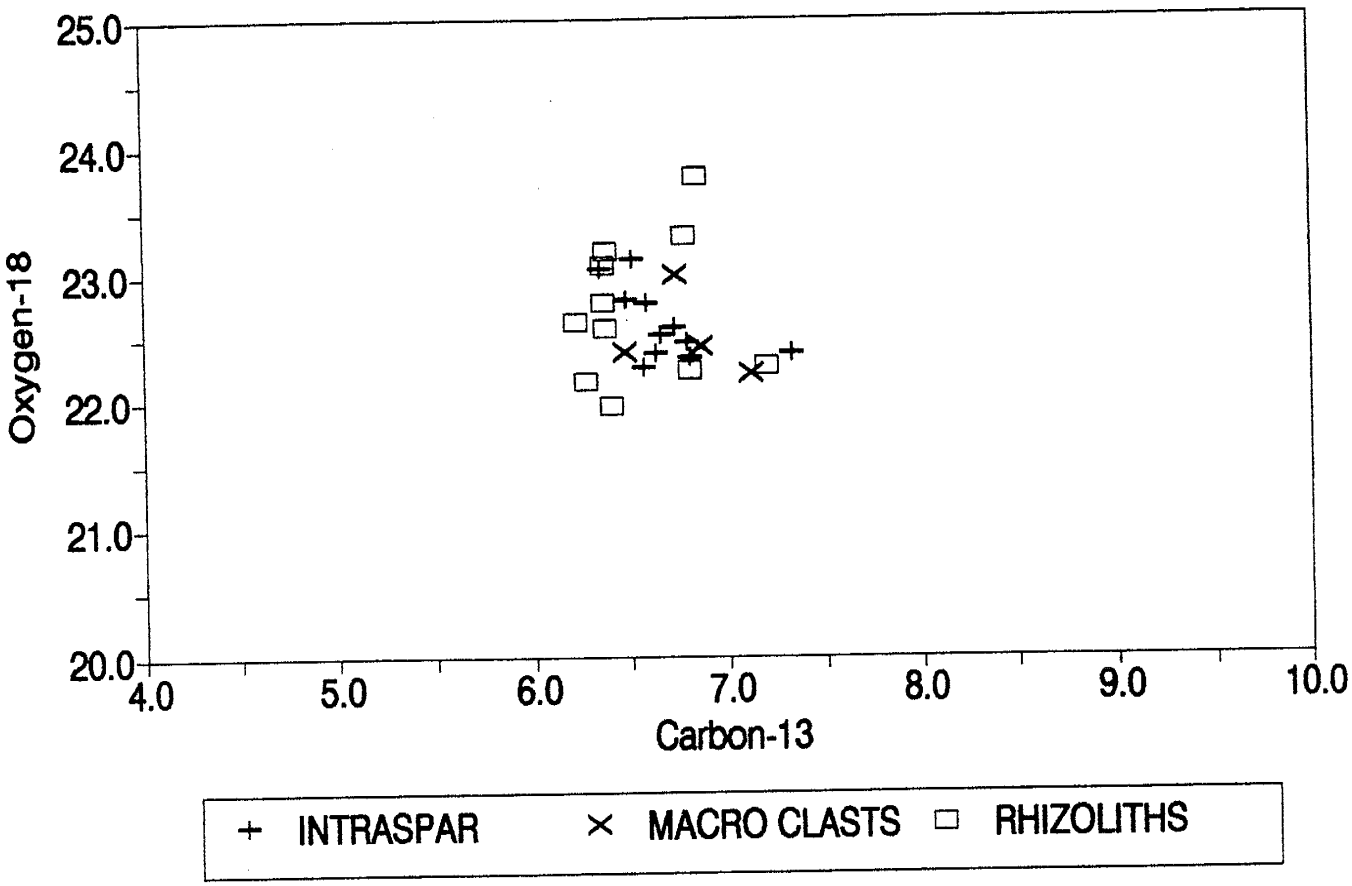

FIG. 21 - An isotopic scatter plot of intrasparrudite samples, macroscopic micritic clasts and micrite filled rhizoliths. The trend seen in Fig. 20 is obliterated by the inclusion of the other micrite-rich sample groups.

primary grains that comprise NRDC#1. The micritic intrasparrudite samples have been subdivided based on their associated textures. This subdivision is the key to visualizing isotopic fractionation effects. The samples in Fig. 20 are not associated with terra rossa layers or other features that might affect the isotopic value. The resulting graph displays a distinct trend of increasing $\delta^{13}C$ but decreasing $\delta^{18}O$ values with depth. By adding other sample groups to Fig. 20, the trend becomes less obvious. Macroscopic micritic clasts taken were sampled from different associated textures, such as: terra rossa horizons, porous zones, and rhizoliths (Fig. 21). The rhizoliths sampled were composed of micrite cement with a frequent very thin iron-stained borders separating the rhizoliths from the matrix. The crescent shaped clasts occur in intrasparrudite accumulations and they appear similar to the other micritic allochems. The rhizoliths are plotted with the micritic clasts (Fig. 21) to demonstrate that without careful sample identification and segregation, the trend exhibited by the micritic intrasparrudite would be obliterated. The scatter plots in Fig. 20 and 21 illustrate the overprinting of isotopic fractionation processes that blur distinctive trends.

TRANSLUCENT LAMINATED BANDS (TLB)

The TLB were sampled downward across the bands. These bands are void-filling cements that grew from the edges of the void inward. Cathodoluminescence observations that show the cement grew

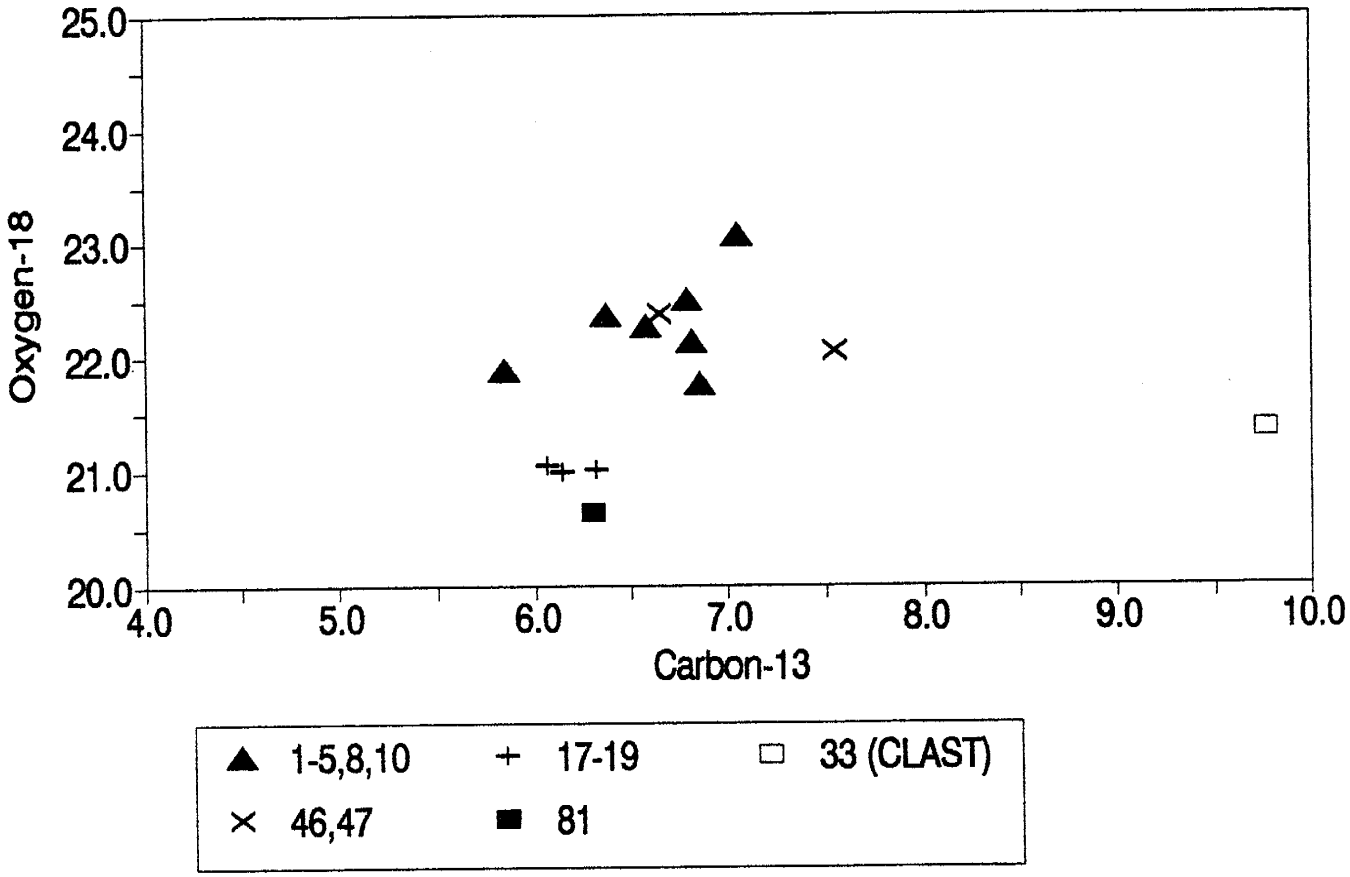

FIG. 22 - An isotopic scatter plot of the NRDC#1 TLB samples. Many of the samples have isotopes values that fall outside the "Restricted Range" of Fig. 15.

in a geochemically open system, which explains the lack of an isotopic trend. The source of both the carbonate and fluid that precipitated the spar will greatly influence the isotopic composition of the spar. Thereby, the lack of any trend seen in Fig. 22 indicates the sample groups were formed in difference isotopic environments.

SHRUBS

Two shrub regions were sampled in NRDC#1, the upper shrub group, samples 37,38,41-45, and the lower shrub group, samples 75-80. Both shrub groups (Fig. 23) display limited ranges in $\delta^{18}O$ composition. The average $\delta^{18}O$ values of the two shrub groups are very similar, and within $0.1^{0}/_{00}$ of each other. Both shrub groups show a general trend of increasing $\delta^{13}C$ values with depth. However, the range in $\delta^{13}C$ values of samples 37,38 and 41-44 is about $0.1^{0}/_{00}$ whereas the range in variation of the lower shrub layer is $0.8^{0}/_{00}$. The isotopic range of both $\delta^{13}C$ and $\delta^{18}O$ for both shrub groups is more constricted than for any other texture. This might be due to secondary processes. The upper shrub group is overlain by a terra rossa horizon that might have homogenized the underlying samples. The lower shrub group have been bisected by a desiccation crack filled with spar cement. Recognition of a isotopic trend in the shrub layers is complicated by probable secondary processes.

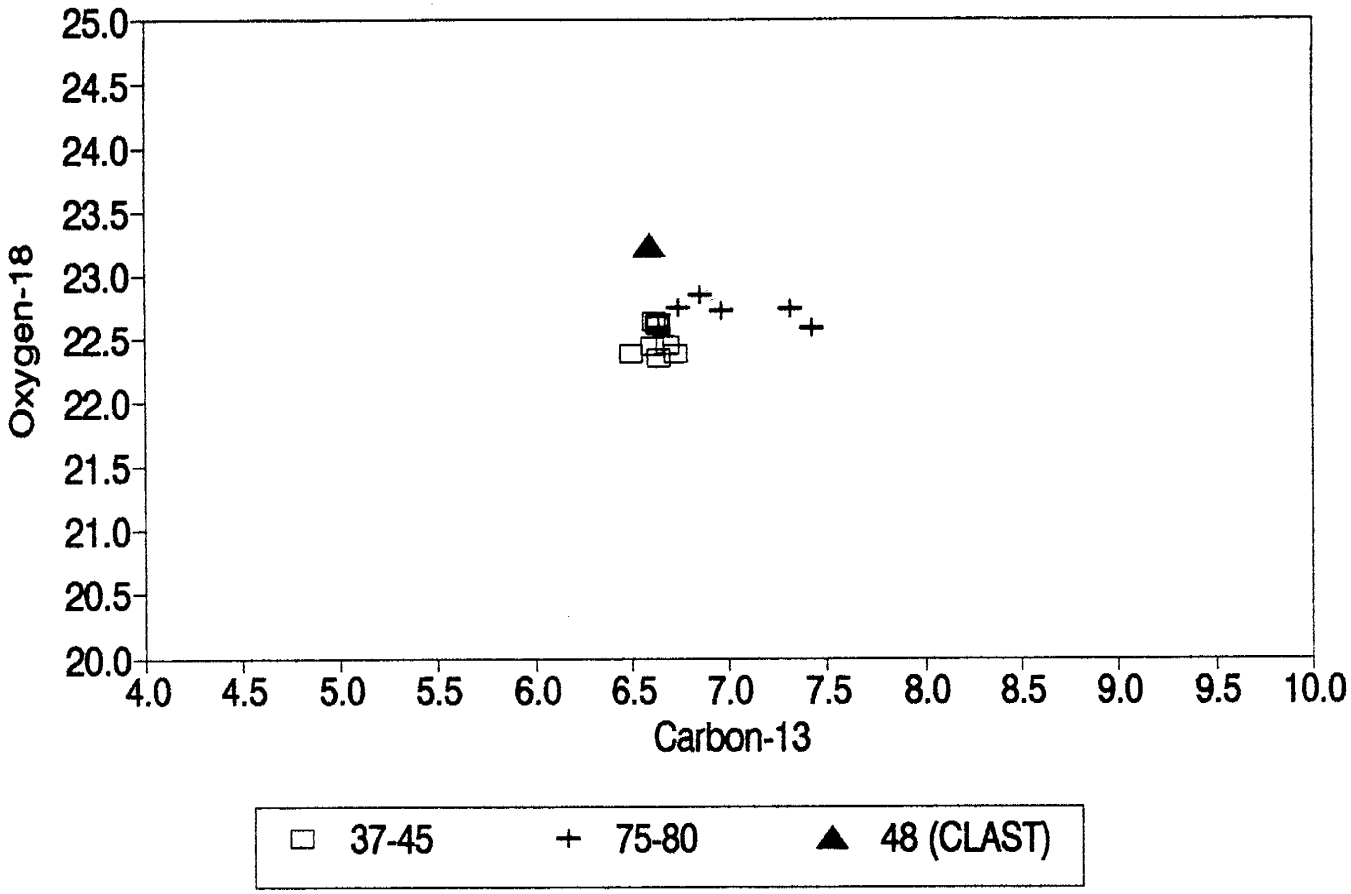

FIG. 23 - An isotopic scatter plot of NRDC#1 shrub samples. The two large sample groups have nearly identical average $\delta^{18}O$ but differing average $\delta^{13}C$ compositions. The shrub clast has a similar $\delta^{13}C$ value as the upper group, but an elevated $\delta^{18}O$ value.

TRAVERTINE RAFTS

The raft samples that were collected are the combination of a thin, elongate primary grain coated by a set of cements. The cements composed the majority of each sample, with the spar versus micrite ratio probably even. Thereby, each raft sample is a mixture of primary and secondary carbonate. Sample 54, is anomalously depleted in $\delta^{13}C$ but enriched in $\delta^{18}O$. It clearly displays neomorphic spar cross-cutting spar/micrite layers. The other raft sample groups display a rather narrow range of $\delta^{18}O$ values but a larger variation in $\delta^{13}C$ composition (Fig. 24). At least some raft samples, like the TLB samples, have been isotopically affected by post-depositional processes.

RHIZOLITHS

Rhizolith samples containing micrite cement were graphed (Fig. 25) to examine if the isotopic trend seen was present. The horizontal spar rhizoliths were not included in Fig. 25 because of limited sampling. The rhizolith sample groups in Fig. 25 are based on spatial and petrological analysis. The micrite rhizoliths are similar to the vertical rhizoliths described by Mount and Cohen (1984). The rhizoliths display a generalized trend of decreasing $\delta^{18}O$ value with decreasing depth. Rhizolith samples 6,12,14 and 15 have $\delta^{18}O$ values above $23^{0}/_{00}$, while samples 25,30,31 and 34 average slightly over $22.5^{0}/_{00}$. The stratigraphically lowest rhizolith specimens 64,68,74 average slightly under $22^{0}/_{00}$, The upper rhizolith samples $\delta^{13}C$ composition display a tendency to decrease

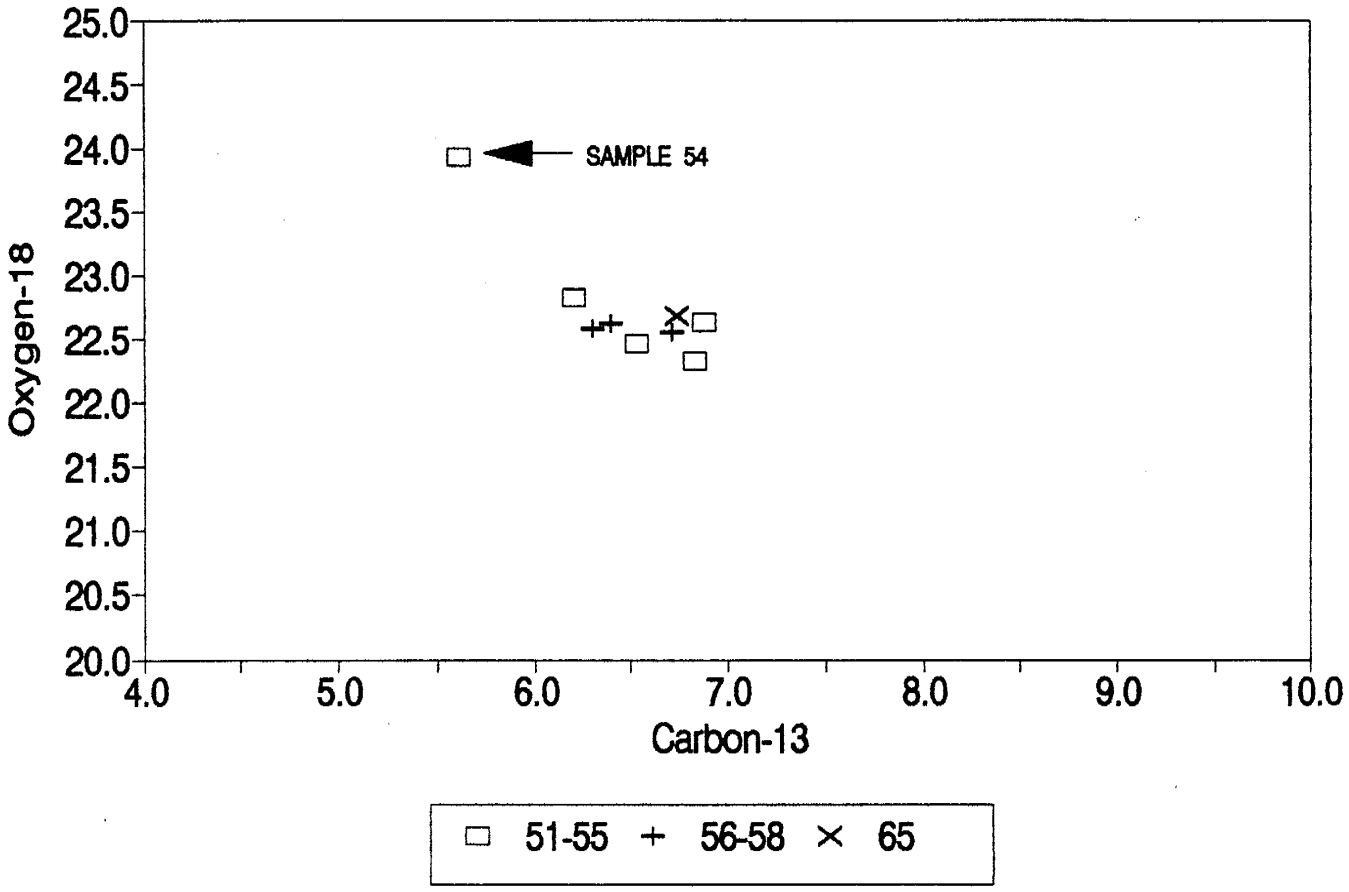

FIG. 24 - An isotopic scatter plot of the NRDC#1 raft samples. The sample groups were chosen based on stratigraphic position, which is reflected in their decreasing sample number. Sample 54 is specially noted because it displays neomorphic crystal growth across the spar then micrite isopachous cement layers.

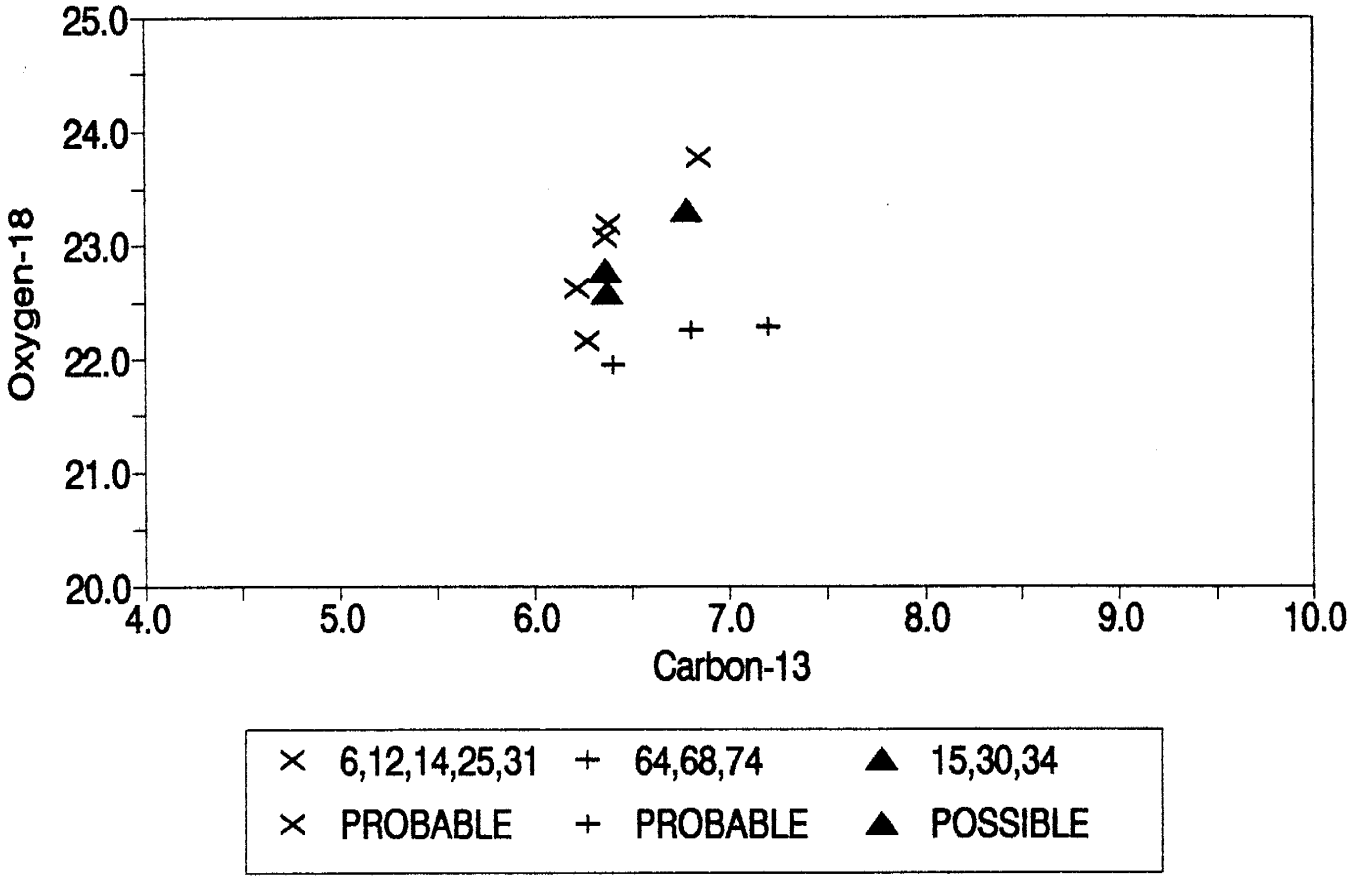

FIG. 25 - An isotopic scatter plot of the NRDC#1 rhizolith samples. Samples were grouped by their relative stratigraphic position. Due to damaged thin sections and the difficulty in differentiating micritic cement from later deposited micritic clasts in hand specimen, the categories "probable" and "possible" are used.

with depth, however the lower rhizolith samples 64,68,74 display a broad range of values. The common trend of decreasing $\delta^{18}O$ values with depth indicates that the intrasparrudite and rhizolith sample groups recorded a similar depositional trend.

TERRA ROSSA

Subaerial exposure horizons are markers that indicate fresh-water diagenesis may have affected or reset underlying isotopic trends (Allan and Matthews, 1982). These horizons may also chronicle paleoclimatic changes. Terra rossa samples were graphed to determine if any trends were preserved. Fig. 26 presents a similar $\delta^{18}O$ trend to the rhizoliths. The upper terra rossa sample group, 9 and 20, has a $\delta^{18}O$ average value of $23^{0}/_{00}$. Samples from the middle group, 27,36,50 and 62, averaged near $22.6^{0}/_{00}$ and the lowest terra rossa sample, 100, was just below $22^{0}/_{00}$. The $\delta^{13}C$ value of the terra rossa horizons (Fig. 26) also fall into a distinct pattern of increasing relative isotopic concentration with depth. Sample 27 has the elevated $\delta^{18}O$ value of the first group, but the $\delta^{13}C$ value fits in perfectly with the second group. The terra rossa best parallels the intrasparrudite trend of increasing $\delta^{13}C$ but decreasing $\delta^{18}O$ with depth. This indicates that terra rossa horizons might record paleo-environmental changes.

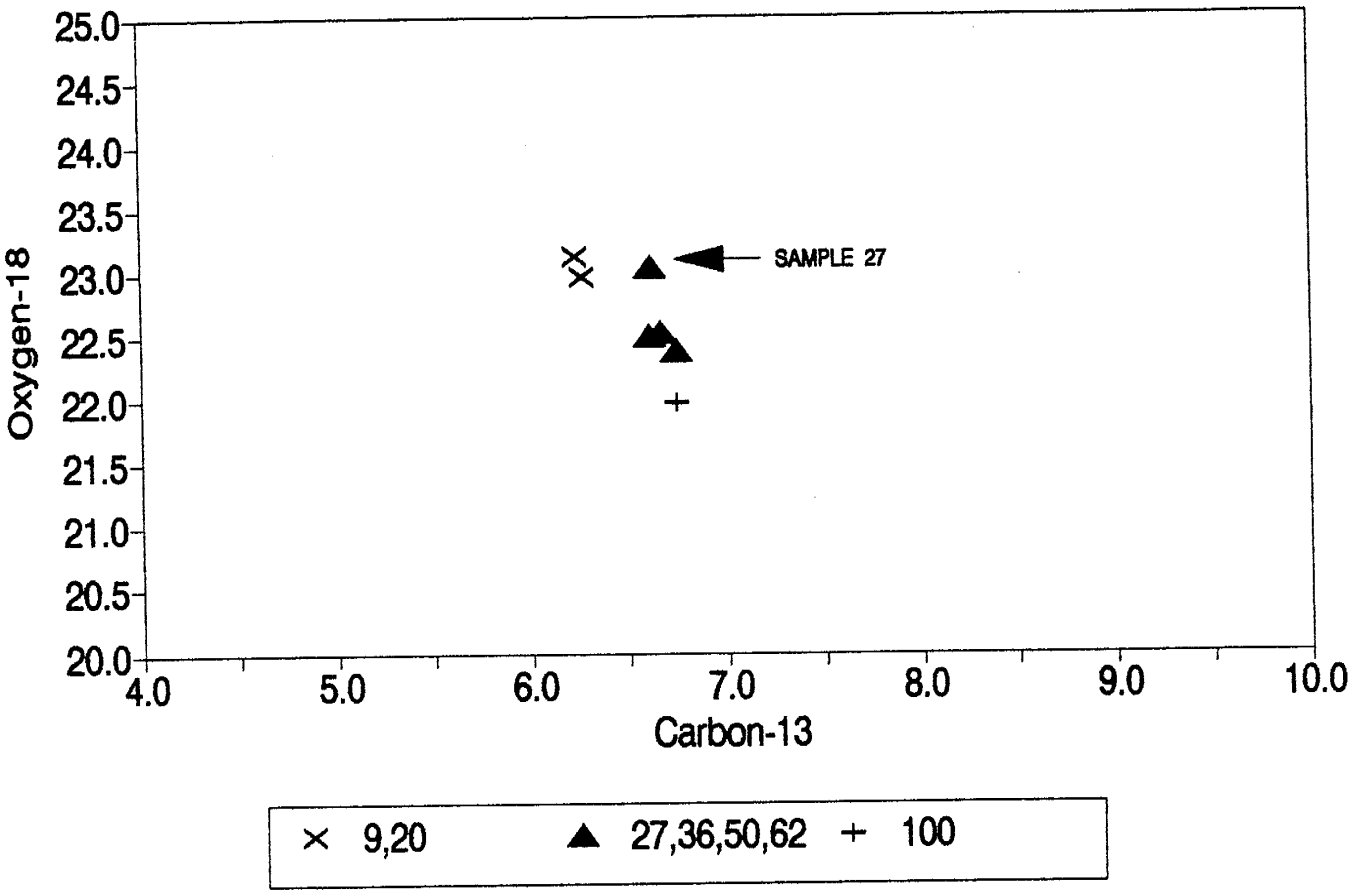

FIG. 26 - An isotopic scatter plot of NRDC#1 samples taken from terra rossa horizons. The three sample groups display an overall trend of decreasing $\delta^{18}O$ but increasing $\delta^{13}C$ with depth. Sample 27 does not fall on this trend, but has a $\delta^{13}C$ value of the second group and a $\delta^{18}O$ value of the first group.

SPAR CEMENT

Calcite spar cement is found throughout the intrasparrudite of NRDC#1. The three secondary groups seen in Fig. 27 are stalactites, spar (which was not associated with TLB), and terrarossa horizons. The stalactites display the most enriched $\delta^{18}O$ and the most depleted $\delta^{13}C$ values in the entire secondary spar data. The spar cement and terra rossa samples have similar isotopic ranges. The trend in the terra rossa samples would have been difficult to notice if all the spar samples were grouped together. Without textural segregation of the spar samples, the recognition of an isotopic trend in the terra rossa samples would not have occurred.

TRENDS WITHIN TEXTURES

The isotopic composition of travertine is not completely independent of texture, but texture is probably just one factor in the variety of processes that have affected NRDC#1. The different processes act to obscure individual trends within the isotopic data. The fact that trends are seen within a single texture is not solid evidience that different textures have different δ values. It may be a secondary process where one texture is more susceptible to alteration. But two different trends are each represented by two different data sets. The data from NRDC#1 and RBTS indicate fairly well that isotopic composition of travertine is co-dependent with respect to texture.

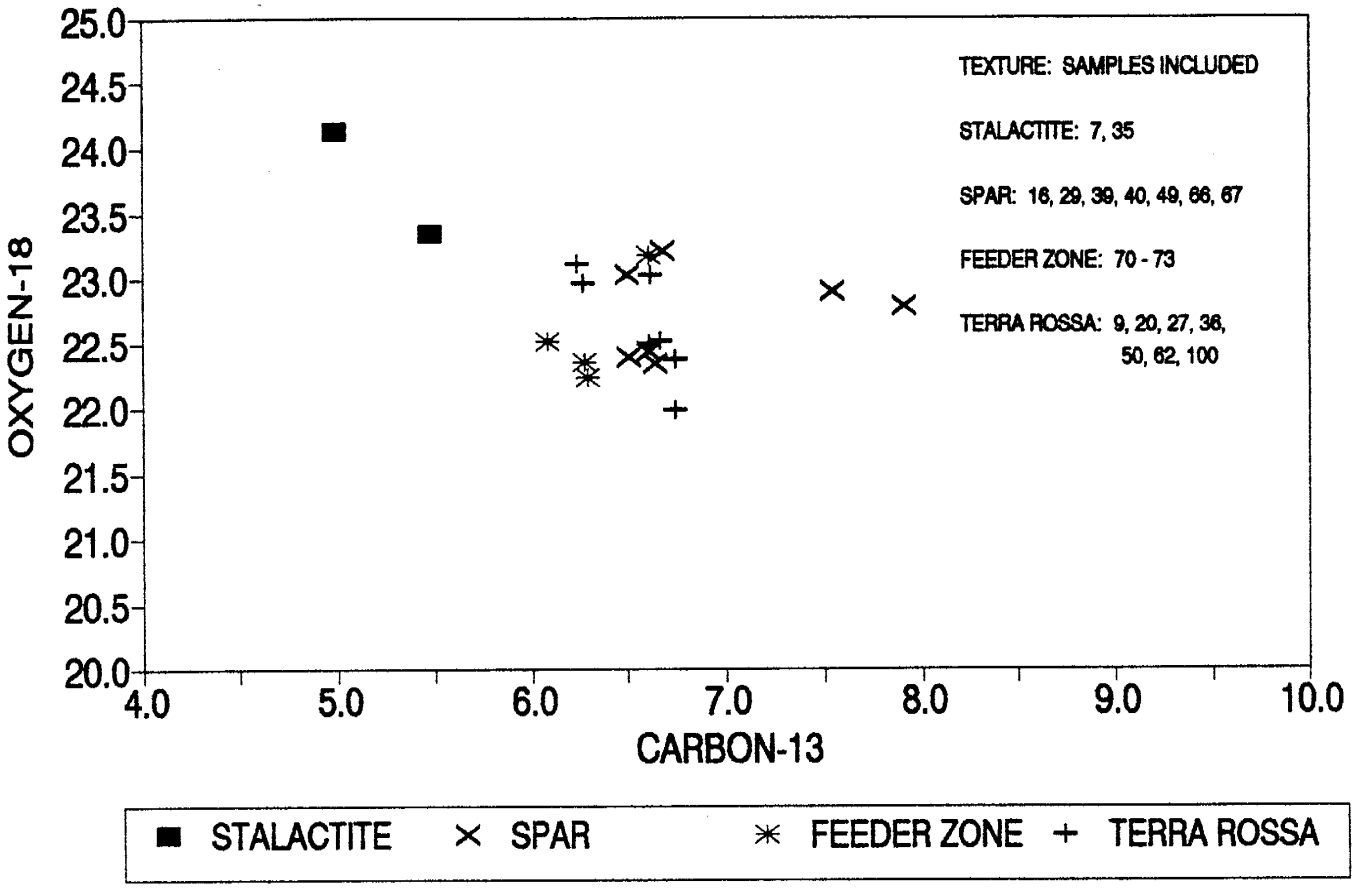

FIG. 27 - An isotopic scatter plot of NRDC#1 spar cement samples. The stalactite samples have a totally independent isotopic value from the other groups, whereas the terra rossa samples and the spar cement samples do show some similarity in composition.

The segregated texture scatter plot (Fig. 19) does not show any distinct isotopic ranges for the different textural groups. The only place where a texture occupies a completely separate isotopic range is the two stalactite samples (Fig. 27). Yet, there are definite and distinct trends within textures in the NRDC#1 sample data. The factor that defines the intrasparrudite (Fig. 20) and terra rossa (Fig. 26) trends is stratigraphic depth which is a measure of deposition over time. Time is the other variable in conjunction with textures that allows definition of trends.

Two important depositional trends are seen in the NRDC#1 and the RBTS isotopic data. Both the RBTS (Fig. 14) and the linear sampled micrite (Fig. 18) data show well defined peaks. Because of the terra rossa horizons that bound the micrite and the multiple cycles in the RBTS isotopic data, it appears possible that this trend is a seasonal or yearly trend. The $\delta^{18}O$ peak of the linear sampled micrite rich allochems occurs nearly midway through the traverse, possibly implying a biogenic bloom or seasonal variation had depleted the fluid in $\delta^{16}O$. A biogenic bloom would also increase the $\delta^{13}C$ of the fluid, however, both RBTS and the micrite data show a depression in $\delta^{13}C$ values compared to the enriched $\delta^{18}O$ value in the samples. The $\delta^{18}O$ peak may be due to increased evaporation due to higher temperatures.

The second important textural trend is the increasing $\delta^{13}C$ but decreasing $\delta^{18}O$ With depth. This trend is distinct within the intrasparrudite (Fig. 20) and terra rossa (Fig. 26) sample groups. It is also apparent in the rhizolith samples (Fig. 15) to a lesser

degree. The intrasparrudite and terra rossa trends are similar, but not parallel. Other textural sample groups show definite signs of multiple processes and complex cementation and thereby their data should be considered as unknown combination of factors and not representative of their groups original isotopic signature. The congruent trends in "primary" (intrasparrudite) and secondary (terra rossa) textures supports the trends' validity.

The lack of a broad trend in viewing the entire data set isdue both to the initial heterogeneity in textural variation and to the later secondary alteration and depositional processes. Each process has affected only certain sample groups and the multiple processes increase the distortion of a general trend. The total cumulative effect of the multiple processes is to blur detailed micro-trends and obscure any general trend. Viewing the NRDC#1 isotopic data without detailed textural analysis might lead to an incorrect "simplifying assumption".

DISCUSSION OF DEPOSITIONAL ENVIRONMENT

Because the age of NRDC#1 has not been accurately determined by radiometric or biostratigraphic means, incorporation into a regional paleoclimatic reconstruction has not been attempted. The highly variable nature of travertine deposition, especially within the Riley travertine, indicates that conclusions regarding the depositional environment, drawn from the travertine within NRDC#1 must be limited to a very small area around NRDC#1. However, broad paleoclimatic conclusions drawn from the isotopic data of NRDC#1 might pertain to laterally adjacent regions of the North Riley travertine.

PETROLOGIC EVIDENCE

Some recent studies about paleoclimatic changes recorded in travertines assume continuous deposition (for example, see Livnat and Kronfeld, 1985). An important conclusion of this study is that deposition of the first 10 ft (3.1 m) of NRDC#1 was not continuous. The abundance and spacing of terra rossa horizons is prime evidence of intermittent deposition. In the uppermost 10 ft (3.1 m) of NRDC#1, terra rossa horizon spacings are on the order of 6 in. (15 cm) while in the second interval they occur at approximately 1 ft (0.3 m) intervals. Episodic deposition may result from seasonal or groundwater effects.

The disturbed layering seen in shrub layers indicates that

subaqueous deposition was also intermittent. Shrub layers are indicators for a shallow (certainly within the photic zone, probably 20 ft (6.1 m) or less), stable, subaqueous environment and biogenic deposition (Folk and Chafetz, 1983). The best preserved shrub horizon is only 6 in. (15 cm) region in the upper 20 ft (6.1 m) of NRDC#1, and it has a major desiccation crack splitting and offsetting the layers. Folk suggests (personal communication, 1991) that shrub layering with thin micrite beds might define a yearly growth for some travertine deposits. If so, the shallow pool that produced the best shrub layer only lasted for 7 years. Travertine deposition at the site where NRDC#1 was later drilled occurred in short-lived pools.

During periods of subaqueous travertine deposition in NRDC#1, biogenic deposition helped produce travertine. Much of the upper portion of NRDC#1 was biogenically induced or precipitated. The peloids, oncoids and some coated grains that comprise the majority of the interclasts within the intrasparrudite were probably produced at the bottom of the pools by algal mats similar to those described by Friedman et al. (1973); though the Riley's algal mats would have been in fresh water. The large number of intraclasts were probably generated by the desiccation of algal mats once the pools had dried up. Shrub layers are a direct product of microbial activity (Folk and Chafetz, 1983), and the presence of rhizoliths indicates macrophytes were sometimes present. During much of travertine deposition at the site of NRDC#1, organisms played a large role in aiding travertine accumulation and morphology.

The clasts seen in NRDC#1 also aid in paleoenvironmental reconstructions. Travertine intraclasts seen in the core indicate that periodic flooding or a change in the fluid flow affected travertine accumulation. Fluid flow can change as the result of either biogenic deposition changing stream morphology, (Slack, 1967) or a change in the position of the fluid source (Chafetz and Folk, 1984). A diversion in fluid flow will halt travertine deposition in a previously active environment and initiate travertine deposition in a region previously inactive. The zone of previous deposition will undergo desiccation and possibly polygonal cracking (Warren, 1982) which generates travertine clasts.

Almost all of the clasts in NRDC#1 are travertine clasts that were re-deposited within the North Riley. The extreme $\delta^{13}C$ composition of the TLB clast (sample #33) and the enriched $\delta^{18}O$ composition of a shrub clast (sample #48) indicate periods of clast transport over large distances and probably different travertine depositing areas of the Riley. The paucity of non-travertine clasts suggests localized fluid flow within the Riley. Clasts demonstrate the continually changing center of deposition.

The different cement morphologies also indicate non-uniform environment after deposition. Most travertine rafts have two different cements coating them, micrite cements with geopetal features and spar cements with terra rossa glaebules fill the voids between rafts and lithify the deposit. This sequence of cements in commonly seen coating rafts two times or more. The cyclicity of the cement layers is good evidence of a changing microenvironment

around the rafts during lithification. The sequence of scalenohedral calcite (sometimes coated by a thin Fe-mineraloid) followed by rhombohedral spar also suggests differing environments of cementation. The Given and Wilkinson (1985) model of abiotic sedimentary carbonates states that the scalenohedral crystals are formed by rapid precipitation in a meteoric-vadose zone while the later rhombohedral spar is generated in the meteoric-phreatic environment. This model explains the range in size of the rhombohedral and scalenohedral spar as a function of the time spent in each of the spar's respective growth domains. The occurrence of two different morphologies of spar cement is the progression of diagenesis during changing environments and perhaps burial (Given and Wilkinson, 1985). Deposition and diagenesis of the North Riley travertine occurred in differing enviroments.

ISOTOPIC EVIDENCE

Although it is not possible to uniquely determine the temperature of deposition without knowing the $\delta^{18}O$ of the water, it is possible to determine the approximate range of temperatures which would be needed to account for the range of carbonate values. To do this we need to assume a reasonable temperature for travertine deposition. Based on other temperatures determined by Lorah and Herman (1988), we will assume 25°C. Using this temperature, the average $\delta^{18}O$ of carbonate and α, an average water value is calculated by using the equilibrium fractionation equation;

$$1000 \ln \alpha = (2.78 \times 10^6 / T (^0K)^2) - 3.39$$

where α is the isotopic fractionation factor and assuming temperature of 25^0C for the deposition of $CaCO^3$ yields $27.9^0/_{00}$ for 1000 ln α. Then using an isotopic fractionation equation with the computed 1000 ln α and an average $\delta^{18}O$ $CaCO_3$ of $22.75^0/_{00}$, solving for $\delta^{18}O$ of the deposition fluid;

$$1000 \ln \alpha - \delta^{18}O\ CaCO_3 - \delta^{18}O\ H_2O$$

yields $5.15^0/_{00}$ for $\delta^{18}O$ H_2O. Now the fluid's temperature range at the time of deposition can be found by solving for a new 1000 ln α by substituting the maximum and minimum $\delta^{18}O$ $CaCO_3$ values. The TLB samples 17-19 had the lowest $\delta^{18}O$ values at $21^0/_{00}$, which yields a depositional temperature of 33.5^0C. The pore-filling fluids that produced the TLB's might have been deposited directly from an underground fluid that did not contact the atmosphere and thereby cool. A raft sample that has undergone neomorphism has a $\delta^{18}O$ value of almost $24^0/_{00}$, which yields a depositional temperature of 19^0C. Paleoclimatic isotopic equations suggest that the fluids that formed the travertine in NRDC#1 ranged from 19^0C to 34^0C. Whether or not the absolute values of this temperature range is correct, because of the initial assumption of a $\delta^{18}O$, a range of 14^0C can explain the range in carbonate values given a constant $\delta^{18}O$ of the fluid.

The source of the fluid is meteoric, but whether it is surficial meteoric or re-circulated meteoric surface is difficult to discern. The travertine deposited by surficial meteoric waters have fluid temperatures up to 26^0C (Slack, 1967) whereas deeply

circulated meteoric water was hotter than 35^{0}C at the spring source (Herman and Lorah, 1987). A travertine depositing stream can show a temperature change of nearly 17^{0}C, from an initial 35^{0}C, upon emergence of the fluid, to 18.5^{0}C over a 3 mi (4.8 km) course (Herman and Lorah, 1987). Even if the temperature of the fluid measured in NRDC#1 seems surficial, the fluid that originated from the orifice may have been heated, re-circulated meteoric water. Because the distance the fluid travelled from the spring's origin to NRDC#1 is not known, the source of the fluid is not clear. The large range in the temperature of the fluids that deposited the Riley travertine appears more likely to have been heated in the subsurface than strictly surficial meteoric.

Within the Rio Grande Rift, there are several possible thermal sources for the fluids that deposited travertine in NRDC#1. Travertine deposits are associated with volcanic terrains (Friedman, 1970; Fitzmaurice, 1990) and rifts (Livat and Kronfeld, 1985). The fluids that deposit travertine may derive heat from magmatic sources and/or basinal sources. Within the Rio Grande Rift, elevated heat flow and groundwater temperatures have been measured by Barroll and Reiter (1990), which could be due to upper crustal magma or deep-circulating fluids. Thus, there are thermal sources within the Rio Grande Rift to heat the fluid.

The lack of aragonite can provide a very important temperature constraint on the travertine depositing fluid. At 40^{0}C is the temperature depositional boundary of the aragonite/calcite mineral phase. The two factors that commonly produce aragonite are heated

fluids and biogenic activity. Because no macroscopic invertebrate fossils were found in NRDC#1 and X-ray diffraction studies on the Riley by Barker (1983; 1984) detected no aragonite, the absence of aragonite within NRDC#1 is expected. Although Folk (personal communication, 1991) has mentioned the extreme difficulty in identifying aragonite relicts and pseudomorphs in travertine deposits. The absence of aragonite provides good evidence that the isotopically calculated fluid temperatures of deposition are within the correct range.

The $\delta^{18}O$ composition of the two textural trends seen in the RBTS and NRDC#1 data seem to record temperature changes. Both the RBTS and the linear sampled intarsparrudite display a well-defined $\delta^{18}O$ peaks. The peaks appear to chronicle a cyclic temperature change, probably seasonal changes in fluid temperature or changes in the fluid's isotopic composition. Biogenic blooms of algae and bacteria, which greatly contributed to travertine deposition in NRDC#1, could also be responsible for the seasonal cycle. The "broad" isotopic trend of decreasing $\delta^{18}O$ with depth seen in the intrasparrudite, terra rossa and rhizolith sample groups can be interpretated as a paleoclimatic warming trend. The fact that the "broad" trend is seen in multiple textures helps validate the assumption that the each texture's original isotopic composition has been preserved.

The "broad" $\delta^{13}C$ and $\delta^{18}O$ trend seen in NRDC#1 does record a warming trend in the fluid temperature over time, but this is not necessarily caused by paleoclimatic changes. An important aspect

of the depositional environment can probably be seen in the $\delta^{13}C$ trend. Within some previous studies a trend exists in these data sets showing a consistant decrease in difference in the precipitate and the fluid ($\Delta^{13}C$). In Fig. 28 the mechanics of the carbonate-rich solution depositing $CaCO_3$ were examined at the instance of sampling, as if the stream was frozen in time to clarify the relationships of pH, temperature $\delta^{13}C$ of the fluid, the difference in $\delta^{13}C$ between the solution and the precipitate and chemical concentration of $(HCO_3)^-$. A change occurs in $\delta^{13}C$ of the fluid, from $-2.89^0/_{00}$ at the beginning of the ditch, to $2.38^0/_{00}$ at 25 yd (22.8 m) downstream (Fig. 28). This trend is accompanied by a decrease in the difference between the $\delta^{13}C$ of the fluid and the travertine formed from it. It also corresponds with an increase in pH downstream. The $(HCO_3)^-$ concentration decreases downstream as pH rises and also correlates to the increase in $(CO_3)^{-2}$ concentration. Farther downstream another spring flows into the original (S-1) stream. The mixing of carbonate waters affects the chemical and isotopic composition of a stream in a non-linear fashion (Wigley and Plummer, 1976).

In order to explain the parallel trends of increasing pH and $\delta^{13}C$ of the fluid but decreasing $\Delta^{13}C$ with distance downstream, an explanation is proposed here based or a review of the data of

FIGURE 28. GEOCHEMICAL AND ISOTOPIC CHANGES IN A TRAVERTINE DEPOSITING SYSTEM

(SELECTED DATA FROM CHAFETZ ET AL., 1991)

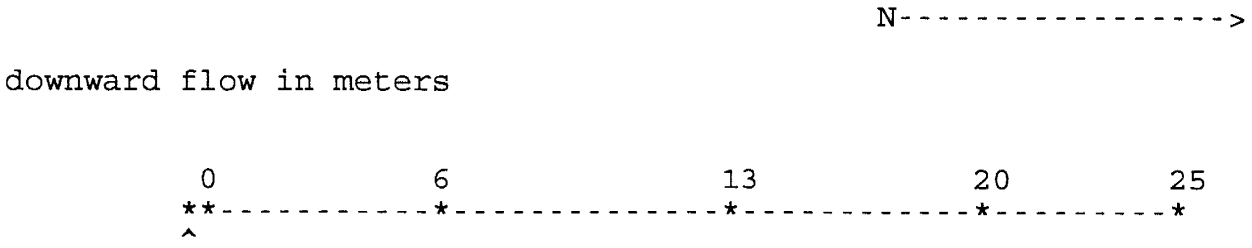

downward flow in meters

SPRING S-1

Sample Site	meters	T^{0}C	pH	$\delta^{13}C_{fluid}$	$\Delta^{13}C_{diff}$*
June 14th					
SPRING S-1	0	33.2	6.35	-2.89	
Ditch-0	0	32.0	6.80	-1.49	6.35
Ditch-6	6	31.5	6.95	0.12	
Ditch-13	13	31.5	7.13	0.49	
Ditch-20	20	30.0	7.23	1.55	
Ditch-25	25	30.2	7.30	2.35	2.38
June 20th					$[HCO_3]^-$
SPRING S-1	0	33.2	6.10	-2.18	1665
DITCH-25	25	32.0	7.11	2.35	1140

$\Delta^{13}C_{diff}$* = The average difference over several sampling events between $\delta^{13}C$ of the water and solid precipitate at the site, in per mil.

$[HCO_3]^-$ = the concentration of bicarbonate ion in solution, measured in ppm.

Chafetz et al., (1991 ; Dandurand et al., (1982); Friedman, (1970); Lorah and Herman, (1988) and Usdowski et al., (1979). Fig. 29 represents a model of pH and carbon isotope fractionation involving a carbonate-rich solution feeding a calcite-depositing travertine system. The first condition for the model is a temperature below 40^0C. If the temperature of the fluid is greater than 40^0C, then aragonite is deposited preferentially to calcite (Pursell et al., 1985 in Fitzmaurice, 1990). To avoid the complications of phase changes and calcite/aragonite codeposition, the model is based on calcite deposition.

The three main mechanisms in this model are: change in pH of the solution due to chemical deposition, the fractionation of carbon isotopes by calcite precipitation, and the fractionation of carbon isotopes by degassing carbon dioxide. The initial conditions of the system are: a spring or seep, a solution with greatly elevated [(Ca^{+2})], $(HCO_3)^{-1}$, $(CO_3)^{-2}$] and [CO_2] and a flow regime.

The pH of the system changes as the system evolves. As the fluids rush out of the vent, they are supersaturated in CO_2 (which is a measure of the total carbonate in solution) with respect to the surrounding atmosphere and there is an excess Ca^{+2} in solution. By the application of Le Chatelier's Principle, the solution, which has an elevated concentration of CO_2, attempts to come to equilibrium with the atmosphere. Besides directly degassing

FIGURE 29 : A MODEL OF ^{13}C ISOTOPIC ENRICHMENT IN A GENERALIZED TRAVERTINE-DEPOSITING STREAM

T°C VARIABLE (BELOW 40°C)

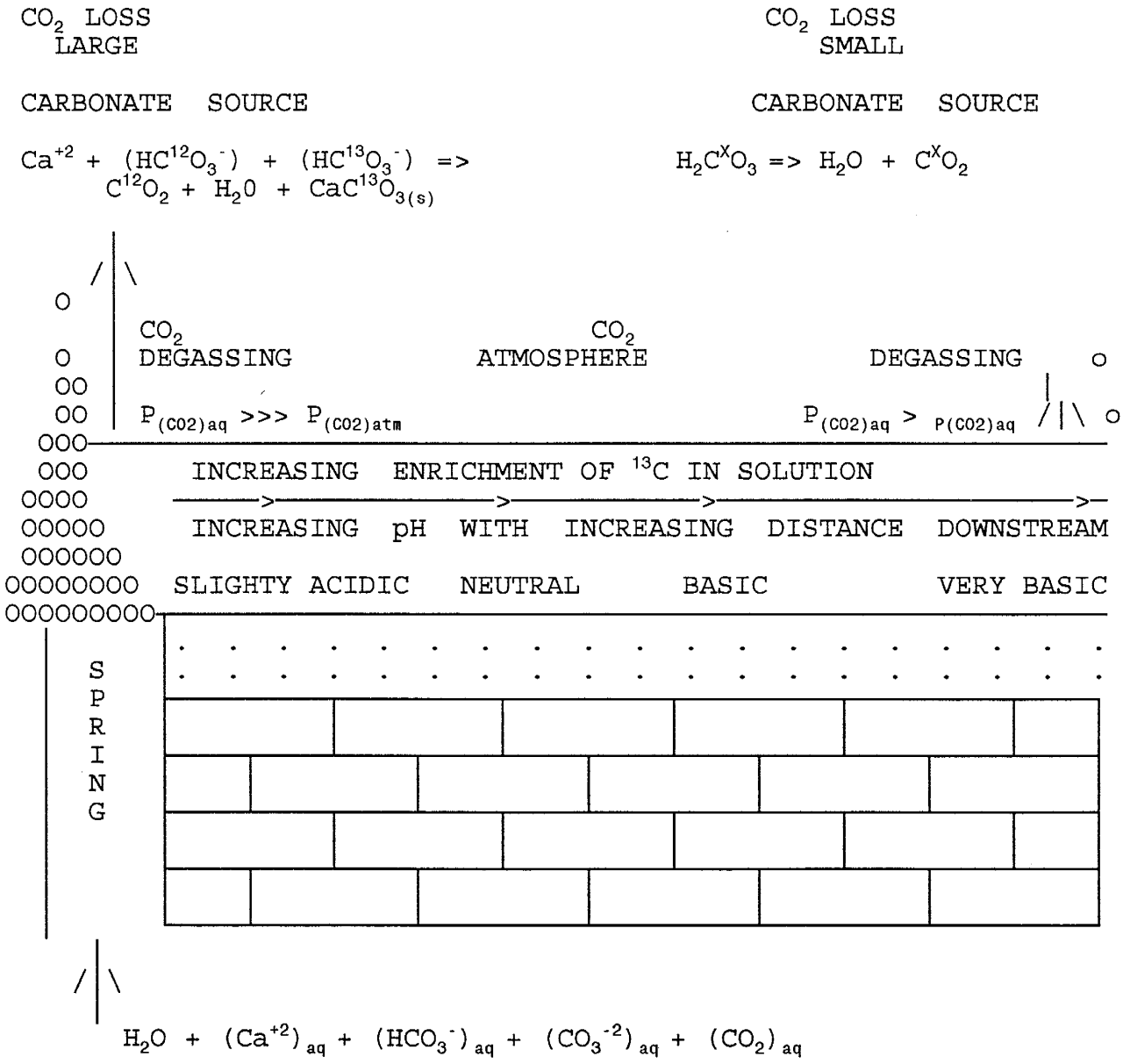

aqueous CO_2 into the atmosphere, carbonate reactions occur in the solution to expedite CO_2 degassing and equilibrium with the atmosphere.

(1) $Ca^{+2} + 2(HCO_3)^-_{(aq)} \text{ ---> } CaCO_{3(s)} + H_2O_{(l)} + CO_{2(g)}\uparrow$

(2) $H^+_{(aq)} + (HCO_3)^-_{(aq)} \text{ <---> } H_2CO_{3(aq)} \text{ --> } H_2O + CO_{2(g)}\uparrow$

(3) $Ca^{+2}_{(aq)} + (CO_3)^{-2}_{(aq)} \text{ ---> } CaCO_{3(s)}$

(aq) = aqueous or in solution
(s) = solid
(l) = liquid
(g)^ = gaseous phase released into atmosphere environment
(Usdowski et al., 1979)

$K(1) = (H_2CO_3) / (CO_2) + (H_20) = 10^{(-2.59)}$

$K(2) = (H^+)\ (HCO_3^-) / (H_2CO_3) = 10^{(-3.76)}$ (Fisher, 1979)

As the fluids leave the vent and enter an "open system", the solution starts off slightly acidic (Chafetz et al., 1991) or neutral (Dandurand et al., 1982) or rarely slightly basic (Usdowski et al., 1979). As the solution begins to flow downstream, nucleation of $CaCO_3$ begins in a solution supersaturated in total dissolved carbonate and undergoing very rapid degassing. The initial $CaCO_3$ formed will generate CO_2, because most fluids just leaving the vent are slightly acidic to neutral, and thereby Eq.1 will produce the majority of $CaCO_3$. The very small amount of fluid in the environment, or microenvironment surrounding the initial molecules of $CaCO_3$ will be affected almost immediately by the rapid degassing and solution turbulence. The initial $CaCO_3$formed was probably in equilibrium with

the microenvironmental fluid, for an instant, but rapid degassing and associated solution turblence will change the overall fluid chemistry and isotopic signature almost immediately. This initial $CaCO^3$ molecules suspended in solution will merge with other $CaCO_3$ formed elsewhere in the fluid and form a grain and precipitate. The carbon isotopic signature of this grain will not appear to be in equilibrium with the fluid presently surrounding the grain, because the present fluid did not form the grain.

Downstream, however, the pH of the fluid has risen and becomes basic so that $CaCO_3$ production is governed by Eq. 3, a non- degassing reaction. The fluid has mostly degassed and is only slightly supersaturated with total carbonate with respect to the atmosphere (Fig. 29). The solution chemistry does not change as rapidly downstream as it does near the vent (Fig. 29). The fluid downstream, which is generating very little CO_2 from $CaCO_3$ formation, is likely to have a fairly uniform environment relative to the microenvironment of the fluid that produced $CaCO_3$. Any microenvironment downstream that forms $CaCO_3$ will more closely resemble the surrounding fluid than a microenvironment near the vent resembling it's surrounding fluid. The solution is in a higher state of chemical disequilibrium closer to the vent, and is more likely to display a greater carbon isotopic disequilibrium.

The travertine deposited in NRDC#1 could have been formed by a fissure ridge or sloping fan morphology. Both deposit types produce ponds where the biogenic deposition could have occurred. In both deposits fluid flow is subject to change in direction in accordance

with deposition. Both deposits are stable enough to produce 20 to 30 ft (6.1-9.1 m) accumulation, and both deposits have moving sources of emerging fluids. If a warm-spring orifice moved closer to the depositional site of NRDC#1, relatively, then the isotopic trend would be the same as seen in the upper portion of the NRDC#1. The $\delta^{13}C$ composition would decrease as the spring orifice moved closer to the depositional site. This trend can be seen by moving backwards through the sampling stations in Fig. 28. The warm spring orifice moving closer to the depositional site of NRDC#1 would increase the temperature of the fluid at the depositional site by allowing less time and distance for the fluid to cool. The progression of orifice movement relative to the site will produce warmer temperatures in the fluid that deposits travertine over time, which will generate a $\delta^{18}O$ trend that *appears* to be a paleoclimatic warming trend. The general isotopic trend and rapidly changing textures seen in the NRDC#1 data might be due to a warm spring fed fissure ridge or sloping fan with relative movement of the spring orifice toward the depositional site of NRDC#1.

CONCLUSIONS

The various textures and features are inter-related with changes in the production of calcium carbonate by biogenic and inorganic processes. NRDC#1 samples a cross section of travertine in which both biogenic and inorganic processes were operating. There are sections in the core where inorganic processes were dominant, such as the spar that comprises terra rossa horizons, and certain areas where biogenic processes were active, such as the shrub layers. But even the stalactite spar has traces of fragmented biogenic calcium carbonate incorporated into the spar and the shrub horizons have spar cement in between most of the "trees in the forest" (Chafetz and Folk, 1984). The travertine in the North Riley travertine is due to the accumulation of calcium carbonate by both biogenic and inorganic processes.

The lack of an overall trend in the scatter plot of all the NRDC#1 isotopic data is due to many factors. Factors such as diagenesis, paleoclimatic changes, neomorphism, organic decay and change in the geometry of deposition have had various effects on the overall NRDC#1 isotopic data. Only by precise micro-sampling and accurate textural identification can the trends be segregated from natural fluctuations and identified distinctly. Without detailed textural analysis of the NRDC#1 isotopic data, one could make an incorrect "simplifying assumption" that isotopic composi- tion is completely independent of textural differences in traver- tine.

Many other correlations and findings, some based on or broadened from previous work are noteworthy. A brief listing of them is presented:

1) The intrasparrudite that forms the great majority of the accumulation is composed of intraclasts, peloids and coated grains. In many cases, peloid grains are in the nucleus of intraclasts.

2) Shrub layers occur in NRDC#1 but are not well-formed. Travertine rafts occur in the NRDC#1 and appear to be composed of micrite and spar cement.

4) Subaerial exposure surfaces are represented by terra rossa horizons in NRDC#1.

5) Other sedimentary features such as desiccation cracks and sediment draping make-up an insignificant accumulation of travertine but are important environmental indicators.

6) There are many examples of diagenesis in NRDC#1 such as spar cement, microstylolites and aggrading neomorphism.

7) The scatter plot of all NRDC#1 isotopic data does not exhibit an overall trend.

8) $\delta^{13}C$ and $\delta^{18}O$ profiles display some similar trends within certain sample groups, but neither isotopic profile reveals consistent textural trends.

9) RBTS and the linear traverse both display a $\delta^{18}O$ depth profile of a well-defined peak. This trend is possibly due to seasonal changes. The $\delta^{13}C$ data does not present a trend that confirms the cause of the $\delta^{18}O$ trend.

10) A broad isotopic trend can be recognized within the dense micritic allochems, terra rossa and rhizolith (partially) sample groups, decreasing $\delta^{18}O$ composition but increasing $\delta^{13}C$ compostion with increasing depth.

11) The decreasing $\delta^{18}O$ isotopic composition with depth within the broad trend suggests a paleoclimatic warming trend.

12) A possible deposition model, for the area where NRDC#1 was drilled, is that a warm spring was the source of the fluid that fed small intermittent pools on a travertine terrace, fan or mound. As the upper portion of the NRDC#1 was depositing, the spring orifice moved relatively closer to the depositional site.

ACKNOWLEDGMENTS

Support for this study was provided by the New Mexico Bureau of Mines and Mineral Resources by Directors Dr. Frank Kottlowski and Dr. Charles E. Chapin and from the New Mexico Tech Department of Geoscience by Dr. John Schlue and Dr. Andrew Campbell.

Invaluable direction and discussion was provided by Dr. Andrew Campbell, Dr. David Johnson and Dr. Peter Mozley along with James Barker and Marc Wilson of the New Mexico Bureau of Mines and Mineral Resources.

In addition, I am very grateful and indebted to the following people for their support and writing expertise: Jody J.Beatty, David E. Beatty, Edward S. Johnson, Lynne Hemmingway, Mr. and Mrs. Israel Bills and Douglas Jones.

BIBLIOGRAPHY

Allan, J.R. and Matthews, P.K., 1982, Isotopic signatures associated with early meteoric diagenesis: Sedimentology, vol. 29, p. 797-817.

Amundson, R. and Kelly, E., 1987, The chemistry and mineralogy of a CO_2-rich travertine depositing spring in the California Coast Range: Geochimica et Cosmochimica Acta, vol. 51, p. 2883-2890.

Bachman, G.O. and Machette, M.N., 1977, Calic soils and calcretes in the Southwestern Unisted States: U.S.G.S. Open file Report 77-794.

Barker, J.M., 1983, Preliminary investigation of the origin of the Riley travertine, Socorro County, New Mexico: New Mexico Geological Society Guidebook 30, p.269-276.

Barker, J.M., 1984, Origin of the Riley travertine as constrained by the clay mineralogy of acid- and EDTA- insoluble residues: New Mexico Bureau of Mines and Mineral Resources Open-file Report 212, p. 6,7.

Barroll, M.W. and Reiter, M., 1990, Analysis of the Socorro Hydrogeothermal system: Central New Mexico: Journal of Geophysical Research, vol. 95, p. 949 963.

Burne, R.V. and Moore, S.L., 1987, Microbialites: Organosedimentary deposits of benthic microbial commmunities: Palaios, vol. 2, p. 241-254.

Chafetz, H.S., 1986, Marine peloids: a product of bacterially induced precipitation of calcite: Journal of Sedimentary Petrology, vol. 56, 812-817.

Chafetz, H.S., Rush, P.F. and Utech, N.M., 1991, Microenvironmental controls on mineralogy and habit of $CaCO_3$, precipitates: an example from an active travertine system: Sedimentology, vol. 38, p.107-126.

Chafetz, H.S. and Butler, J.C., 1980, Petrology of recent caliche pisolites, spherulites and speleothem deposits from central Texas: Sedimentology, vol. 27, p. 497-518.

Chafetz, H.S. and Folk, R.L., 1984, Travertines: Depositional morphology and the bacterially constructed constituents: Journal of Sedimentary Petrology, vol. 54, p.289-316.

Chamberlin, R.M. et al., 1982, Preliminary evaluation of the mineral resource potential of the Sierra Ladrones wilderness study area, Socorro County, New Mexico: New Mexico Bureau of Mines and Mineral Resources Open-file Report 179, p.142-154.

Clayton, R.N., 1962, Oxygen isotope fractionation between calcium carbonate and water: Journal of Chemical Physics, vol. 34, p. 724-726.

Dandurand, J.L., Gout, R., Hoefs, J., Menschel, G., Schott, E. and Usdowski, E., 1982, Kinetically controlled variation of major components and carbon and oxygen isotopes in a calcite-precipitating spring: chemical Geology, vol. 36, p.299-315.

Denny, C.S., 1940, Tertiary geology of the San Acacia area, New Mexico: The Journal of Geology, vol. 48, p. 73-106.

Denny, C.S., 1941, Quaternary geology of the San Acacia area, New Mexico: The Journal of Geology, vol. 49, p.225-239.

Emeis, K.-C., Richnow, H.H. and Kempe, S., 1987, Travertine formation in plitvice National Park, Yugoslavia: Chemical versus biological control: Sedimentology, vol. 34, p. 595-609.

Fisher, R.A., 1979, A biochemical study of the recent calcite deposits along the Lucero uplift, Valencia County, New Mexico: Unpublished Master's Thesis, New Mexico Institute of Mining and Technology, Socorro, 152p.

Fitzmaurice, S.P., 1990, The petrolography, geochemistry, and depositional environments of travertines of the Palm Park Formation (Eocene), Caballo Mountains, New Mexico: Unpublished Master's Thesis, University of Houston, Houston, Texas, 316p.

Folk, R.L., 1962, Spectral subdivision of Limestone types in Classification of Carbonate Rocks, W.E. Ham, ed., Memoirs American Association Petroleum Geologists, vol. 1, p. 62-84.

Folk, R.L. and Chavetz, H.S., 1983, Pisoliths(pisoids) in Quaternary travertines of Tivoli,Italy: in Coated Grains,ed. by T.M. Peryt, Springer-Verlag,Ber*lin, p.474-487.

Friedman, G.M., Amiel, A.J., Braun, M., and Miller, D.S., 1973, Generation of carbonate particles and laminites in algal mats-example from sea-marginal hypersaline pool, Gulf of Aqaba, Red Sea: American Association Petroleum Geologists Bulletin, vol. 57, p. 541-557.

Friedman, G.M., 1967, The Fabric of Carbonate Cement and Matrix and its dependence on the salinity of water: in Depositional environments in carbonate rocks, ed. by G.M. Friedman, Soceity of Economic Paleontologists and Mineralogists Special Publication No. 14, p. 11-20.

Friedman, I., 1970, Some investigations of the deposition of travertine from hot springs-I. The isotopic chemistry of a travertine-depositing spring: Geochimica et Cosmochimica Acta, vol. 34, p. 1303-1315.

Gary, M., McAfee, Jr., R. and Wolf, C.L., editors, 1974, Glossary of Geology; American Geological Institute, Washington, D.C.

Given, R.K. and Wilkinson, B.H., 1985, Kinetic control of morphology, composition, and mineralogy of abiotic sedimentary carbonates: Journal of Sedimentary Petrology, vol. 55, p. 109-119.

Golubic, S., 1991, Modern Stromatolites: A Review: in Calcareous Algae and Stromatolites, R. Riding, ed., Springer-Verlag, p.541-561.

Henning, G.J., et al, 1982, Speleothems, Travertines, and Paleoclimates: Quaternary Research, vol. 20, p. 1-26.

Herman, J.S. and Lorah, M.M., 1987, CO_2 outgassing and calcite precipitation in Falling Spring Creek, Virginia, U.S.A.: Chemical Geology, vol. 62, p. 251-262.

Irion, G. and Muller, G., 1968, Mineralogy, petrology and chemical composition of some calcareous tufa from the Schwavische Alb, Germany: in Recent developments in carbonate sedimentology in Central Europe, G. Muller and G.M. Friedman, eds., p.157-171.

Jones, B., 1989, Calcite rafts, peloids, and micrite, in cave deposits from Cayman Brac, British West Indies: Canadian Journal of Earth Science, vol. 26, p.654-664.

Julia, R., 1983, Travertines: in Carbonate Depositional Environments; ed. P.A. Scolle, D.G. Bebout and C.H. Moore, American Association of Petroleum Geologists, Tulsa, Oklahoma, p.64-72.

Kottlowski, F.E., 1962, Reconnaissance of commercial high- calcium limestones in New Mexico: New Bureau of Mines and Mineral Resources, Circular 60, p. 9,20-21,28.

Lambert, S.J. and Harvey, D.M., 1987, Stable-Isotope geochemistry of groundwaters in the Delaware Basin of Southeastern New Mexico: Sandia Report SAND87-UC-70, pg. 42-51

Leslie, A.B., Tucker, M.E. and Spiro, B., 1992, A sedimentological and stable isotopic study of travertines and associated sediments within Upper Triassic lacustrine Limestones, South Wales, UK: sedimentology vol. 39, 613-629.

Livnat, A. and Kronfeld, J., 1985, Paleoclimatic implications of U-series dates for lake sediments and travertines in the Araua Riff Valley, Israel: Quaternary Research, vol. 24, p.164-172.

Love, K.M. and Chafetz, H.S., 1988, Diagenesis of laminated travertine crusts, Arbuckle Mountains, Oklahoma: Journal of Sedimentary Petrology, vol. 58, p.441-445.

Lorah, M.M., and Herman, J.S., 1988, The chemical evolution of a travertine-depositing stream: geochemical processes and mass transfer reactions: Water Resources Research, vol. 24, no. 9, p.1541-1552.

Massingill, G.L., 1979, Geology of the Riley-Puertecito area, southeastern margin of the Coloroda Plateau, Socorro County, New Mexico: New Mexico Bureau of Mines and Mineral Resources Open-file Report 107, p.12,13,127-128.

McLemore, V.M. and Barker, J.M., 1987, Some geological applications of cathodoluminescence-examples from the Lemitar Mountains and Riley travertine, Socorro County, NNew Mexico: New Mexico Geology, vol. 9, p.37-40.

Mount, J.F. and Cohen, A.S., 1984, Petrology and geochemistry of rhizoliths from Plio-Pleistocene fluvial and marginal lacustrine deposits, East Lake Turkana, Kenya: Journal of Sedimentary Petrology, vol. 54, p. 263-275.

Pazdur, A. and Pazdur, F., 1988, Stable Isotopes of Holocene Calcareous Tufa in Southern Poland as Paleoclimatic Indicators: Quaternary Research, vol. 30, p. 177-189.

Peryt, T.M., 1983, Vadoids: in Coated Grains, ed. by T.M. Peryt, Springer-Verlag, Berlin, p. 437-449.

Slack, K.V., 1967, Physical and chemical description of Birck Creek, a travertine depositing stream, Inyo County, California: U.G.S. Professional Paper 549-A, 19 p.

Usdowski, E., Hoefs, J. and Menschel, G., 1979, Relationship between ^{13}C and ^{18}O fractionation and changes in major element composition in a recent calcite-depositing spring-A model of chemical variations with inorganic $CaCO_3$ precipitation: Earth and Planetary Science Letters, vol. 42, p.267-276.

Warren, J.K., 1982, The hydrobiological significance of Holocene tepees, stromolites and boxwork limestones in coastal salinas in South Australia: Journal of Sedimentary Petrology, vol. 52, p. 1171-1201.

Wigley, T.M.L. and Plummer, L.N., 1976, Mixing of carbonate waters: Geochimica et Cosmochimica Acta, vol. 40, p.989-995.

Winograd, I.J., Szabo, B.J., Coplen, T.B. and Riggs, A.C., 1988, A 250,000-year climatic record from Great Basin vein calcite: Implications for Milankovitch Theory: Science, vol. 242, p. 1275-1280.

APPENDIX

RBTS	ISOTOPIC	SAMPLE	VALUES
Sample #	Carbon-13 PDB	Oxygen-18 SMOW	Oxygen-18 PDB
1	4.52	23.04	-7.59
2	4.63	22.91	-7.71
3	4.66	22.99	-7.64
4	4.32	22.68	-7.94
5	2.58	22.93	-7.69
6	3.52	23.08	-7.55
7	4.07	23.16	-7.47
8	3.22	22.75	-7.87
9	3.46	23.13	-7.50
10	2.68	22.54	-8.07
11	3.22	22.23	-8.37
12	3.45	22.29	-8.32
13	3.47	23.46	-7.18
14	3.38	23.90	-6.75
15	3.21	24.30	-6.37
16	3.28	24.16	-6.50
17	3.59	24.06	-6.60
18	4.07	23.30	-7.33
19	4.30	22.92	-7.70
20	4.50	22.73	-7.88
21	4.86	22.72	-7.90
22	4.47	23.32	-7.31
23	4.39	23.53	-7.11
24	4.10	23.11	-7.52
25	4.22	22.63	-7.99
26	4.09	22.82	-7.80
27	3.85	22.59	-8.02
28	4.03	22.25	-8.36

RBTS	ISOTOPIC	SAMPLE	VALUES
Sample #	Carbon-13 PDB	Oxygen-18 SMOW	Oxygen-18 PDB
29	4.24	21.68	-8.91
30	4.14	22.26	-8.35
31	4.28	22.23	-8.37
32	4.27	22.61	-8.00
33	4.32	22.80	-7.82
34	4.70	22.97	-7.65
35	4.11	22.38	-8.22
36	3.28	22.02	-8.57
37	3.31	22.02	-8.57
38	3.05	22.33	-8.28
39	2.48	21.94	-8.66
40	1.78	22.27	-8.33
41	1.62	22.13	-8.47
42	1.60	22.52	-8.09
43	2.75	22.49	-8.12
44	3.64	22.96	-7.66
45	3.73	23.30	-7.33
46	3.60	23.19	-7.44
47	4.46	22.98	-7.65
48	4.62	23.08	-7.54
49	4.46	23.56	-7.08
50	3.93	23.23	-7.40
51	3.80	22.85	-7.78
52	3.83	22.83	-7.79
53	2.48	23.83	-6.82
54	4.22	22.72	-7.90
55	2.69	24.10	-6.55
56	4.47	22.31	-8.29
57	3.29	22.98	-7.64

NRDC#1	ISOTOPIC	SAMPLE	VALUES
Sample #	Carbon-13 PDB	Oxygen-18 SMOW	Oxygen-18 PDB
1	5.85	21.89	-8.70
2	6.37	22.37	-8.24
3	6.86	21.77	-8.82
4	6.58	22.27	-8.33
5	7.06	23.08	-7.55
6	6.36	23.07	-7.55
7	5.48	23.35	-7.29
8	6.81	22.13	-8.47
9	6.24	23.13	-7.50
10	6.79	22.50	-8.11
11	6.51	23.13	-7.50
12	6.38	23.18	-7.45
13	6.35	23.04	-7.58
14	6.85	23.76	-6.88
15	6.79	23.31	-7.33
16	7.91	22.79	-7.83
17	6.32	21.02	-9.55
18	6.06	21.06	-9.51
19	6.14	21.00	-9.56
20	6.27	22.96	-7.66
21	6.74	22.99	-7.63
22	6.73	22.58	-8.03
23	6.59	22.77	-7.84
24	6.48	22.80	-7.82
25	6.27	22.15	-8.45
26	6.80	22.46	-8.15
27	6.61	23.04	-7.59
28	6.66	22.52	-8.09
29	6.50	23.04	-7.59
30	6.37	22.58	-8.03
31	6.22	22.62	-7.99
32	6.48	22.39	-8.22
33	9.77	21.35	-9.22
34	6.36	22.78	-7.84
35	4.99	24.14	-6.52
36	6.74	22.38	-8.23
37	6.63	22.61	-8.01
38	6.64	22.62	-7.99
39	6.64	22.34	-8.26
40	6.61	22.44	-8.17
41	6.64	22.59	-8.02
42	6.62	22.64	-7.98
43	6.69	22.45	-8.16
44	6.73	22.38	-8.22
45	6.50	22.38	-8.23
46	6.65	22.38	-8.23
47	7.55	22.06	-8.54
48	6.60	23.23	-7.41
49	6.69	23.21	-7.42
50	6.67	22.52	-8.09

NRDC#1	ISOTOPIC	SAMPLE	VALUES
Sample #	Carbon-13 PDB	Oxygen-18 SMOW	Oxygen-18 PDB
51	6.88	22.64	-7.98
52	6.83	22.33	-8.27
53	6.53	22.46	-8.15
54	5.61	23.92	-6.73
55	6.20	22.83	-7.79
56	6.30	22.58	-8.03
57	6.40	22.62	-8.00
58	6.71	22.56	-8.05
59	6.81	22.34	-8.27
60	6.57	22.27	-8.34
61	7.12	22.22	-8.38
62	6.61	22.51	-8.11
63	6.86	22.43	-8.18
64	6.81	22.25	-8.35
65	6.74	22.68	-7.94
66	6.50	22.39	-8.22
67	7.54	22.91	-7.72
68	7.20	22.29	-8.32
69	7.33	22.38	-8.23
70	6.61	23.18	-7.45
71	6.27	22.36	-8.25
72	6.08	22.51	-8.10
73	6.29	22.24	-8.36
74	6.40	21.96	-8.64
75	6.74	22.74	-7.88
76	6.64	22.58	-8.03
77	6.97	22.72	-7.89
78	6.85	22.84	-7.78
79	7.32	22.73	-7.89
80	7.43	22.59	-8.02
81	6.30	20.63	-9.93
82	6.63	22.37	-8.23
83	6.66	22.88	-7.74
84	7.01	23.89	-6.76
85	6.90	23.96	-6.70
86	7.44	23.56	-7.08
87	7.28	22.59	-8.02
88	7.46	23.01	-7.61
89	7.11	23.43	-7.21
90	7.18	23.44	-7.20
91	6.85	23.62	-7.03
92	7.27	23.13	-7.50
93	7.25	23.04	-7.59
94	7.53	22.89	-7.73
95	7.06	22.83	-7.79
96	7.20	21.90	-8.69
97	7.55	22.03	-8.57
98	6.95	22.52	-8.09
99	7.32	22.49	-8.12
100	6.75	21.98	-8.61

SAMPLE	DEPTH	NRDC#1	ISOTOPIC SAMPLE DESCRIPTION
8.2m + " "mm	27ft + " "in	SAMPLE #	TEXTURE(S) OBSERVED AND ASSOCIATED WITH SAMPLE
104.9	4.13	1	TLB
108.0	4.25	2	TLB
111.3	4.38	3	TLB
114.3	4.50	4	TLB
120.7	4.75	5	TLB
127.0	5.00	6	INTRASPARRUDITE; MIC. ALLOCHEM RICH
139.7	5.50	8	TLB
158.8	6.25	7	DIAGENETIC SPAR; STALACTITE
190.5	7.50	10	TLB
203.2	8.00	9	BLOCKY SPAR;TERRA ROSSA
219.2	8.63	11	INTRASPARRUDITE
266.7	10.50	12	INTRASPARRUDITE; PROBABLE RHIZOLITH
270.0	10.63	13	INTRASPARRUDITE
292.1	11.50	14	INTRASPARRUDITE;MIC. ALLOCHEMS;PROBABLE RHIZ.
317.5	12.50	16	SPAR CEMENT
330.2	13.00	15	INTRASPARRUDITE; MIC. ALLOCHEMS; POSSIBLE RHIZ.
349.3	13.75	17	TLB
355.6	14.00	18	TLB
355.6	14.00	19	TLB
374.7	14.75	21	INTRASPARRUDITE "CLASTS" IN TERRA ROSSA
381.0	15.00	20	SPAR CEMENT; TERRA ROSSA
562.1	22.13	23	INTRASPARRUDITE;MULTI-LAYERED COATED GRAINS
571.5	22.50	22	INTRASPARRUDITE;MULTI-LAYERED COATED GRAINS
701.8	27.63	24	INTRASPARRUDITE; SPAR(S)
730.3	28.75	25	INTRASPARRUDITE; PROBABLE RHIZ.
784.4	30.88	26	INTRASPARRUDITE;MULTI-LAYERED COATED GRAINS
784.4	30.88	27	SPAR CEMENT; BLOCKY AND DRUSY; TERRA ROSSA
809.8	31.88	28	INTRASPARRUDITE
866.9	34.13	29	SPAR CEMENT
866.9	34.13	30	INTRASPARRUDITE; PROBABLE RHIZ.
901.7	35.50	31	INTRASPARRUDITE; PROBABLE RHIZ.
977.9	38.50	32	INTRASPARRUDITE W/ MIC. "CLASTS" IN POROUS ZONE;
1168.4	46.00	33	TLB CLAST;FRACTURED
1168.4	46.00	34	INTRASPARRUDITE; POSSIBLE RHIZOLITH
1219.2	48.00	35	SPAR; STACTITE; TRACE INTRACLASTS IN SPAR
1308.1	51.50	36	BLOCKY SPAR; TERRA ROSSA
1327.2	52.25	37	SHRUB LAYER;W/ THIN INTRASPARRUDITE BEDS
1327.2	52.25	38	SHRUB LAYER;W/ THIN INTRASPARRUDITE BEDS
1330.5	52.38	39	SPAR IN VEIN; INTRASPARRUDITE BORDER
1336.8	52.63	40	SPAR IN VEIN; INTRASPARRUDITE BORDER
1346.2	53.00	41	SHRUB LAYER;W/ THIN INTRASPARRUDITE BEDS
1346.2	53.00	42	SHRUB LAYER;W/ THIN INTRASPARRUDITE BEDS
1352.6	53.25	43	SHRUB LAYER;W/ THIN INTRASPARRUDITE BEDS
1352.6	53.25	44	SHRUB LAYER;W/ THIN INTRASPARRUDITE BEDS
1368.6	53.88	45	SHRUB LAYER;W/ THIN INTRASPARRUDITE BEDS
1549.4	61.00	46	TLB
1552.7	61.13	47	TLB
1574.8	62.00	48	SHRUB CLAST SURROUNDED BY INTRASPARRUDITE & SPAR
1581.2	62.25	49	RADIAL & BLOCKY(?) CEMENT PARTIALLY FILLING VOID
1692.4	66.63	50	BLOCKY SPAR; TERRA ROSSA; Fe BANDS DOMAL

SAMPLE	DEPTH	NRDC#1	ISOTOPIC SAMPLE DESCRIPTION
8.2m + " "mm	27ft + " "in	SAMPLE #	TEXTURE(S) OBSERVED AND ASSOCIATED WITH SAMPLE
1694.9	66.73	51	RAFTS;SPAR/MICRITE CEMENT LAYERS
1701.8	67.00	52	RAFTS;SPAR/MICRITE CEMENT LAYERS
1708.2	67.25	55	RAFTS;SPAR/MICRITE CEMENT LAYERS
1720.9	67.75	53	RAFTS;SPAR/MICRITE CEMENT LAYERS
1720.9	67.75	54	STYL RAFTS;MICROSPAR IN SPAR/MIC. CEMENT LAYERS
1835.2	72.25	56	RAFTS;SPAR/MICRITE CEMENT LAYERS
1847.9	72.75	58	RAFTS;SPAR/MICRITE CEMENT LAYERS
1854.2	73.00	57	INTRASPARRUDITE & SPAR(RARE)
1866.9	73.50	59	INTRASPARRUDITE; MICRITIC ALLOCHEM RICH
1879.6	74.00	60	INTRASPARRUDITE; MICRITIC ALLOCHEM RICH
1886.0	74.25	61	INTRASPARRUDITE W/MIC. "CLAST" IN YELLOW MATRIX
1898.7	74.75	62	YELLOW TERRA ROSSA-LIKE MATRIX
1917.7	75.50	63	INTRASPPARRUDITE "CLASTS" Fe(OH) IN POROUS ZONE
1955.8	77.00	64	INTRASPARRUDITE; MIC. ALLOCHEMS; PROBABLE RHIZ.
1955.8	77.00	66	BLOCKY & RADIAL CEMENT
1962.2	77.25	65	RAFTS;POSSIBLE STYL AND MICROSPAR,
2000.3	78.75	67	SPAR CEMENT
2101.9	82.75	68	INTRASPARRUDITE;MIC. ALLOCHEMS;PROBABLE RHIZ.
2108.2	83.00	69	INTRASPARRUDITE
2152.7	84.75	70	BLOCKY SPAR (Fe STAINING)
2197.1	86.50	72	BLOCKY & RADIAL CEMENT;Fe & Mn DOMAL
2197.1	86.50	73	SPAR (RADIAL + BLOCKY); Fe STAINED
2203.5	86.75	71	BLOCKY SPAR;Fe DOMAL
2295.7	90.38	74	INTRASPARRUDITE;MIC. ALLOCHEMS; PROBABLE RHIZ.
2730.5	107.50	75	SHRUB LAYER;INTRASPARRUDITE THIN BEDS
2736.9	107.75	76	SHRUB LAYER;INTRASPARRUDITE THIN BEDS
2736.9	107.75	77	SHRUB LAYER;INTRASPARRUDITE THIN BEDS
2743.2	108.00	78	SHRUB LAYER;INTRASPARRUDITE THIN BEDS
2749.6	108.25	79	INTRASPARRUDITE & SHRUB LAYER; (50/50)
2800.4	110.25	80	INTRASPARRUDITE & SHRUB LAYER; (50/50)
2935.4	112.63	81	TLB
2863.9	112.75	82	INTRASPARRUDITE FILLING DESICCATION CRACK
3683.0	145	83	INTRASPARRUDITE;MIC. CLAST;SPAR MATRIX
3708.4	146	84	INTRASPARRUDITE
3759.2	148	85	INTRASPARRUDITE;MIC. ALLOCHEMS & SOME CEMENT
3733.8	147	86	INTRASPARRUDITE
3708.4	146	87	INTRASPARRUDITE
3733.8	147	88	INTRASPARRUDITE
3759.2	148	89	INTRASPARRUDITE
3784.6	149	90	INTRASPARRUDITE
3810.0	150	91	INTRASPARRUDITE
3835.4	151	92	INTRASPARRUDITE
3860.8	152	93	INTRASPARRUDITE
3886.2	153	94	INTRASPARRUDITE
3911.6	154	95	INTRASPARRUDITE
3911.6	154	96	INTRASPARRUDITE;MIC.ALLOCHEMS;IN POROUS ZONE
3937.0	155	97	INTRASPARRUDITE
3886.2	153	98	SPAR CEMENT
4165.6	164	99	INTRASPARRUDITE;MIC. ALLOCHEMS CLASTS
4114.8	162	100	SPAR CEMENT; TERRA ROSSA

NORTH RILEY TRAVERTINE DRILL CORE #1
THIN SECTION AND PLANCHETTE LIST

THIN SECTION NUMBER	STRATIGRAPHIC DEPTH		RELATED ISOTOPIC SAMPLE(S) NUMBER
	meters	ft' in"	
1	8.33	27' 4"	1-6
2	8.81	28' 11"	22,23
3	9.19	30' 2"(r)	
4	9.19	30' 2"(l)	
5	9.22	30' 3"	32
6	9.45	31' 0"	35
7	9.41	30' 10.5"	33,34
8	9.80	32' 2"	48,49
9	9.78	32' 1"(l)	46,47
10	9.78	32' 1"(r)	46,47
11	8.56	28' 1"	17-19
12	9.93	32' 7"	50-55
13	9.55	31' 4"	37-40
15	9.58	31' 5"	40-44
17	9.63	31' 7"	44,45
18	8.41	27' 7"	10
19	8.43	27' 8"	9,11
21	8.92	29' 3"	24
23	9.02	29' 7"	26-28
24	10.52	34' 6"	
25	10.54	34' 7"	74
26	10.22	33' 6.5"	65,67
27	10.24	33' 7"	
29	10.08	33' 1"(r)	56,58,59
30	10.08	33' 1"(c)	56,58
31	10.08	33' 1"(l)	56,57,58
32	10.20	33' 5.5"	64-66
33	10.17	33' 4.5"	65
35	10.59	34' 9"	
38	10.99	36' 0.5"	75,76
39	10.36	34' 0"	70
40	10.39	34' 1"	
41	10.41	34' 2"	72,73
42	10.43	34' 2.75"	71
44	10.97	36' 0"	77, 78
45	11.07	36' 4"	81,82
46	10.36	34' 0"	70,72
47	10.40	34' 1.5"	71,73

(l)=left (c)=center (r)=right
depth measured in decreasing order: 30'12" = 31' 0"

DESCRIPTION OF THIN SECTIONS OF NRDC#1

Abbreviations

Spar	= Calcite cement crystals 10 microns or larger (Folk, 1962)
TLB	= Translucent laminated bands (see text)
Rhiz(s)	= Rhizolith(s)
Onc	= Oncolite
Fe	= Iron-mineral(oid) phase
Pspar	= Previously deposited $CaCO_3$ that has undergone neomorphism(Pseudospar)
Pel	= peloids
Cgr	= coated grains (Vadoids - Peryt,1983) (Pisoids - Folk and Chafetz,1983)
Xtals	= crystals
Desi	= desiccation caused cracks
Int	= Intraclasts

Definition of (%)

M = Mostly > 70%	S = Some > 10% - < 25%
VC = Very Common > 50% - < 70%	R = Rare > 5% - < 10%
C = Common > 25%- < 50%	VR = Very Rare <5%

#	FABRIC (%)	COMPOSITION
1)	TLB (C)	Distinct thin laminations
	Micrite (C)	Pel grains (VC), Int (C)
	Moldic Pores (VR)	Possible Rhiz, Fe staining around vug
	---	---
2)	Rhiz (Horizontal) (C)	Drusy xtals on edge, then Fe, then equant spar in center
	Moldic Pores (S)	
	TLB (R)	
	Micrite (S)	Int (S), Cgr (VR)
	---	---
3)	Micrite (VC)	Pel grains (VC), Onc (VR), Shrub clast (VR)
	Moldic Pores (R)	
	Rhiz (Horizontal) (C)	Drusy xtals on edge, then Fe, then equant spar in center
	---	---
4)	Very similar to 3)	
	---	---
5)	Moldic Pores (C)	
	Micrite (C)	Pel grains (M), Int (S)
	---	---
6)	Moldic Pores (C)	Probable Rhiz
	Micrite (C)	Int (M), Cgr (C), Onc (VR), TLB and Shrub clasts (VR)
	TLB (R)	

#	FABRIC (%)	COMPOSITION
7)	Moldic Pores (C) Micrite (C)	Rhiz (C) Int (M), Cgr (C), Desi (?), TLB clasts (R), Shrub clast (VR)
8)	Moldic Pores (R) Micrite (C) Shrubs (S) Spar (C)	 Int (C), shrub clast (R) Distorted layers Crystals are elongate when in contact with pores
9)	Moldic Pores (C) Spar (VC) Pspar (R)	 Matrix and coating travertine rafts Pspar grains cross micrite/spar layers
10)	Moldic Pores (C) Micrite (C) TLB (S)	Probable rhiz Int (C), Shrub-cored grains (R) Bladed crystals
11)	Moldic Pores (S) TLB (M) Micrite (R)	Possible rhiz at base Pel grains
12)	Moldic Pores (S) Spar (M)	 Surrounding Rafts (M), Cgr (VR)
13)	Moldic Pores (C) Micrite (VC)	 Shrubs (M), pel grains (S)
15)	Moldic Pores (C) Micrite (C) Shrubs (C)	 Int (C)
17)	Very similar to 15)	
18)	Moldic Pore (VR) TLB (M) Micrite (VR)	 Onc (S), Int (C)
19)	Moldic Pores (VC) Micrite (C)	Fe, possible rhiz(s) Cgr (VC), pel grains (C)
21)	Moldic Pores (VC) Micrite (C)	Fe in drusy xtals, equant or blocky in center Int (C), Cgr. (S)(some coated grains "free floating" in spar cement
23)	Moldic Pores (C) Micrite (VC)	 Int (VC), Cgr (C), pel grains (C) many peloids have spar centers)

#	FABRIC	COMPOSITION
24)	Moldic Pores (C)	Fe rinds on equant or spar
	TLB (C)	Xtals > 1mm
	Pspar (C)	Vague outline on rafts remains
25)	Moldic Pores (C)	Possible rhiz
	Pspar (C)	Spar growing across multiple generations of intraclasts
	Spar (C)	Composing the matrix
26)	Moldic Pores (C)	Possible rhiz
	Spar (VC)	Surrounding rafts (C),
	Micrite (R)	Pel grains (C), Int (VC)
27)	Moldic Pores (S)	
	Spar (VC)	Surrounding rafts (C), dark colored spar (C)
	Micrite (R)	Pel grains
29)	Moldic Pores (S)	Probable rhiz
	Micrite (S)	Int (C), Cgr(S)
	Spar (VC)	Surrounding rafts (fish hook looking raft with 3 alternating layers. Most intense bio by moldic pores, maybe cyanobacteria grew on stem?).
30)	Moldic Pores (S)	Fe glaebules (Jones, 1989) stain spar
	Spar (C)	Matrix between rafts
	Pspar (R)	Raft cements recrystallized
	Micrite (C)	Int (M), Pel (R)
31)	Moldic Pores (S)	
	Rafts (S)	
	Pspar (VC)	(Possibly TLB but banding is truncated by moldic pores in areas, showing that light(spar)/dark is mirrored around spar center).
32)	Moldic Pore (C)	Possible rhiz
	Micrite (S)	Int (M), Cgr (C)
	Spar (C)	
33)	Moldic Pores(C)	Possible rhiz
	Spar (VC)	Inclusions of Int and Pel
35)	SLIDE DAMAGED	
	Moldic Pores (C)	Vertical rhiz or desi
	Micrite (VC)	Int (C), Pel grains (C)

#	FABRIC	COMPOSITIONS
38)	Moldic Pores (S)	
	Micrite (S)	Thin layers of pel between shrubs
	Shrubs (M)	Superior example
	Spar (R)	Coating isopachous shrubs
39)	Micrite (R)	Int (M), Cgr (S)
	Spar (S)	Spar banded, domal > stromlike?, later blocky spar invades domal bands
	Moldic Pores (VC)	Rhiz? Fe-staining
40)	Moldic Pores (S)	
	Spar (VC)	Fe rind staining spar
	Micrite (S)	Int (C)
41)	Moldic Pores (S)	
	Spar (M)	Fe-stained blocky spar
	Pspar (VR)	Colloidal-looking Fe crossing rafts
42)	Moldic Pore (S)	Possible rhiz?
	Spar (M)	Fe-strands in spar have domal look
	Pspar (S)	Neomorphic spar across shrub layer
44)	Moldic Pore (R)	
	Shrubs (M)	
	Micrite (S)	Thin horizontal layers between shrubs
45)	SLIDE DAMAGED	
	TLB (M)	Bladed crystal growth
	Moldic Pores (R)	
	Spar (S)	Coating perimeter of vugs
46)	Moldic Pore (R)	Probable rhizolith
	Spar (VC)	Fe-stain pervasive, possible rafting obliterated, less altered away from center
	Pspar (S)	Highly altered in center
	Micrite (S)	Varying multi-layered Cgr (C)
47)	Moldic Pores (R)	
	Spar (VC)	Fe-filaments and black Mn? in equant spar.
	Micrite (R)	Pel grains
	Pspar (R)	Highly altered areas, probably ex-rafts in region.